ADVANCED LECTURES 1986

PARAMETRIZATION OF PHYSICAL PROCESSES IN ATMOSPHERE AND OCEAN MODELS

VOL 1

DRS D J CARSON AND H CATTLE

.nj

Advanced Lecture 1

Introduction to parametrization and ocean models and the representation of orographic effects in atmospheric models

1.1 Introduction to parametrization

The title of this lecture series: "The parametrization of physical processes in atmosphere and ocean models" may require a little elaboration, for the models are, of course, themselves constructed from equations for the physical concepts of conservation of mass, momentum, and heat and, in the case of the atmosphere, of water substance and of the ocean, of salt. In order to do this, we shall here follow closely the discussion of Smagorinsky (1981), from which the time-space domain for characteristic atmospheric phenomena shown in Figure 1.1 is drawn. This is typical of the free atmosphere (away from the lower boundary). Note that it covers a 10 order of magnitude span of horizontal dimension, but does not include sizes, for example of cloud water droplets (< 1 mm). There is a major energy peak at around 3000 to 6000 km, corresponding to a zonal wavenumber of 5 to 8 (the number of waves of wind or temperature around a latitude circle). There are second peaks corresponding to tropical cyclones, fronts, cumulus convection, tornadoes, cloud and clear air turbulence. They are generally intermittent phenomena and thus may not appear in the spectrum taken at any one time. Usually, because of computer limitations, a numerical model can at most resolve a two order of magnitude span of scales in this spectrum (Figure 1.2). Hence a global model with a horizontal grid size of 100 km can resolve wavelengths of 400 km or larger up to the planetary size (about 40,000 km). Their interactions with smaller scales must be dealt with by other methods, which means that they must be parametrized, That is, their integrated effects on the grid scale must be represented in terms of the variables explicitly resolved - the "large scale" or "grid scale" variables. For the atmosphere these constitute the macroscale wind, temperature and humidity; for the ocean the current, temperature and salinity. As noted by Smagorinsky a parametrization allows for a two way interaction between the resolved and parametrized parts of the spectrum; it also usually introduces empirical constants (parameters) that enter into the prescription. An example of such a parameter is the eddy viscosity coefficient in a turbulent parametrization. Thus what is at issue here is the representation of those processes that take place on scales smaller than can be resolved on, in the case of a finite difference model, the model grid or, in the case of a spectral model, at wavelengths smaller than the truncation wavelength of the model. Since, for a spectral model, inclusion of these processes involves a transformation from wavenumber space to physical space on a finite grid, the term "physical processes" in the title of this lecture series might be appropriately replaced by the term "sub grid-scale", therefore.

Note that characteristic space and time scales for the ocean are very different to those for the atmosphere. Thus, for example, although the upper ocean responds rapidly to imposed atmospheric forcing, the deep ocean response time is of the order of centuries or more, whilst the "synopic scale" eddies of the ocean (the equivalent of the atmospheric cyclones and anticyclones of middle latitudes) have

horizontal scales of order only tens of kilometers or so (Figure 1.3).

What, then are the main processes to be parametrized? For the atmosphere, parametrized processes make contributions to all three of the momentum, thermal energy and water vapour equations, and thereby indirectly to the mass balance (Figure 1.4). Those directly affecting the thermal energy equation involve, firstly, radiative processes in both the solar and terrestrial infrared parts of the spectrum, the scattering, absorption or transmission of which will in general depend on the changing content of water vapour and liquid water particles. Thus cloudiness must be parametrized, both layer cloud due to large scale (dynamical) condensation and convective cloud. The effects of latent heat released by condensation must also be allowed for in the thermal energy equation. Further, if hydrological processes in the atmosphere are to be correctly represented, both precipitation and evaporation must be parametrized. The interaction of the atmosphere with its lower boundary is of particular importance. For forecasting models, this is because the near surface conditions in which we live are of interest to us all, whilst for climate research the lower boundary represents one of the major sources and sinks of atmospheric energy. For example, the atmospheric circulation loses about half its energy via the stress at the surface. Moreover the atmosphere is largely transparent to solar radiation whilst much of that which reaches the surface is absorbed and then fed back up by infrared radiation and through turbulent transfer of sensible and latent heat. Aspects which require parametrization, therefore, are both the heat, water and momentum fluxes from the surface itself and their associated transfers through the atmospheric boundary layer. The former may require more or less detailed models of the underlying surface - of soil moisture and heat conduction, for example.

The correct representation of the surface fluxes is also of crucial importance for modelling of the ocean, which itself is driven by the net heat flux across the ocean surface (the sum of the net solar and infrared radiative fluxes and the sensible and latent heat flux), the surface stress and the precipitation less evaporation difference. Whilst not important for day to day weather forecasting, ocean models are becoming of increasing importance to the meteorologist from the point of view of the construction of interactive models of the ocean-atmosphere climate system. In such models, the fluxes at the air-sea interface must be provided by the atmospheric model which itself passes back the updated conditions at the sea surface (Figure 1.5).

Processes required to be parametrized in ocean models include the turbulent transfer of heat, momentum and salt though the oceanic boundary layer (the ocean "mixed layer") and convective overturning to deeper layers. In high latitudes, the presence of sea ice on the ocean surface also needs to be represented. As noted above, the time and space scales of the ocean are very different to that for the atmosphere. Ocean models are restricted just as much by limitations of computer capacity as atmospheric models, so that, again, the finest resolution that can be achieved at present on a global grid is about 1 degree of latitude and longitude. Such models are unable, therefore, unlike their atmospheric counterparts, to resolve the synoptic scale oceanic eddies. This represents a further restriction on the nature of current large scale ocean model simulations. Whilst the nature of

atmospheric modelling is probably well known to most, the nature of ocean modelling will be less familiar. In the next section, therefore, a brief summary of aspects of ocean modelling will be given.

1.2 Some aspects of ocean models

We shall restrict the discussion here only to prognostic models of the ocean, omitting consideration of the so-called diagnostic models which provide a means of combining conservation principles with data. A range of models have, to date, been run in coupled mode with atmospheric models. Some of these are very simple "slab" representations, whereby the upper ocean mixed layer is represented by a column of water of constant depth a few tens of metres in thickness with no dynamics. The water temperature then responds to the imposed heat flux through an equation of the form:

$$\Delta T = \frac{Q_N}{\rho c_p h} \Delta t \qquad (1.1)$$

Such a model was used, for example by Manabe and Stouffer (1980) in a series of CO_2 integrations and in the Meteorological Office has been used by Mitchell with a low resolution version of the Met O 20 climate model. More sophisticated representations of the upper ocean mixed layer are also available, but will not be discussed here as they are dealt with extensively in Lecture 6. Dynamical ocean models range from advective mixed layer models to eddy resolving quasi-geostrophic models run over a limited domain and global primitive equation models. For the discussion here, we shall restrict ourselves to a description of the primitive equation model of Bryan (1969), also described by Semtner (1974) and recently rewritten to be efficient on modern vector computers by Cox (1984). In doing so, we shall note most of the features necessary for parametrization in an ocean modelling context.

The basic equations of the Bryan model, written down in spherical polar coordinates are as follows: (see over)

$$\frac{\partial u}{\partial t} + Lu - \frac{uv\tan\varphi}{a} - fv = -\frac{1}{\rho_0 a\cos\varphi}\frac{\partial p}{\partial\lambda} + \kappa\frac{\partial^2 u}{\partial z^2} + A_M\left\{\nabla^2 u + \frac{(1-\tan^2\varphi)u}{a^2} - \frac{2\sin\varphi}{a^2\cos^2\varphi}\frac{\partial v}{\partial\lambda}\right\}, \quad (1.2)$$

$$\frac{\partial v}{\partial t} + Lv + \frac{u^2\tan\varphi}{a} + fu = -\frac{1}{\rho_0 a}\frac{\partial p}{\partial\varphi} + \kappa\frac{\partial^2 v}{\partial z^2} + A_M\left\{\nabla^2 v + \frac{(1-\tan^2\varphi)v}{a^2} + \frac{2\sin\varphi}{a^2\cos^2\varphi}\frac{\partial u}{\partial\lambda}\right\}, \quad (1.3)$$

$$\frac{\partial p}{\partial z} = -\rho g \quad , \quad (1.4)$$

$$\frac{1}{a\cos\varphi}\frac{\partial u}{\partial\lambda} + \frac{1}{a\cos\varphi}\frac{\partial}{\partial\varphi}(v\cos\varphi) + \frac{\partial w}{\partial z} = 0 \quad , \quad (1.5)$$

$$\frac{\partial\theta}{\partial t} + L\theta = \kappa\frac{\partial^2\theta}{\partial z^2} + A_H\nabla^2\theta \quad , \quad (1.6)$$

$$\frac{\partial S}{\partial t} + LS = \kappa\frac{\partial^2 S}{\partial z^2} + A_H\nabla^2 S \quad , \quad (1.7)$$

$$\rho = \rho(T, S, p) \quad . \quad (1.8)$$

In the above, we have the advection operator,

$$L(\sigma) = \frac{1}{a\cos\varphi}\frac{\partial}{\partial\lambda}(u\sigma) + \frac{1}{a\cos\varphi}\frac{\partial}{\partial\varphi}(\cos\varphi\, v\sigma) + \frac{\partial}{\partial z}(w\sigma) \, ,$$

the horizontal Laplacian operator,

$$\nabla^2\sigma = \frac{1}{a^2\cos^2\varphi}\frac{\partial^2\sigma}{\partial\lambda^2} + \frac{1}{a^2\cos\varphi}\frac{\partial}{\partial\varphi}\left(\cos\varphi\frac{\partial\sigma}{\partial\varphi}\right) \, ,$$

and the Coriolis parameter,

$$f = 2\Omega \sin\varphi \quad .$$

The first two of these ((1.2) and (1.3)) represent conservation of momentum, the third (1.4) is the hydrostatic assumption, (1.5) is an in compressibility condition, (1.6) and (1.7) are equations for potential temperature, θ, and salinity (S) predictions and (1.8) the equation of state for sea water, by which the density is non-linearly related to temperature, salinity and depth. The model is formulated for conditions of arbitrary grid spacing on a latitude-longitude grid and for oceans of arbitrary coastline, bottom topography and connectedness so that it can be set up for any ocean basin or group of basins. Any distribution of levels can be chosen in the vertical. The horizontal grid currently being employed with this model in Met O 20, which is identical to that of their atmospheric general circulation model (AGCM) grid, is illustrated in Figure 1.6. Grid points over land are, of course, effectively ignored by the ocean model. Values of the basic variables u, v, (components of the currents), Θ, and S are integrated forward in time by finite difference approximations to the above equations, with the exception that the solution for the velocity field is complicated by the fact that, in order to remove the effects of fast external gravity waves, a rigid lid condition, w = 0, is imposed at the upper boundary. By this means a longer timestep can be taken than would otherwise be the case. Indeed, for long spin up runs in which the model must be integrated for periods of the order of centuries, it is essential that as long a timestep is used as possible if such runs are to be computationally feasible. In fact, in this case, techniques for using a longer timestep in the more slowly adjusting parts of the system must be used. This entails using a longer timestep for the adjustment of the temperature and salinity fields (of the order of days) than for the velocity fields (up to several hours, depending on the grid size), and with depth, in which case the heat capacities of the lower layers must be adjusted. This has the effect of distorting the dynamics of the waves in the model, which is acceptable, provided the detailed character of the spin up is unimportant and an equilibrium solution is sought (see, e.g. Bryan and Lewis, 1979; Killworth et al., 1984). In essence, the complications which arise from imposition of the surface boundary condition, w = 0, are that the calculation of the velocities must be split into separate calculation of their baroclinic and barotropic parts, the latter via the solution of a Poisson equation for a non divergent streamfunction which gives the vertically integrated flow. As noted above, a variable bottom topography is allowed in the model, with respect to which, the flow is assumed to parallel the slope so that:

$$w = -\frac{u}{a\cos\phi}\frac{\partial H}{\partial \lambda} - \frac{v}{a}\frac{\partial H}{\partial \phi} \qquad (1.9)$$

Referring back to equations (1.2), (1.3), (1.6) and (1.7), it will be noted that these include both horizontal and vertical diffusion terms on their right hand sides. It is sometimes said that that these allow representation of oceanic eddies unresolved by the model grid. However, for grids of the resolution of, for example, Figure 1.6 the horizontal diffusion coefficients, A_H and A_M, for heat/salt and momentum are necessarily chosen for reasons of computational stability

(see Bryan et al., 1975). This, on such, for the ocean, "coarse resolution" grids, results in the values of these coefficients taking values several orders of magnitude higher than can be inferred for example, from regional scale eddy resolving models which means that the models are highly viscous. It is not until the grid length is brought down to a size of the order of 1 degree of latitude/longitude that the two effectively correspond (Semtner, A.J., pers. comm.) and even then the validity of using constant values across the whole model domain must be questioned.

In the model, the specified momentum, heat and fresh water fluxes which go to drive the ocean circulation effectively pass directly into the top layer of the model ocean (of the order of tens of metres in thickness) which communicates with the deeper layers via vertical diffusion, convective adjustment and large scale vertical motion. Except where convective adjustment immediately takes place as a result of layer instabilities, the model therefore effectively has a constant depth slab representation of the upper ocean mixed layer. The inadequacies of this are illustrated in Figure 1.7 which shows the characteristic variation of mixed layer depth at OWS P over a seasonal cycle. Note the rapid spring shallowing and winter deepening, in particular. The topic of improved representations of the upper ocean mixed layer will be taken up again briefly in Lecture 4 and, as already noted, more extensively in Lecture 6. Convection in ocean models will be discussed as part of Lecture 8 which will also generally address the parametrizatio n of convection in atmospheric models.

As noted above, the representation of the fluxes at the air-sea interface in atmospheric models is a crucial one for coupled ocean-atmosphere modelling. The whole question of parametrization of sur face processes will be dealt with extensively in Lectures 2 and 3 (to be given by D.J. Carson), which, though concentrating on the treatment for the land surface will touch on processes relevant to the ocean also. Lectures 4 and 5 will deal primarily on parametrizations of the atmospheric boundary layer in depth, whilst parametrization of clouds and radiation will be dealt with in Lectures 7 and 9. From a purely climate modelling context, lecture 10 will deal with the question of sea ice. For the remainder of this lecture, I want to briefly touch on recent improvements to the representation of the mid-latitude flow which have been brought about by the introduction into models of envelope orography and the parametrization of gravity wave drag.

1.3 The parametrization of orographic drag in atmospheric models

A particular problem experienced in the use of atmospheric models in the past has been that, as their resolution is increased to better than about 4 degrees of latitude, the flow in the mid-latitudes of the northern hemisphere westerlies in winter tends to become too strong at the surface in association with excessively deep low pressure areas over the North Atlantic and Pacific Oceans. Figure 1.8 shows an example taken from the so-called "third annual cycle" integration of the Met O 20 AGCM. It compares the mean sea level pressure distribution averaged over 8 northern hemisphere winters (December to February from the model with a "climatology" derived from the 3 years of operational model analyses. Such behaviour is general and is common to both grid point and spectral atmospheric models. Two recent

solutions to this problem have been to introduce the concept of envelope orography and parametrization of gravity wave drag.

The representations of land surface orography in models are, of necessity, markedly smoothed compared to reality. As an example, the topopography of the Met O 20 AGCM is shown in Figure 1.9. Jarraud et al. (1986) list four main effects which the presence of orography can have the larger scale flow:

** The dynamical low level blocking (barrier) effect over a wide range of scales;

** Generation of smaller scale vertically propogating gravity waves and their dissipative effect on the large scale flow in the troposphere and stratosphere;

** Low level drag associated with very short scales of the orography (up to a few hundred metres)

** Secondary effects due to interactions with precipitation, snow cover, surface temperature, cloud cover etc.

Envelope orography is essentially one way of representing the first of these. As noted by Jarraud et al., several approaches have been used to enhance the low level blocking effect of mountains in numerical models. Some correspond to a more or less explicit blocking of the low level flow (e.g. Egger, 1972). Many others correspond essentially to an increase in the height of the mountains used in models. For example, (Gerrity, 1985) a "silhouette" orography is used for global operational prediction at NMC, Washington. This orography approximately simulates the cross section of the mountains presented to the flow. At ECMWF Wallace et al. (1983) proposed the use of an "envelope orography" constructed, from the mean orography by adding to it twice the square root of the variance over each grid square, as computed from a much finer resolution dataset. Its use in the ECMWF model was found to achieve a significant improvement, including reduction of systematic errors. Some unfavourable aspects of the scheme in the ECMWF model have more recently been investigated by Jarraud et al. (1986).

The importance of the second effect of orography listed above, that of vertically propogating gravity waves, has been advocated by a number of authors in the past (e.g. Lilly, 1962). More recently parametrizations of the drag exerted by gravity waves on the large scale circulation of atmospheric models have been tested at the Canadian Climate Centre by Chouinard et al. (1983) by Palmer et al. (1985) and Slingo and Pearson (1986) in the Met O 20 AGCM and Kitchen et al. (1985) in the Meteorological Office operational Numerical Weather Prediction (NWP) model. An outline of the parametrization described by Palmer et al. for the Met O 20 AGCM will be given here, though for details of the approximations and assumptions involved, together with appropriate derivations, the reader is referred to their paper.

The parametrization essentially consists of two parts. An expression for the stress, τ_{gs} , due to gravity wave drag at the surface and a means of deducing the profile of the stress, $\tau_g(z)$, progressively upwards, from which the impact on the large scale

velocity field can be derived via:

$$\frac{D\underset{\sim}{V}}{Dt} + \ldots = \frac{1}{\rho}\frac{\partial \tau_g}{\partial z} \qquad (1.10)$$

The surface drag is given by an expression of the form:

$$\tau_{gs} = k \rho_s N \underset{\sim}{V}_s s^2 \qquad (1.11)$$

where k is an empirical ("tunable") constant, chosen as 2.5×10^{-5} m^{-1}; $\underset{\sim}{V}_s$ and ρ_s are the are the wind and density in the lowest layer of the mode N is the Brunt-Vaisala frequency (a buoyancy parameter) given by:

$$N^2 = \frac{g}{\bar{\theta}}\frac{\partial \bar{\theta}}{\partial z} \qquad (1.12)$$

It is evaluated using values of temperature, T, on the first two sigma levels (in layer numbers 10 and 11 of Figure 1.10). s^2 is the variance of the sub grid-scale topography as determined from a fine resolution orographic dataset. Above the surface, the stress can be shown to be related to the vertical displacement, δh, of isentropic surfaces so that:

$$\tau_g = - k \rho N U \delta h^2 \qquad (1.13)$$

where U is the magnitude of the component of the wind in the direction of the surface gravity wave stress. Further, Palmer et al. show that a "wave Richardson number" can be defined by:

$$\tilde{Ri} = Ri\left[\frac{1 - \frac{N\delta h}{U}}{\left(1 + Ri^{1/2}\left(\frac{N\delta h}{U}\right)\right)^2}\right] \qquad (1.14)$$

where Ri is the Richardson number of the basic atmospheric state given by:

$$Ri = \frac{\frac{g}{\bar{\theta}}\frac{\partial \bar{\theta}}{\partial z}}{\left|\frac{\partial \underset{\sim}{V}}{\partial z}\right|^2} \qquad (1.15)$$

They also make an assumption that if, over a particular layer, $\tilde{Ri} > 1/4$ then no stress is absorbed in that layer. In order to derive the stress profile as a function of height, therefore, the calculated surface stress is first carried over to the next layer up and a preliminary value of δh, determined from (1.13). Ri is also calculated, again using values of V and T on adjacent sigma levels (Figure 1.10). A value for $\tilde{Ri}$ can then be derived from (1.14). If $\tilde{Ri} > 1/4$ then the stress at the sigma layer boundary is set equal to the value below. If $\tilde{Ri} < 1/4$ then it is reset to 1/4 and a new value of δh derived. A new value for the gravity wave stress in that layer is then obtained from (1.13). In either case, the process is then repeated successively for higher layers, after which the consequences for the large scale velocity field are determined from (1.10).

One point of practical importance mentioned by Palmer et al. is

that it is found necessary to first apply the wave absorption technique at the boundary between layers 9 and 10, rather than 10 and 11, otherwise, in some cases, it is found that a large amount of drag acts on quite a shallow layer (25 mb) as a result of the weak winds in layer 11. As they note, this is quite reasonable since it does not make sense to use the scheme on layers shallower than the amplitude of the sub grid-scale orography. The stress at the boundary between layers 10 and 11 is calculated by assuming that the acceleration due to the wave drag is equal in the lowest two layers.

We illustrate the impact of envelope orography and gravity wave drag parametrizations by reference to recent results by Slingo and Pearson (1986) who tested them in multi-annual cycle integrations of the Met O 20 model. The gravity wave drag parametrization followed the formulation of Palmer et al. just described whilst the envelope orography used was that employed by Wallace et al.(1983). However in early experiments with such an orography the large increments added in some areas (notably over the Andes) led to spurious oscillations in the modelled geopotential height fields. The problem was overcome by limiting the value of the increment to 1500 m. In the following, this "truncated envelope orography" experiment will be referred to as TENV and the gravity wave drag experiment as GRAV.

We illustrate the results from Slingo and Pearson's paper with reference to the impact on the surface (pmsl) pressure fields. Figure 1.11 shows the pmsl distributions, averaged over the four northern hemisphere winters of the experiments, from both TENV and GRAV, which should be compared to that for the control integration in Figure 1.8b. In both cases there are substantial improvements to the pattern in the northern hemisphere, whilst southern hemisphere results are essentially unchanged. In GRAV the Icelandic low is now in its correct position (although the central pressure is still slightly too low), and the high pressure area to the south has now weakened. The near-surface flow over Europe is thus weaker and more south-westerly than in the control experiment, in good agreement with the observations. In TENV, however, the low pressure is in the same position as the control (although less deep) and the high has moved further north. In both experiments the high pressure cells over northern Asia and America are much better represented. The Aleutian low is still too deep in GRAV and in this area results from TENV are closer to the observed pressures. It is worth remarking that the control integration produced a realistic pmsl distribution in the northern summer (not shown). Results from GRAV for that season were found to be very close to the control, indication that the stability-dependence incorporated into the parametrization effectively "turned off" the scheme - a desirable feature. In TENV, on the other hand, the summer simulation was degraded in that the intensities of the northern hemisphere continental lows and oceanic highs were exaggerated and the pressure was found to be too high over the north pole. As noted by Slingo and Pearson, it would appear that in this season the elevated land surface led to too pronounced a thermal forcing of the continental heat lows, leading to a compensating increase in pressure over the oceans.

Whilst the deficiencies in the results from TENV were sufficiently serious to warrant rejection of envelope orography as a solution to the westerly problem in the 11 layer model and adoption of gravity wave drag, as Slingo and Pearson point out, the question as to what is the best recipe for constructing an orographic dataset for an AGCM remains open and it is quite conceivable that a more carefully constructed envelope orography would yield better results than they

found, at least in winter, though use of mean elevations certainly seems more appropriate to calcuation of the surface heat balance, which is an important factor in summer.

****

.nj

Advanced Lecture 1 - References

Bryan, K., 1969, A numerical method for the study of the circulation of the world ocean. J.Comput. Phys., 4, pp 347-376.

Bryan, K. and L.J. Lewis, 1979, A water mass model of the world ocean. J. Geoph. Res., 84, pp 2505-2517.

Bryan, K., S. Manabe and R. Pacanowski, 1975, A global ocean-atmosphere climate model. Part II: The oceanic circulation. J.Phys Ocean., 5, pp 30-46

Chouinard, C., M. Beland and N McFarlane, 1985, The positive impact of gravity wave drag and envelope orography on medium range weather forecasts. Amer. Met. Soc. 7th Conf. Numer. Weath. Predict., pp 336-339.

Cox, M.D., 1984, A primitive equation, 3-dimensional model of the ocean. GFDL Ocean Group Technical Report No. 1.

Egger, J., 1972, Incorporation of steep mountains into a numerical forecasting model. Tellus, 24, pp 324-335.

Gerrity, J.P., 1985, NMC/GFDL medium range prediction model. Res. Activities in Num. Modelling, Report No. 8, WMO, Geneva, p 5.4.

Jarraud, M., A.J. Simmons and M. Kanamitsu, 1986, Impact of an envelope orography in the ECMWF model. Proceedings, ECMWF Seminar 1985 on Physical Parametrization for Numerical Models of the Atmosphere.

Killworth. P.D., J.M. Smith and A.E. Gill, 1984, Speeding up ocean circulation models. Ocean Modelling, No. 56.

Kitchen, J.E., M.J. Carter and A.P. Day, 1985, Results of a trial of a parametrization of gravity wave drag in the operational forecast model. Met. O 11 Tech. Note No. 205.

Lilly, D.K., 1972, Wave momentum flux. A GARP problem. Bull. Am. Met. Soc., 20, pp 17-23.

Manabe, S. and R.J. Stouffer, 1980, Sensitivity of a global climate model to an increase of CO_2 concentration in the atmosphere. J. Geophys. Res., 85, No. C10, pp 5529-5554.

Palmer, T.N., G.J. Shutts and R. Swinbank, 1986, Alleviation of a systematic westerly bias in general circulation and numerical weather prediction models through an orographic gravity wave drag parametrization. Quart. J.R.Met. Soc., Submitted for publication.

Richardson, P.L., R.E. Cheney and L.V. Worthington, 1978, A census of Gulf Stream rings, Spring 1975. J.Geoph. Res., 83, No. C2, pp 6136-6143.

Semtner, A.J., 1974, An oceanic general circulation model with bottom topography. Numerical Simulation of Climate Tech. Rep. No. 9, Dept. Met., Univ. of Califonia, Los Angeles.

Slingo, A. and D.W. Pearson, 1976, A comparison of the impact of an envelope orography and of a parametrization of orographic gravity wave drag on model simulations. Quart. J.R.Met. Soc. Submitted for publication. Also appears as Met O 20 Tech. Note DCTN 43.

Smagorinsky, J., 1981, Large-scale climate modelling and small-scale physical processes. Proceedings, JSC study conference on land surface processes in atmospheric general circulation models, Greenbelt, USA, 5-10 Jan. 1981. ICSU/WMO.

Wallace, J.M., S. Tibaldi and A.J. Simmons, 1983, Reduction of systematic forecast errors in the ECMWF model through the introduction of an envelope orography. Quart. J.R.Met. Soc., 109, pp 683-717.

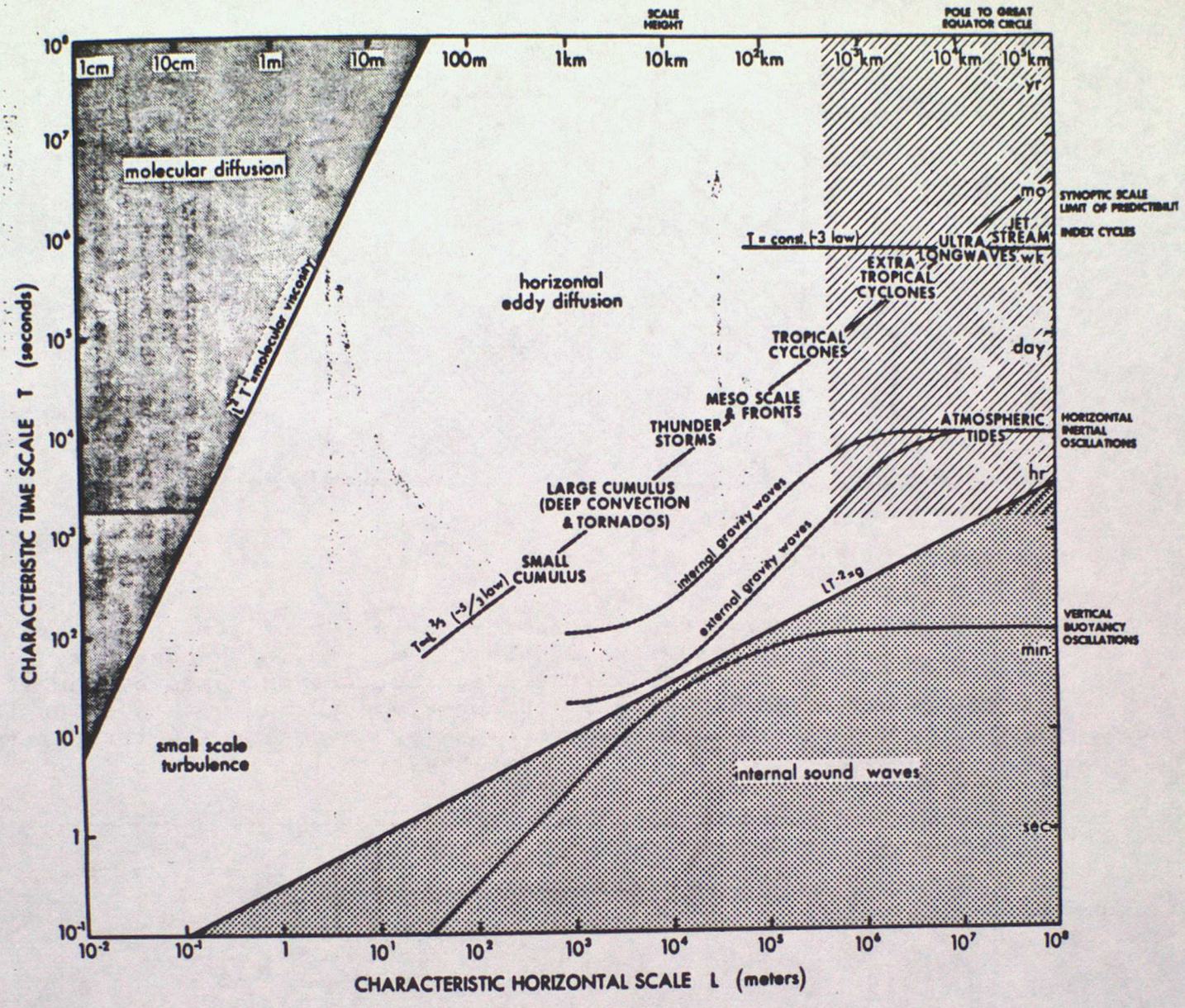

Figure 1.1 A space-time domain for characteristic atmospheric phenomena. The unstippled region encompasses most of the kinetic energy containing phenomena, with the predominance of extra-tropical cyclones, ultralong waves, and the jet stream. The crosshatched area denotes scales and phenomena typically resolved by general circulation models, that is, the macroscale (from Smagorinsky, 1981).

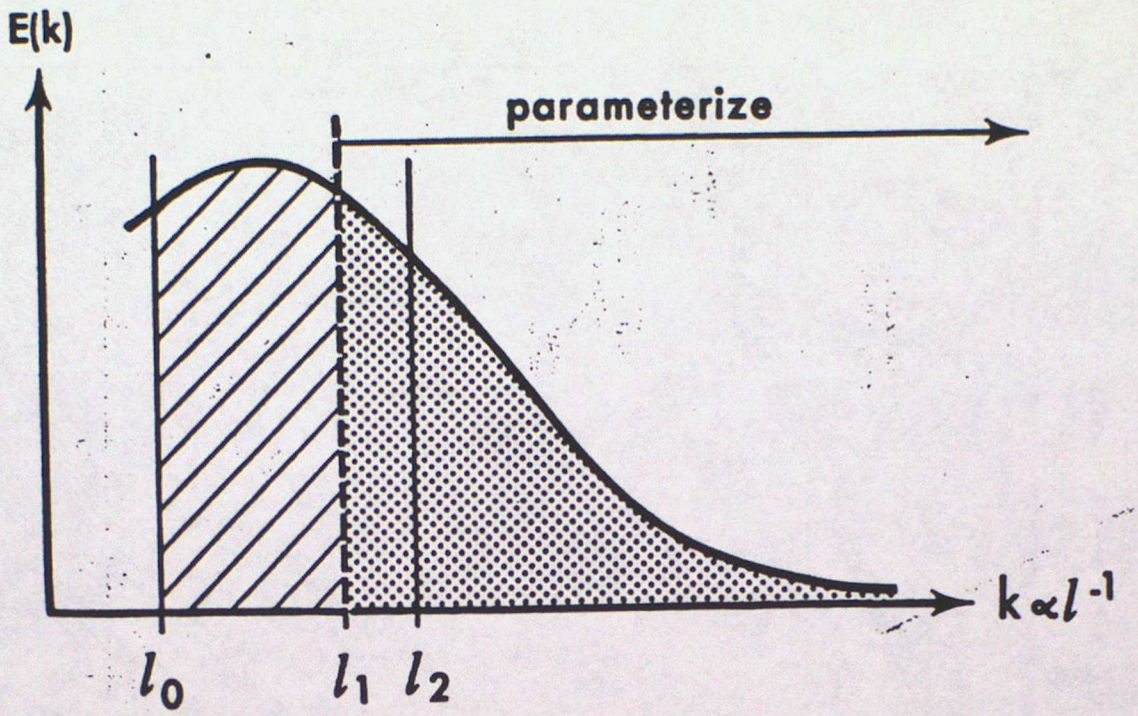

Figure 1.2 The curve represents the variation of atmospheric energy density as a function of wave number $k \propto l-1$. The hatched area is the explicitly resolved part of the spectrum, the macroscale. The stippled area indicates the portion of the energy spectrum within which the physical processes cannot be resolved by a domain with the dimension l_0 and the mesh width l_1 (from Smagorinsky, 1981).

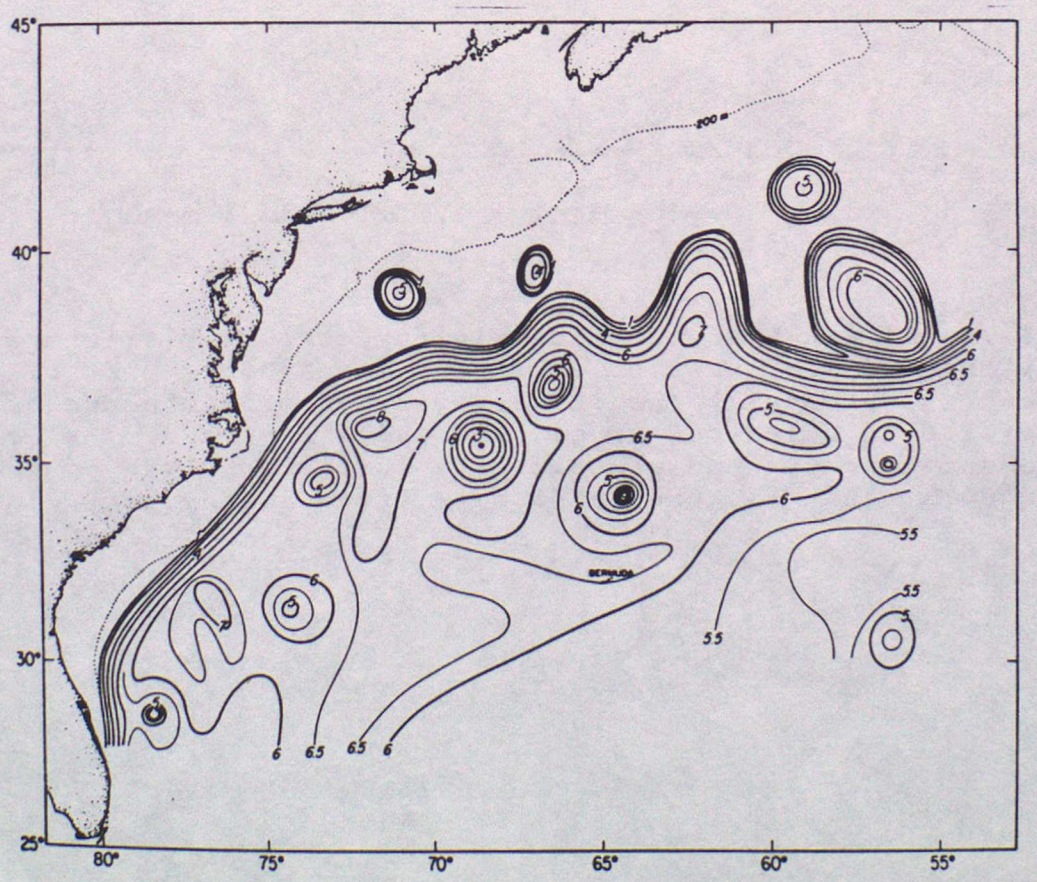

Figure 1.3 Chart of the topography (hectometres) of the 15 isothermal surface showing the Gulf Stream, nine cold-core and three warm-core rings. Contours are based on XBT, CTD, hydrographic and satellite infrared data from the period March 16 to July 9, 1975. (Richardson et al., 1978).

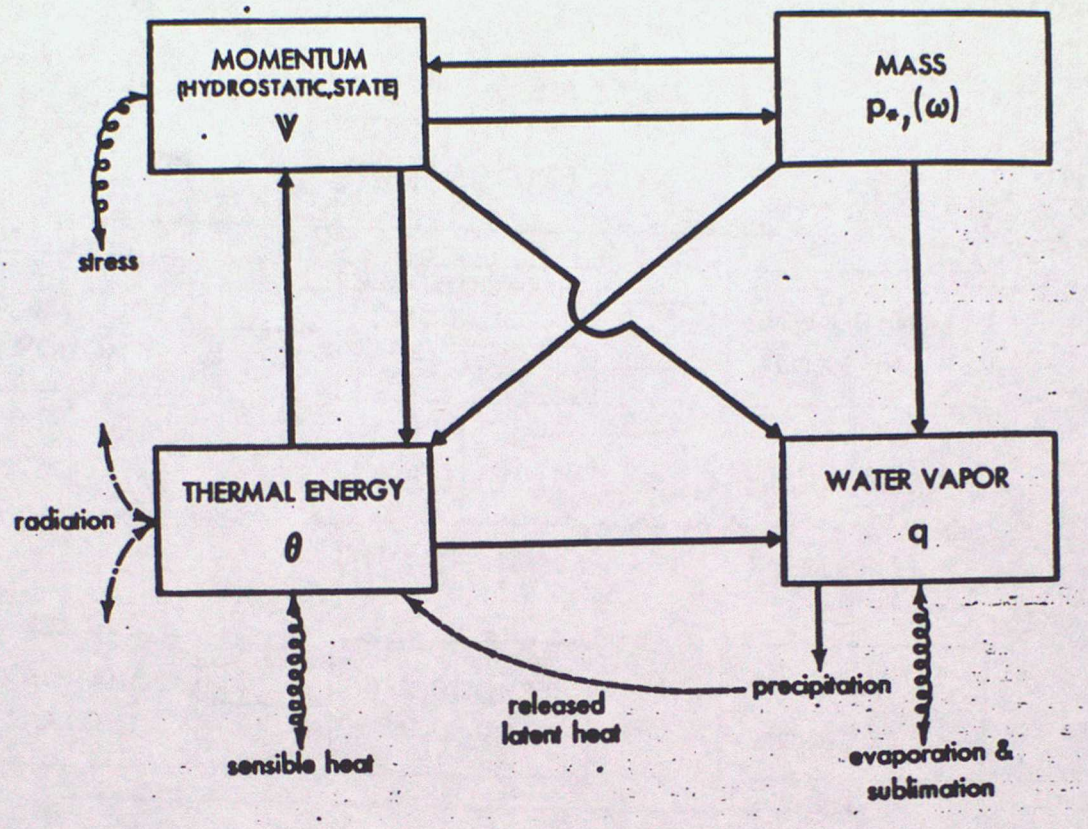

Figure 1.4 A schematic diagram of the relationship of the physical conservation laws which together define the variations of the primary macroscale variables in an elemental volume. Also shown are external sources and sinks of momentum, heat and water vapour (from Smagorinsky, 1981).

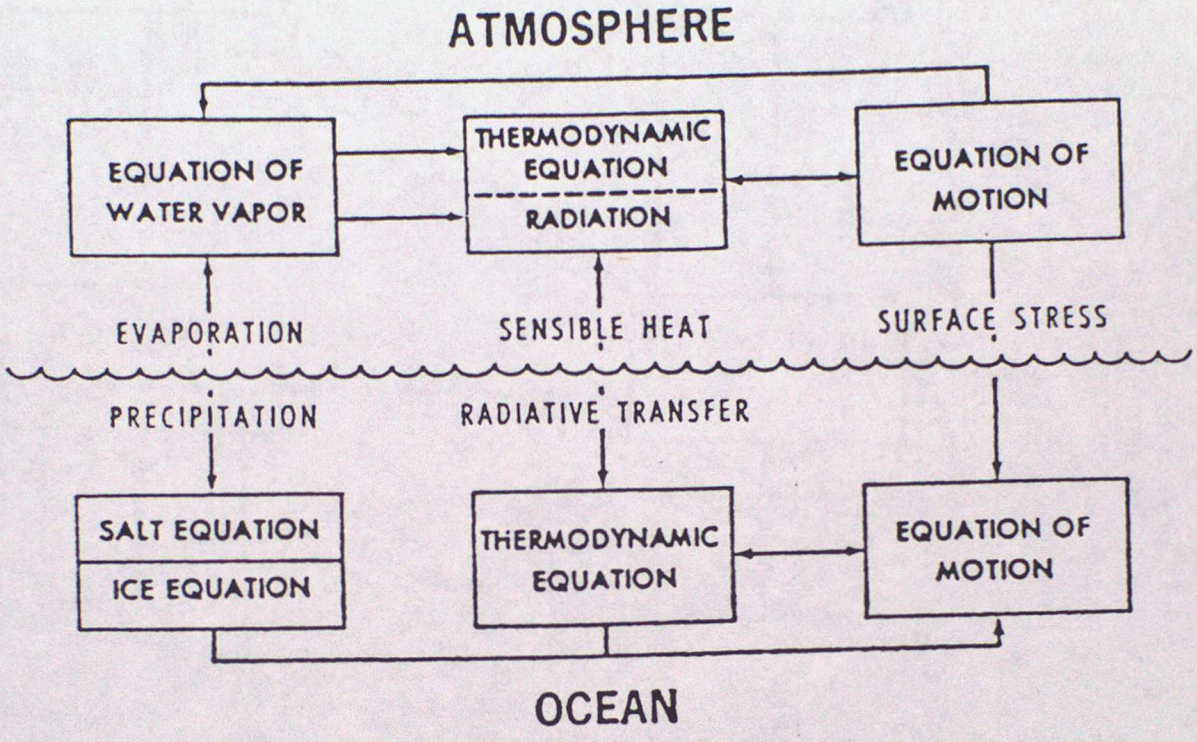

Figure 1.5 Diagram of the coupling of the major components of joint atmosphere-ocean models

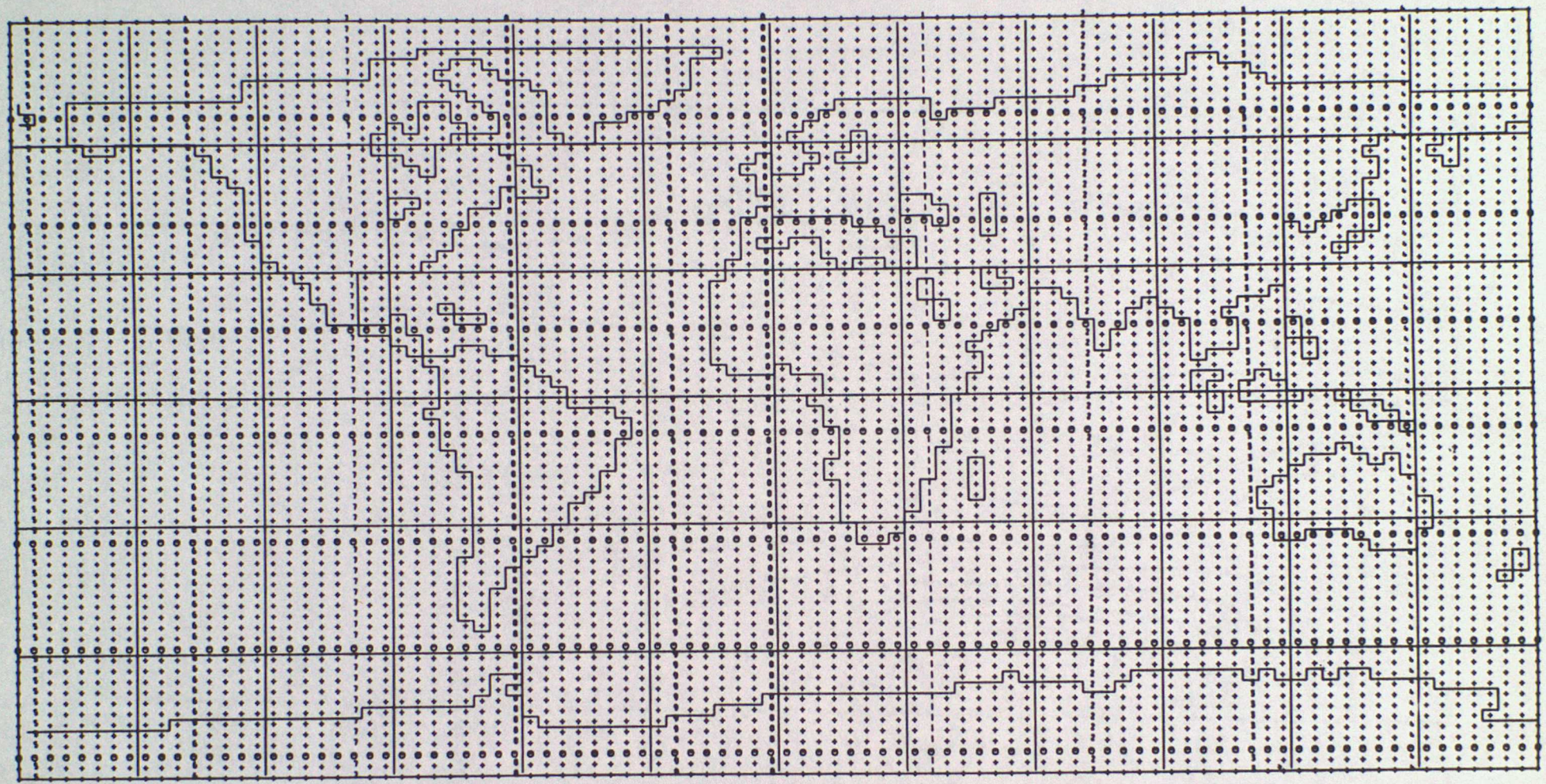

Figure 1.6 Horizontal resolution of the Met O 20 climate model: 2.5 x 3.75 degree latitude-longitude grid.

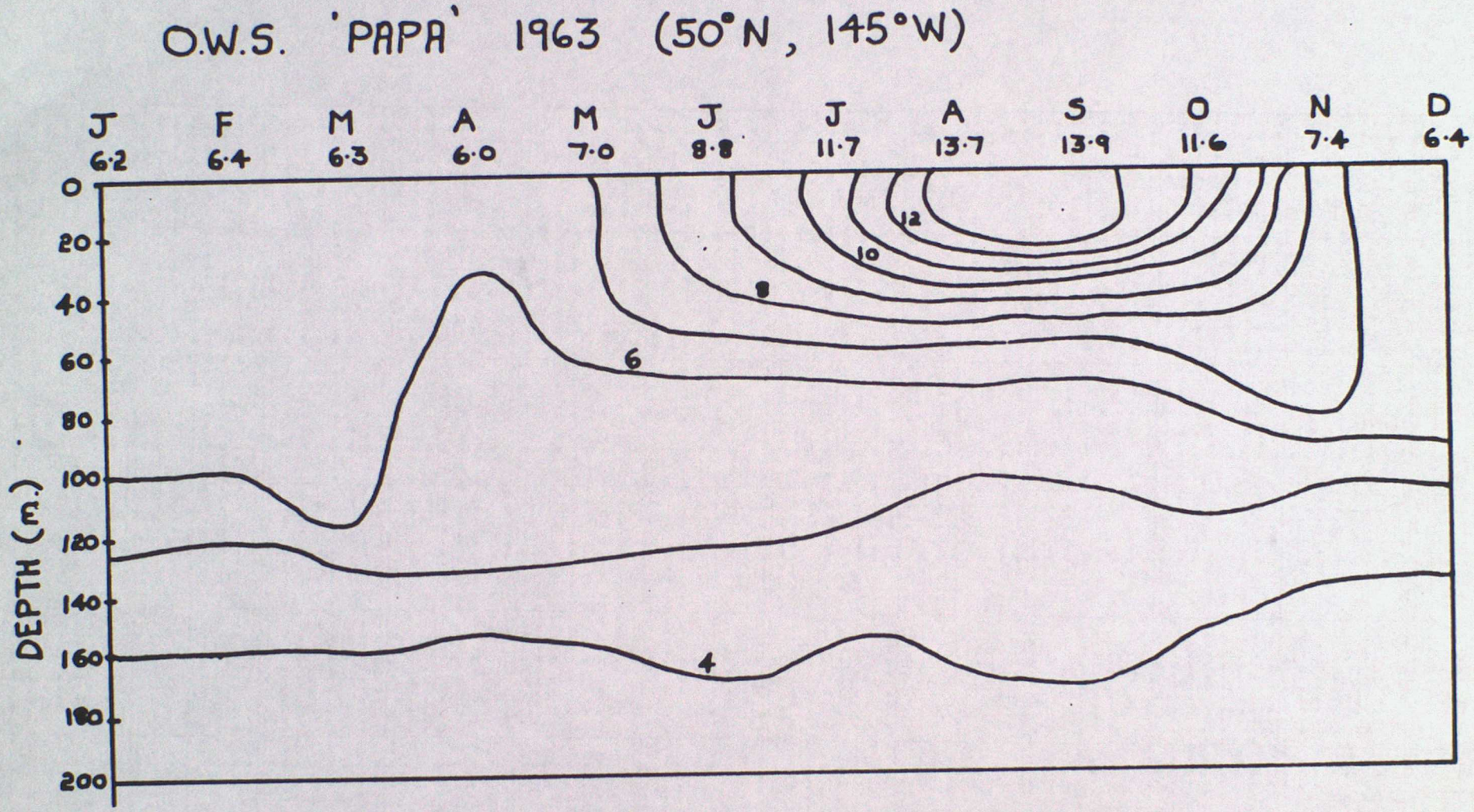

Figure 1.7 Characteristic seasonal variation of temperature with depth at OWS P.

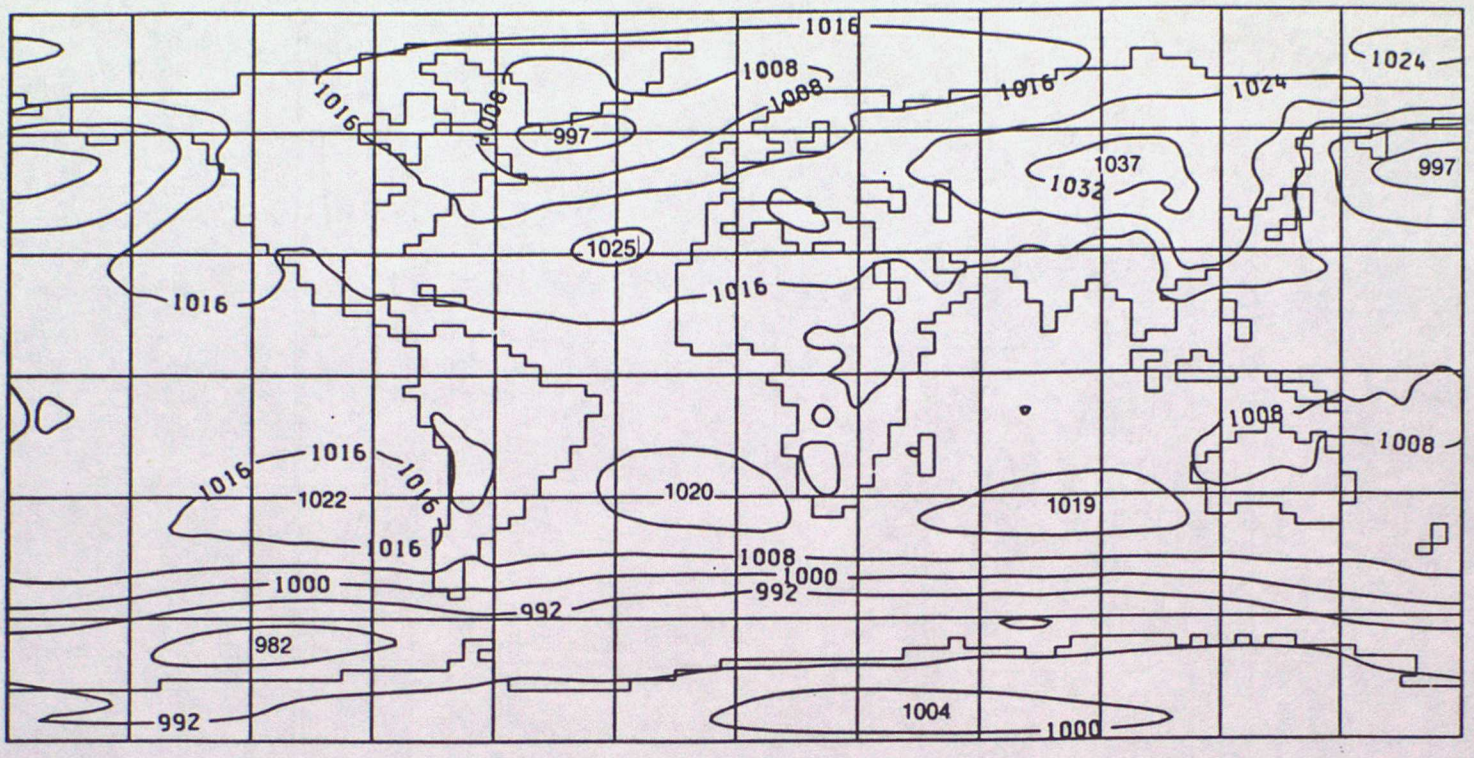

(a)

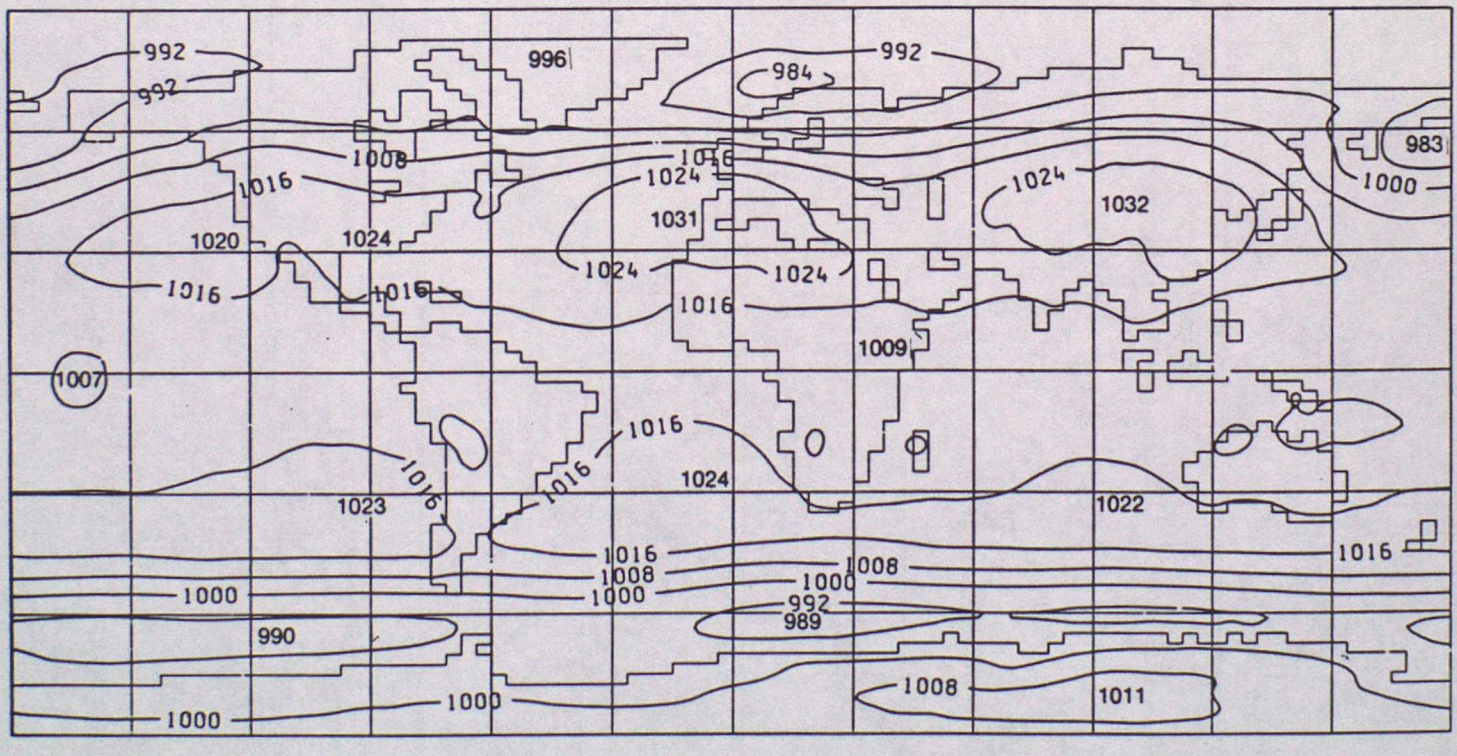

(b)

Figure 1.8 Pressure at mean sea level (pmsl) in millibars for the northern winter season (December to February) for the mean of (a) the three winters 1983/1984 to 1985/1986 derived from Meteorological operational analyses and (b) 8 winters from the third annual cycle experiment of the Met O 20 AGCM. The contour interval is 8 mb (from Slingo and Pearson, 1986).

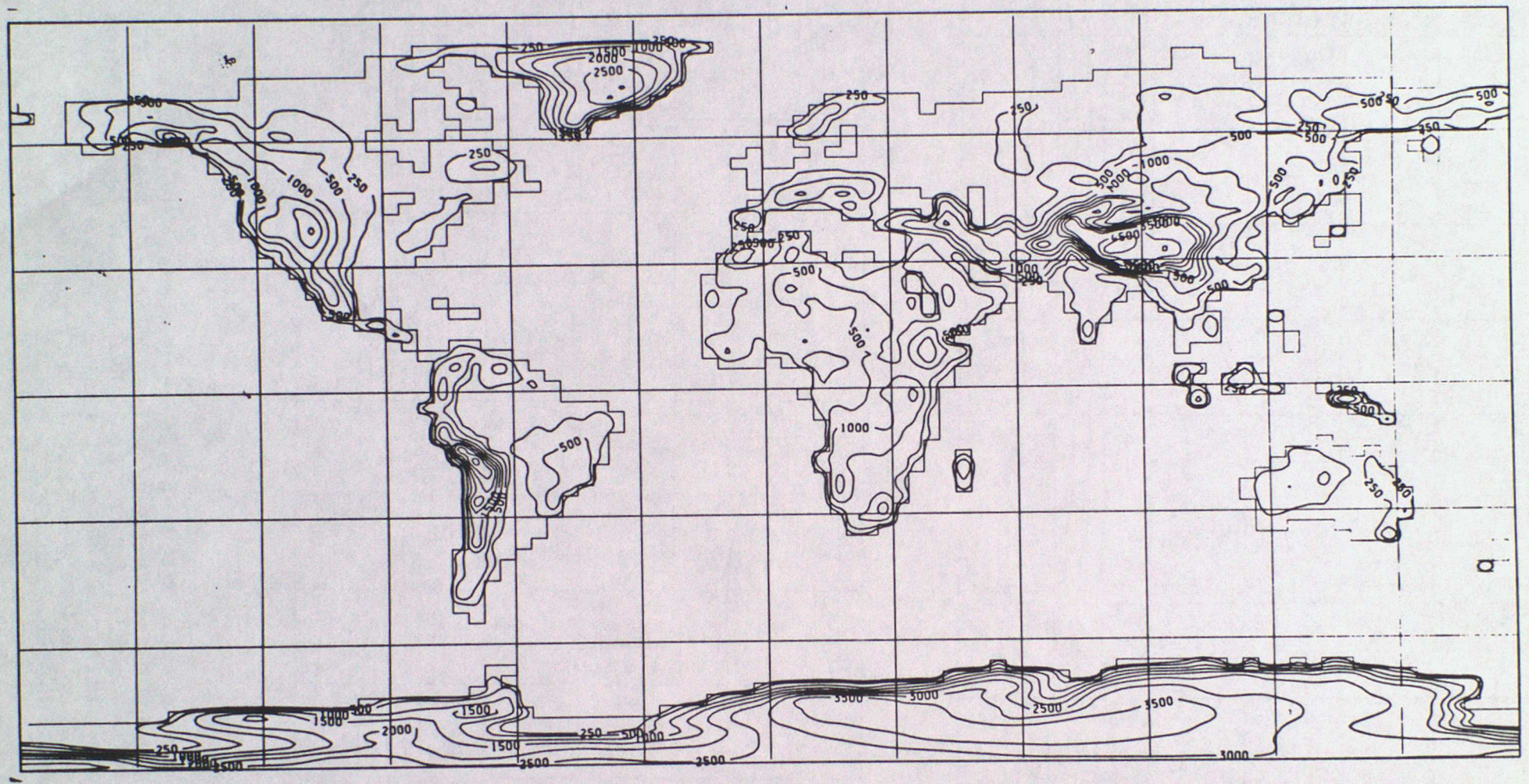

Figure 1.9 Surface elevations for the 2.5 x 3.75 degree version of the Met O 20 AGCM.

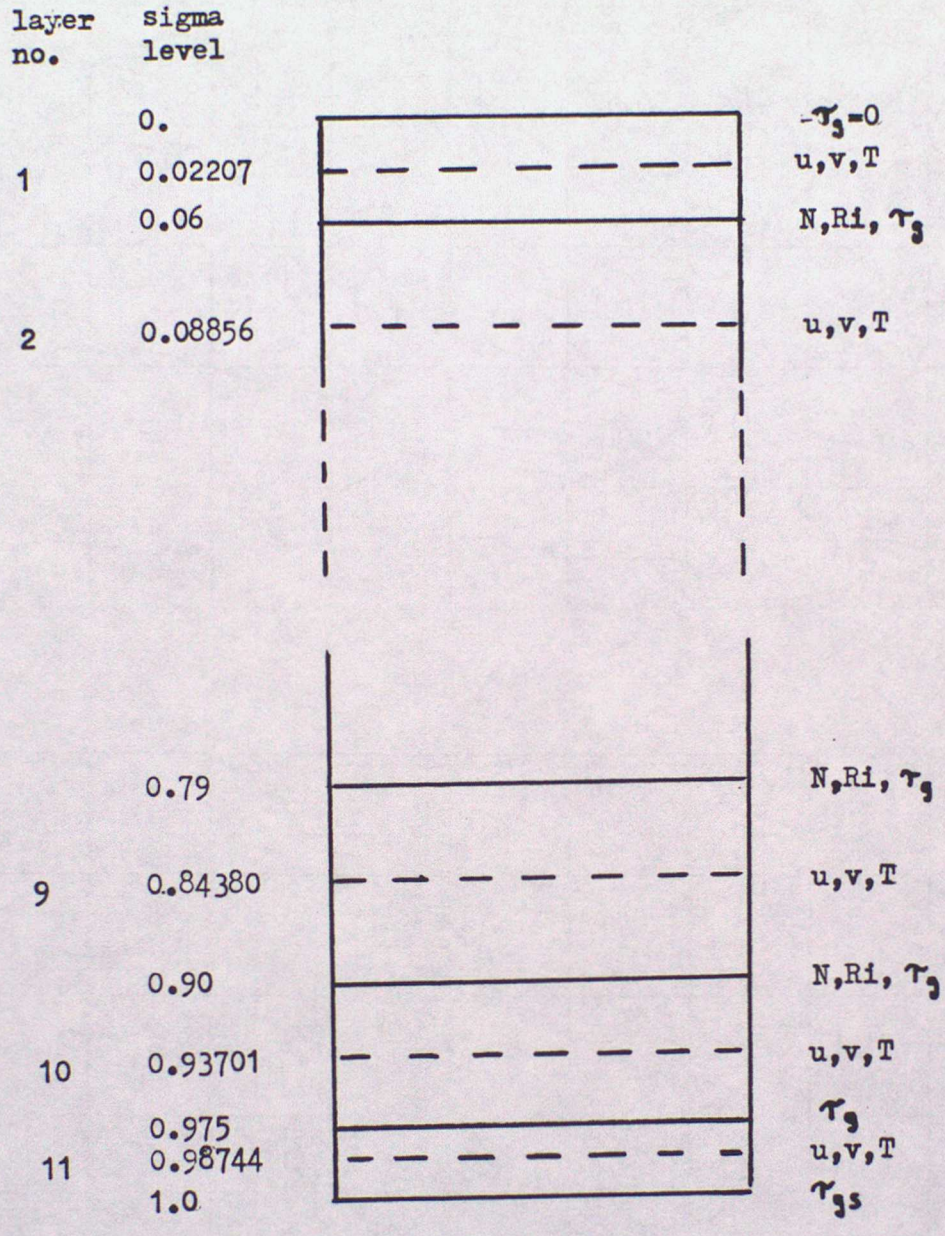

Figure 1.10 Vertical resolution of the Met O 20 11 layer model showing location of primary variables.

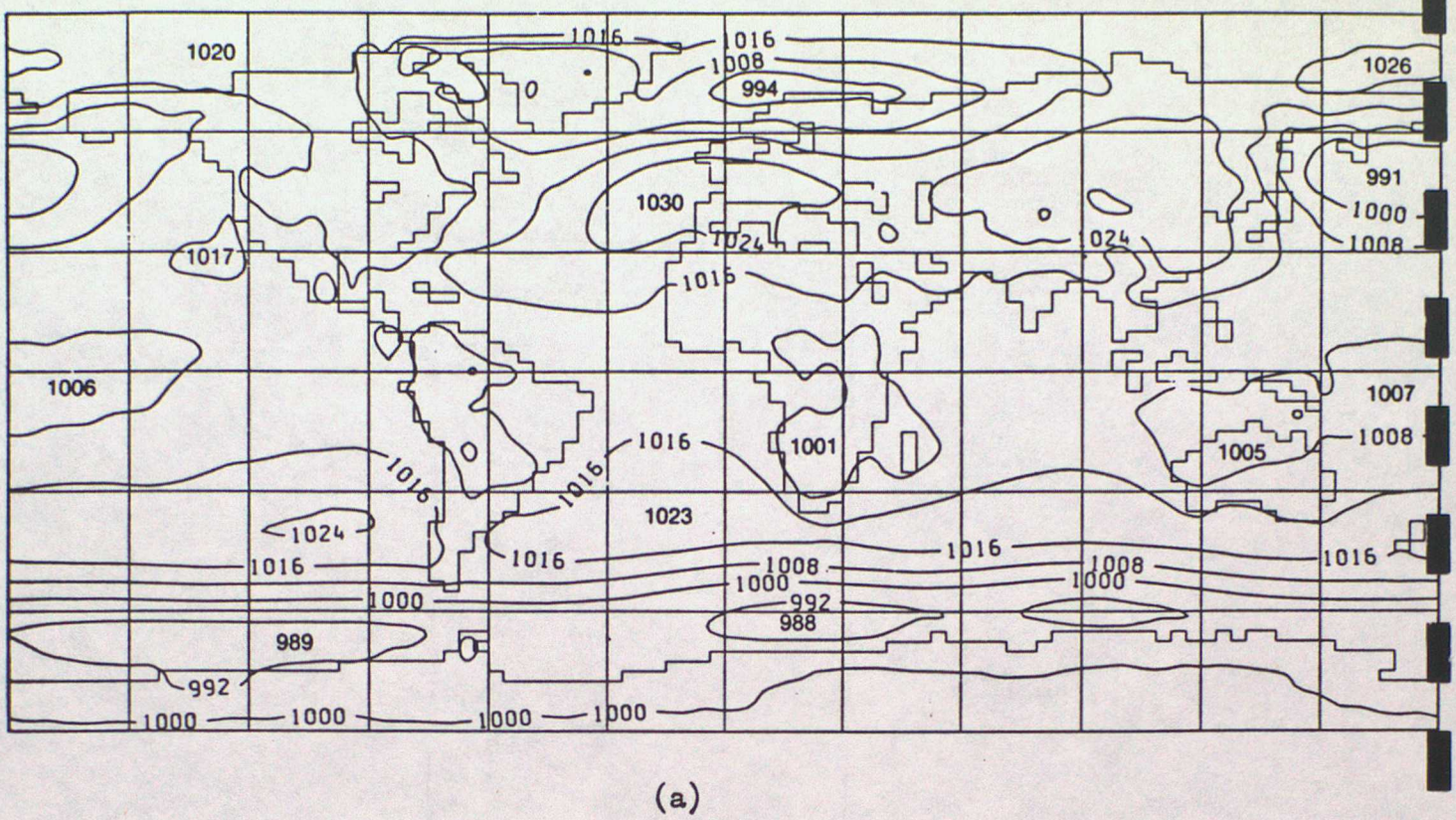

(a)

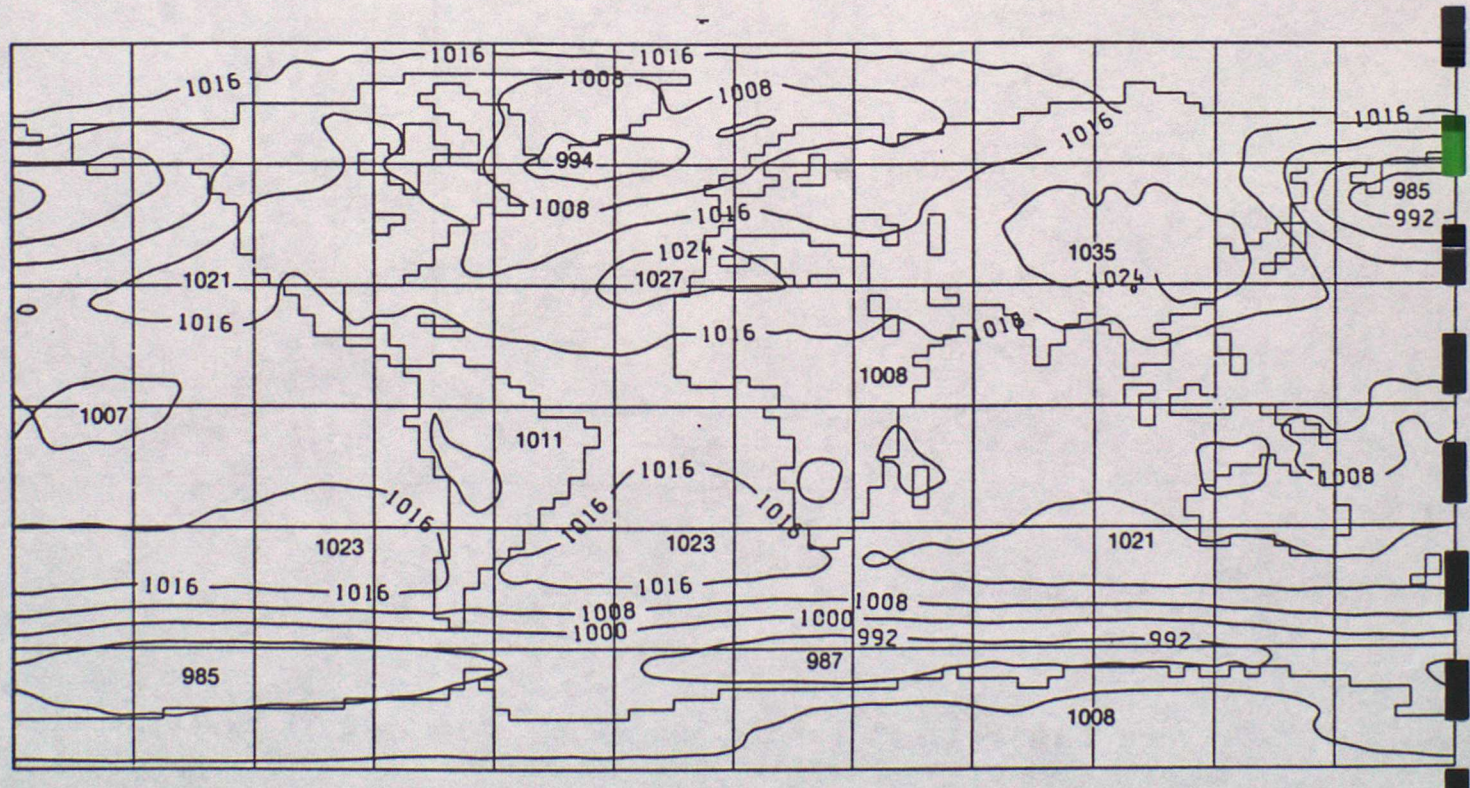

(b)

Figure 1.11 Pressure at mean sea level in millibars for the northern winter (December to February) for the mean of 4 winters from (a) the truncated envelope orography experiment and (b) the experiment with the gravity wave drag scheme. The contour interval is 8 mb. Compare with Figure 1.8 (from Slingo and Pearson, 1986).

LF/M020

AN INTRODUCTION TO THE PARAMETRIZATION OF LAND-SURFACE PROCESSES

D. J. CARSON

Meteorological Office, Bracknell, UK

ABSTRACT

This paper introduces the sub grid-scale, land-surface processes which, it is generally acknowledged, need to be included by parametrization in three-dimensional, numerical models for studying climate and climate change and for numerical weather prediction.

The discussion is restricted, in the main, to the relatively simple case of non-vegetated, land surfaces. The general boundary conditions for momentum transfer and the balance equations for energy and mass (moisture) transfer at a bare-soil surface are identified. The physical character and the parametrization of the varied flux-terms at the surface are considered systematically under the headings: Surface Radiative Properties and Fluxes; Surface Turbulent Exchanges; Soil Heat Conduction and the Land-surface Temperature; and Surface Hydrology and the Soil Water Budget.

Some of the particular problems associated with snow-covered, non-vegetated, land surfaces are described very briefly.

1. Introduction

The atmospheric boundary layer is the lowest layer of the atmosphere characterized by significant vertical flux divergences of momentum, heat and moisture which result directly or indirectly from interactions between the atmosphere and the underlying surface. The turbulent nature of boundary-layer flows is a vital factor in the efficient exchange of momentum, heat and moisture between the Earth's surface below and the 'free' atmosphere above. In general, up until fairly recently, designers and users of global atmospheric general circulation models (AGCMs) and operational numerical weather prediction models (NWPMs) have not been concerned with the details of boundary-layer and surface properties and processes in their own right but mainly for the influence they exert on weather systems and circulation characteristics on the much larger, synoptic or even global scales. However, the recent upsurge in the simultaneous developments of three-dimensional AGCMs for the study of climate and climate change and of increasingly sophisticated and more highly resolved operational NWPMs has resulted in more effort now being directed towards delineating details in boundary-layer structure and in the characteristics of surface climatologies. Studies with AGCMs have indicated considerable sensitivity of their simulations to changes in surface properties such as albedo, soil moisture and surface roughness. Also, some NWPMs now in operational service are expected to forecast the near-surface meteorological variables, and even changes in surface properties. The importance then of 'land-surface processes' and the need

to understand and represent them better in AGCMs and NWPMs are now well established. The respective rôles of these processes in the wider climatological context have been discussed elsewhere.

Following the Joint Scientific Committee Scientific Steering Group on Land-Surface Processes of the World Climate Research Programme (WCP, 1985), I shall adopt the pragmatical definition of land-surface processes as those phenomena which control the fluxes of heat, moisture and momentum between the surface and the atmosphere over the continents. These processes influence both the circulation of the atmosphere, often remotely, and the climate of the surface.

Many important dynamical and physical processes are governed by spatial (and temporal) scales very much smaller than the typical limits of resolution of either a numerical model or an observing system. Such sub grid-scale processes cannot be dealt with explicitly in the models; however, their statistical effects at the resolved scales must be included and are determined in terms of the explicitly resolved variables. This technique is called parametrization and usually introduces empirical terms (parameters) into a model's prescription of the processes. For a fuller discussion of parametrization in numerical models see, for example, Smagorinsky (1982).

My aim here is to introduce the range of sub grid-scale land-surface processes which it is generally recognised need to be represented by parametrizations in climate and numerical weather prediction models. Discussion is restricted in the main to non-vegetated land surfaces and focusses in particular on the surface energy and mass (moisture) fluxes. A more general and fairly comprehensive review of the then current practices in AGCMs was provided by Carson (1982), with an update for Meteorological Office models only in Carson (1986a). As implied above, the parametrization of land-surface processes is a very active field of research and model development and methods labelled 'current' may quickly become susperseded. New approaches ('schemes') are being developed and tested continuously. A single paper cannot do justice to the range and complexity of tried schemes and unresolved problems even in the apparently restricted topic of land-surface processes. The special characteristics and problems of vegetated land surfaces, ice-covered surfaces and the ocean surface are **not** dealt with **here.**
It should be assumed then throughout Sections 2-6 that discussions refer only to non-vegetated, snow-free, land surfaces, unless explicitly stated otherwise. Some of the particular problems associated with snow-covered, non-vegetated, land surfaces will be described briefly in Section 7.

It should also be stressed that there are many factors in a typical AGCM or NWPM which will have a direct or indirect bearing on the character and performance of the land-surface processes but which are not themselves governed directly by, nor specified explicitly in terms of, surface properties. Obvious examples amongst the other physical parametrizations include: components of the radiation scheme; the cloud scheme; the representation of rainfall and snowfall; the delineation of the atmospheric boundary layer and the parametrization of turbulent mixing within it away from the surface; deep convection; etc. A numerical model's general structure with respect to, for example: horizontal domain; spatial and temporal resolutions; distribution and number of surface types; specification of orography; etc will also determine to some extent the quality of its simulations or predictions of the surface and near-surface

climatologies. Such considerations of the general problem of representing the effects of land-surface processes in AGCMs and NWPMs are beyond the scope of this introductory paper.

2. The Boundary Conditions for Momentum, Energy and Mass Transfer at a Bare-soil Surface

A natural and instructive way to delineate and introduce the various land-surface processes of interest is through the boundary conditions for momentum and the balance equations for the energy and mass (moisture) that apply at the surface. Most of the current generation of AGCMs and NWPMs involve such boundary conditions but with varying degrees of complexity and sophistication in their use and in the parametrizations chosen to represent individual components of the system. For the moment, let us consider in turn, the boundary constraints and relations between the momentum, energy and mass fluxes as depicted schematically in Figure 1 as a simplistic, air-soil interfacial problem.

Notation: The subscript o is used to denote surface values of variables and parameters, but only where necessary. In general, terms referred to only at the surface will not be given a subscript; soil fluxes and prognostic surface variables will be subscripted.

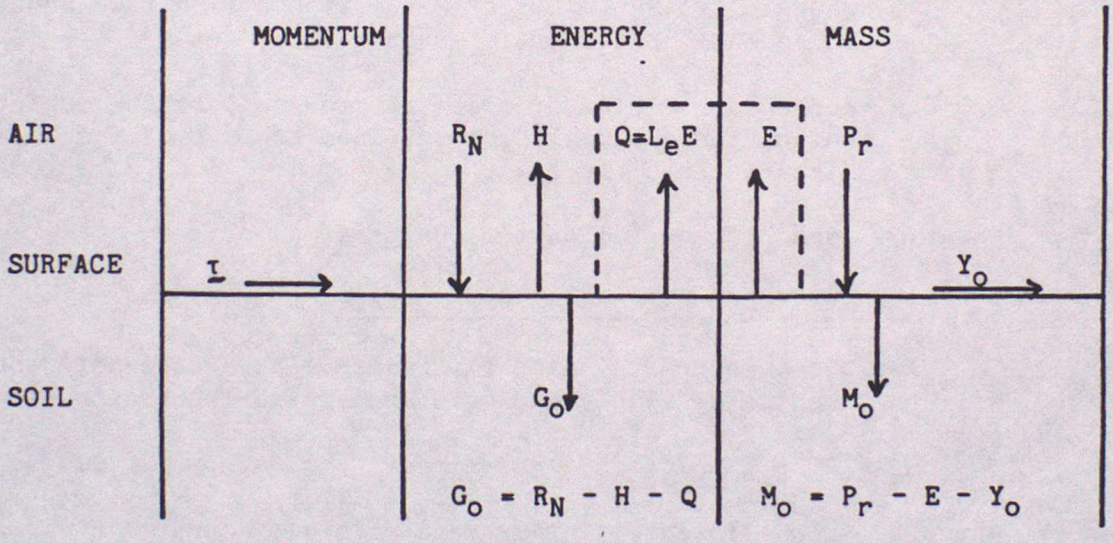

Figure 1. Schematic representation of the fluxes of momentum, energy and mass at a bare-soil surface.

2.1 Surface momentum flux ($\underline{\tau}$)

In an aerodynamic sense the atmospheric boundary layer is simply the lowest layer of the atmosphere under the direct influence of the underlying surface from which momentum is extracted and transferred downward to overcome surface friction. Thus the aerodynamically rough land surface provides a sink for atmospheric momentum, the removal of which at the surface is represented by the viscous drag, or horizontal shearing stress, $\underline{\tau}$, which, by convention, is a vectorial measure of the downward flux of horizontal momentum.

The surface boundary conditions for momentum transfer are:

a. NO-SLIP CONDITION: ie, the mean horizontal wind vector is zero at the surface.

b. $\underset{\sim}{\tau}$ (at the surface) is parallel to the limiting wind direction as the surface is approached.

$\underset{\sim}{\tau}$, the horizontal shearing stress, has SI units of Nm^{-2}.

2.2 The surface energy flux balance

The energy flux balance at a bare-soil surface may be expressed as

$$G_o = R_N - H - Q \qquad (1)$$

where R_N is the net radiative flux at the surface (defined positive towards the surface);

H is the turbulent sensible heat flux (defined positive when directed upward from the surface into the atmosphere);

$Q=L_eE$ represents the latent heat flux due to surface evaporation (defined positive when directed upward from the surface), where E is the turbulent water vapour flux (see Eqn (2)) and L_e is the latent heat of evaporation; and

G_o represents a flux of heat into the soil at the surface, and which, conventionally, is defined to be positive when directed into the soil.

The flux terms in Eqn (1) have SI units of Wm^{-2}.

2.3 The mass flux balance at the surface

For our purposes the mass flux balance at a bare-soil surface will be taken to be simply the moisture flux balance expressed as

$$M_o = P_r - E - Y_o \qquad (2)$$

where P_r is the intensity of surface rainfall;

E is the surface evaporation rate (turbulent flux of water vapour);

Y_o denotes intensity of surface runoff; and

M_o represents the net mass flux of water into the soil layer.

As defined, the flux terms in Eqn (2) strictly have SI units of kg m^{-2} s^{-1}; however, it is fairly common practice to refer to the rates involved in terms of a representative depth (of water) per unit time.

Note:

1. The evaporative flux, E, appears explicitly in both Eqns (1) and (2) and thus provides a direct and important coupling between the surface heat and moisture budgets.

2. A knowledge of heat conduction and water transport in the soil is needed to parametrize the terms G_o and M_o, respectively. In AGCMs and NWPMs this leads usually to the reformulation of Eqn (1) as a prognostic equation for the 'surface temperature', T_o, and of Eqn (2) as a prognostic equation for the mass of water stored in a specified depth of surface soil layer, ie the 'soil moisture content'. Further details of these soil processes and their representation in Eqns (1) and (2) are described more fully in Sections 5 and 6.

The boundary conditions and surface balance equations of Sections 2.1-2.3 involve a wide range of sub grid-scale physical and dynamical processes in both the atmosphere and the soil. It is convenient to consider the nature and parametrization of the various individual components under the following Section headings:

Section 3 Surface Radiative Properties and Fluxes (vid. R_N);

Section 4 Surface Turbulent Exchanges (vid. $\underset{\sim}{\tau}$, H, Q and E);

Section 5 Soil Heat Conduction and the Land-Surface Temperature (vid. G_o); and

Section 6 Surface Hydrology and the Soil Water Budget (vid. P_r, Y_o and M_o).

3. Surface Radiative Properties and Fluxes

Since solar radiation provides most of the energy needed to maintain the general circulation of the atmosphere and since the major input of this energy to the Earth-atmosphere system occurs at the surface, it seems natural to start a discussion of land-surface processes by considering the surface radiative properties and fluxes. The term R_N in Eqn (1) acknowledges the importance of, and the need to determine, the net imbalance of radiative fluxes to and from the land surface expressed simply here as the sum of the net short-wave radiative flux, R_{SN}, and the net long-wave radiative flux, R_{LN}, ie

$$R_N = R_{SN} + R_{LN} \qquad (3)$$

The components of R_{SN} and R_{LN} are shown schematically in Figure 2. Note the convention that the net radiative fluxes are positive when directed towards the surface.

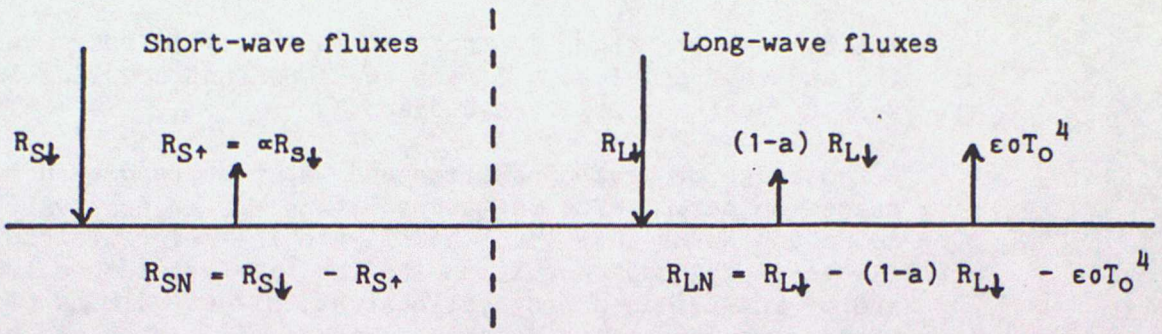

Figure 2. Schematic representation of the short- and long-wave radiative flux balances at a bare-soil surface.

3.1 Surface short-wave radiation balance

$$R_{SN} = (1-\alpha)\ R_{S\downarrow} \qquad (4)$$

where $R_{S\downarrow}$ is the downward short-wave radiative flux, including both the direct solar flux and diffuse radiation from the sky, and

α is the surface short-wave reflectivity or albedo.

3.2 Surface long-wave radiation balance

$$R_{LN} = a\ R_{L\downarrow} - \varepsilon\sigma T_o^4 \qquad (5)$$

where $R_{L\downarrow}$ is the downward long-wave radiative flux,

a is the surface absorptivity to long-wave radiation,

$\varepsilon\sigma T_o^4$ is the long-wave radiative flux emitted at the surface,

T_o is the surface temperature,

ε is the long-wave emissivity of the surface, and

σ is the Stefan-Boltzmann constant.

It is common practice to simplify Eqn (5) further by combining the definition of ε with Kirchoff's law to give $a=\varepsilon$. Eqn (5) then reduces to

$$R_{LN} = \varepsilon(R_{L\downarrow} - \sigma T_o^4) \qquad (6)$$

and Eqn (3) becomes

$$R_N = (1-\alpha)\ R_{S\downarrow} + \varepsilon\ (R_{L\downarrow} - \sigma T_o^4) \qquad (7)$$

The parametrization of the radiative fluxes $R_{S\downarrow}$ and $R_{L\downarrow}$ is beyond the scope of this discussion. They are not normally classed as land-surface processes and may be regarded here as externally given forcing factors. It should be stressed though that a correct evaluation of $R_{S\downarrow}$ and $R_{L\downarrow}$ is a crucial element in establishing

sensible energy and moisture balances at the surface. The prediction of T_o is dealt with in Section 5. The remainder of this section concentrates on the surface radiative parameters, ε and α.

3.3 Surface long-wave emissivity (ε)

ε is known to have a wavelength dependence and to vary according to the character of the surface as discussed for example by Buettner and Kern (1965), Kondratyev (1972), Paltridge and Platt (1976) and Kondratyev et al (1982). Values quoted for the vertical emissivity range from 0.997 for wet snow to 0.71 for quartz. Kondratyev et al (1982) comment that, on average, the relative emissivities of natural underlying surfaces lie within the range 0.90-0.99 and they cite several authors who have inferred that 0.95 may be assumed as the mean relative emissivity of the Earth's surface. They do caution however that the problem of measuring the emissivity of natural surfaces is far from solved and that existing techniques will need to be improved to make such measurements on a large scale.

Although there are exceptions, the most common practice in AGCMs and NWPMs is still to assume explicitly or implicitly that all surfaces act like perfect black bodies for long-wave radiation with $\varepsilon=1$. To a large extent this simply reflects the preoccupation of numerical modellers with other apparently more important and immediate problems with their physical parametrizations. I am sure that the increasing complexity and sophistication of land-surface descriptions in models will also generate more critical and discriminatory approaches to the specification of ε. This is most likely to be the case, for example, with the further development of models which attempt to include the explicit effects of vegetation in the climate system (see, for example, the models of Deardorff (1978) and Sellers et al (1986)).

3.4 Surface short-wave albedo (α)

α depends on the solar zenith angle, the spectral distribution of the solar radiation incident on the surface and whether that radiation is direct or diffuse, as well as on the character of the surface as determined by the vegetation (its type, density and state), the soil type, the soil moisture and whether the surface is snow- or ice-covered. Although generally a long way removed from representing the full complexity of its functional dependence on all such quantities, nevertheless α in AGCMs and NWPMs is usually accorded some variation with the broad character of the surface. In AGCMs it has a specified geographical dependence (see, for example, Carson (1982)) and in many models it is still the only land-surface or soil parameter which is given such a geographical variation (see, for example, Carson (1986a)).

A good illustration of the current status of the global specification of α suitable for use in large-scale atmospheric models is the recent work of Wilson and Henderson-Sellers (1985) on which is based the distribution of grid-box, snow-free, land-surface albedos used in the Meteorological Office operational weather forecasting and climate models (Carson, 1986a). Wilson and Henderson-Sellers (1985) have compiled detailed, global, 1° x 1°, latitude-longitude data sets of land cover and soils, respectively. These data can be manipulated to provide the corresponding characteristics for each model grid-box.

Table 1 gives their proposed albedo values, with a seasonal variation, for each of 23 selected land types; Table 2 gives typical bare-soil albedos as a simple function of soil colour and state of surface wetness.

Land Type Component	Annual	Summer	Winter
1 Water	0.07	0.07	0.07
2 Ice	0.75	0.60	0.80
3 Inland lake	0.06	0.06	0.06
4 Evergreen needleleaf tree	0.14	0.14	0.15
5 Evergreen broadleaf tree	0.14	0.14	0.14
6 Deciduous needleleaf tree	0.13	0.14	0.12
7 Deciduous broadleaf tree	0.13	0.14	0.12
8 Tropical broadleaf tree	0.13	0.13	0.13
9 Drought deciduous tree	0.13	0.13	0.12
10 Evergreen broadleaf shrub	0.17	0.17	0.17
11 Deciduous shrub	0.16	0.17	0.15
12 Thorn shrub	0.16	0.16	0.16
13 Short grass and forbs	0.19	0.20	0.18
14 Tall grass	0.20	0.17	0.22
15 Arable	0.20	0.25	0.16
16 Rice	0.12	0.12	0.12
17 Sugar	0.17	0.17	0.17
18 Maize	0.19	0.22	0.16
19 Cotton	0.19	0.22	0.17
20 Irrigated crop	0.25	0.25	0.25
21 Urban	0.18	0.18	0.18
22 Tundra	0.15	0.17	0.12
23 Swamp	0.12	0.12	0.12

Table 1. Short-wave albedos proposed by Wilson and Henderson-Sellers (1985) for 23 different types of surface cover.

Colour class	Light	Medium	Dark
Moisture state	wet dry	wet dry	wet dry
Albedos	0.18 0.35	0.10 0.20	0.07 0.15
Average	(0.26)	(0.15)	(0.11)

Table 2. Short-wave albedos proposed for bare soils by Wilson and Henderson-Sellers (1985).

Wilson and Henderson-Sellers propose that each grid-box effective α can be calculated from the algorithm

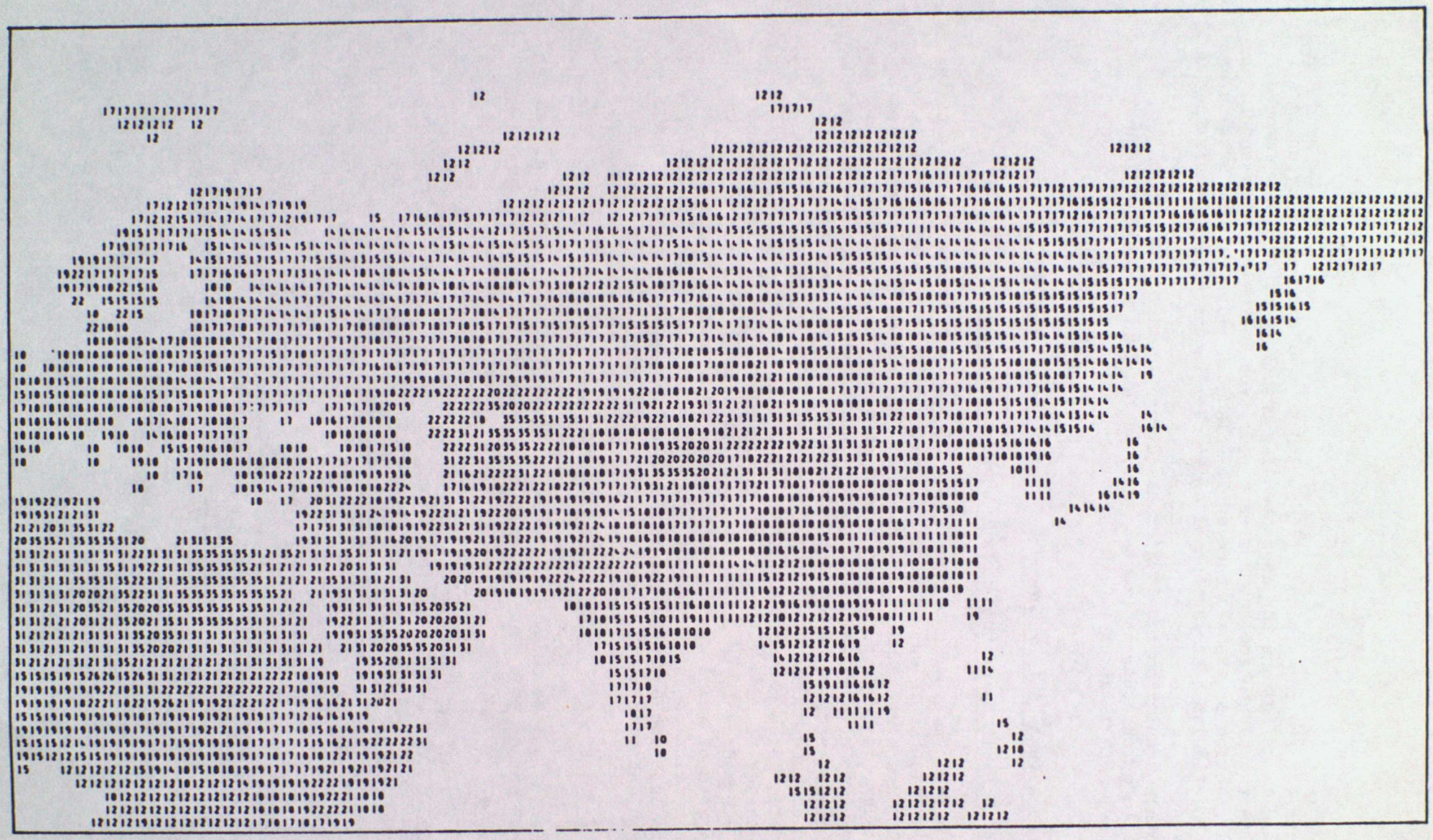

Figure 3. Snow-free land-surface albedos (%) used in the Meteorological Office's 15-level, global operational NWPM.

$$\alpha = \sum_{i=1}^{23} (f_{vi}\ \alpha_{vi}) + f_s\ \alpha_s \qquad (8)$$

where α_{vi} are the albedos of the 23 different land-cover types in Table 1 and f_{vi} are the corresponding fractions of grid-box covered; α_s is the albedo for the dominant soil type in the grid-box and f_s is the fraction of exposed bare soil. Figure 3 illustrates a section of the particular distribution of snow-free, land-surface albedos used currently in the Meteorological Office's 15-level, global, operational weather prediction model which has a regular, 1.5° x 1.875°, latitude-longitude horizontal grid, ie the typical mid-latitude grid-length is about 150 km.

4. Surface Turbulent Exchanges

4.1 Definition of the surface turbulent fluxes

The atmospheric boundary layer (planetary boundary layer; mixing layer) is the lowest layer of the atmosphere under the direct influence of the underlying surface. The flow in the atmospheric boundary layer is turbulent except possibly in very stable conditions, for example, such as those that prevail often at night in the presence of strong surface-based temperature inversions. The velocity, temperature, humidity and other properties in a turbulent flow can be considered as random functions in space and time and it is usually necessary to resort to a statistical approach to the calculation of many boundary-layer properties. In particular this introduces the concepts of mean values, fluctuations and variances into the description of the turbulent properties of the flow. For example, if ξ is some conservative quantity which fluctuates because of the turbulent motion, then it is usually written as

$$\xi = \bar{\xi} + \xi' \qquad (9)$$

where $\bar{\xi}$ is some suitably defined mean value of ξ and ξ' is called the turbulent or eddy fluctuation (see schematic illustration in Figure 4).

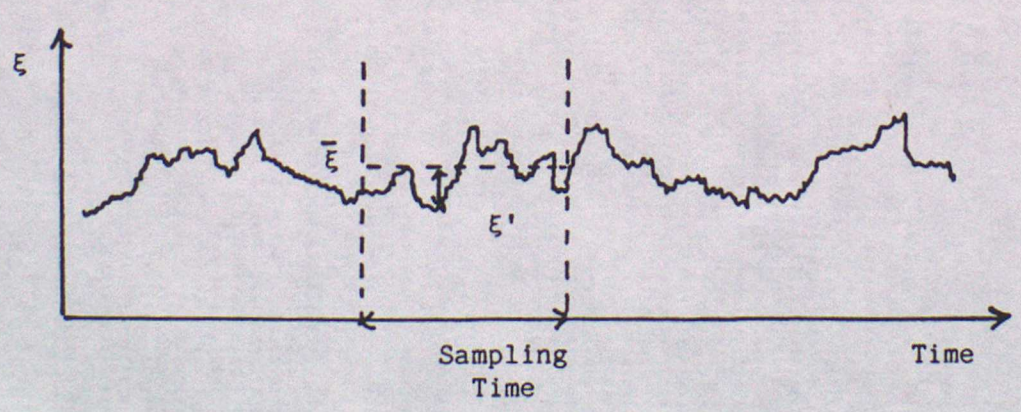

Figure 4. Schematic representation of the mean value, $\bar{\xi}$, and the eddy fluctuation, ξ', determined for a particular sampling time from a time-trace of the fluctuating quantity ξ.

In the notation of Eqn (9), the term $\overline{w'\xi'}$, represents the eddy covariance of ξ and the vertical velocity component of the flow, w, and denotes the mean vertical turbulent flux of ξ at a given height in the atmospheric boundary layer. Let

$$F_\xi = (\overline{w'\xi'})_o \qquad (10)$$

denote the surface value of the mean vertical turbulent flux of ξ, then, in the context of our discussion of land-surface processes, the surface turbulent fluxes of particular interest are:

a. Momentum flux ($\underline{\tau}$)

$$\underline{\tau} = \rho(-(\overline{w'u'})_o, -(\overline{w'v'})_o) \qquad (11)$$

where u, v are the components of the horizontal wind vector, $\underline{V}$, and ρ is a representative mean air density near the surface (the bar notation to denote a mean value will be dispensed with except where essential to the interpretation of the terms involved). The conventional interpretation and vectorial character of the surface shearing stress, $\underline{\tau}$, were discussed in Section 2.1. The direction of $\underline{\tau}$ is determined by the limiting wind direction as the surface is approached. An important parameter, the surface friction velocity u_*, is defined in terms of the magnitude of $\underline{\tau}$ such that

$$|\underline{\tau}| = \rho u_*^2 \qquad (12)$$

b. Sensible heat flux (H)

$$H = \rho c_p(\overline{w'\theta'})_o = -\rho\, c_p\, u_*\theta_* \qquad (13)$$

where the potential temperature θ is used as the temperature which is conserved in the large-scale mixing and c_p is the specific heat of air at constant pressure. θ_* (like u_* in Eqn (12)) is introduced as a scaling parameter defined in terms of H and u_*, and is negative for a positive H (ie upward from the surface). The role of H in the surface energy balance is seen in Eqn (1).

c. Water vapour flux (E)

$$E = \rho(\overline{w'q'})_o = -\rho u_* q_* \qquad (14)$$

where q is the specific humidity and q_* is the corresponding surface scaling parameter (defined negative for positive evaporation from the surface). E, the surface evaporation rate, is not only an important direct component of the moisture flux balance at the surface (vid. Eqn (2)) but also appears in the latent heat flux term $Q = L_e E$ in the surface energy balance (vid. Eqn (1)).

From Eqns (11)-(14) our general expression Eqn (10) for the surface turbulent flux F_ξ can be extended to

$$F_\xi = (\overline{w'\xi'})_o = -u_*\xi_* \qquad (15)$$

which defines the surface scaling value ξ_* (for example as for u_*, θ_* and q_*) in terms of u_* and the mean vertical turbulent flux of ξ at the surface.

4.2 The surface-flux layer

Adjacent to the surface we can identify a shallow layer in which the turning of the wind with height may be ignored and the vertical fluxes of momentum, heat and water vapour may be approximated closely by their surface values (ie for many practical purposes the turbulent fluxes in this layer may be assumed to be virtually constant with height). The layer so-defined is often referred to as the constant-flux layer. However, this terminology can mislead the unwary (note, for example, that the turbulent fluxes generally have their largest vertical gradients at the surface) and it is better to use the more appropriate term of surface-flux layer.

4.3 Monin-Obukhov similarity theory

The Monin-Obukhov similarity hypothesis for the surface-flux layer is the most widely accepted approach for describing the properties of the surface layer. Brought down to the very simplest terms, similarity methods depend on the possibility of being able to express the unknown variables in non-dimensional form, there being suitable argument for saying there exist a length-scale, a velocity-scale (or time-scale) and a temperature- (and humidity-) scale relevant in doing this. The non-dimensional forms are then postulated to be universal in character and this will hold as long as the scales remain the relevant ones.

The Monin-Obukhov similarity hypothesis for the fully turbulent surface-flux layer (where the Coriolis force is neglected) states that for any transferrable property, the distribution of which is homogeneous in space and stationary in time, the vertical flux-profile relation is determined uniquely by the parameters

$$\frac{g}{T},\ \frac{|\tau|}{\rho},\ \frac{H}{\rho c_p},\ \frac{E}{\rho} \qquad (16)$$

where g/T is the Archimedean buoyancy parameter, g is the acceleration due to gravity and T is a representative air temperature in the surface layer. From Eqns (12)-(14) these are equivalent to the set

$$\frac{g}{T},\ u_*,\ \theta_*,\ q_* \qquad (17)$$

where θ_* and q_* can be combined to give

$$\psi_* = \theta_* + 0.61T\, q_* \qquad (18)$$

which is very akin to a virtual potential temperature scaling value.

Instead of using the buoyancy parameter g/T it is convenient to use the length-scale, L, defined uniquely by g/T, u_* and ψ_* by the relation.

$$L = \frac{Tu_*^2}{kg\,\psi_*} = -\frac{\rho c_p T u_*^3}{kg\,(H+0.61c_p TE)} \qquad (19)$$

and called the Monin-Obukhov length. k is the von Kármán constant ($\simeq 0.4$) and is conventionally introduced solely as a matter of convenience. L is effectively constant in the surface-flux layer. The turbulent flow is classed as unstable when $L < 0$ (ie when the net surface buoyancy flux is positive); stable when $L > 0$ (ie when the surface buoyancy flux is negative); and neutral when $|L| \to \infty$ (ie when the surface buoyancy flux is zero).

Thus L, u_*, θ_*, q_* may be taken as the set of basic parameters which uniquely determine the relationships between the surface-layer vertical gradients of wind, potential temperature and specific humidity to the corresponding surface turbulent fluxes. Dimensional analysis leads to the vertical flux-gradient relationship expressed in the general form

$$\frac{\partial \xi}{\partial z} = \frac{\xi_*}{kz}\,\phi_\xi(z/L) \qquad (20)$$

where z is height above the surface. $\phi_\xi(z/L)$ is hypothesized to be a universal function of z/L only which may be of different form for each mean transferrable property, ξ, and which has to be established empirically from analysis of surface-layer data. The overall observational evidence is that the ϕ_ξ decrease with unstable stratification (ie when $L < 0$) and increase with stable stratification ($L > 0$). For specified functions for ϕ_ξ, Eqn (20) can be integrated to provide flux-profile relationships for the surface layer, viz:

$$\frac{k[\xi(z)-\xi(z_r)]}{\xi_*} = \int_{\zeta_r}^{\zeta} \frac{\phi_\xi(\eta)}{\eta}\,d\eta \equiv \Phi_\xi(\zeta,\zeta_r) \qquad (21)$$

where $\zeta = z/L$ and $\zeta_r = z_r/L$, where z_r is some reference height at which ξ is known. In practice, Eqn (21) used in conjunction with Eqns (12)-(14) allows us to estimate the surface turbulent fluxes of momentum, heat and moisture from a knowledge of the corresponding surface-layer profiles of wind, potential temperature and humidity.

4.4 The Monin-Obukhov similarity functions (ϕ_ξ)

The general character of the similarity functions is fairly well established over a limited range of stability conditions, centred on neutral, but their specification for extreme stability conditions (both stable and unstable) is much more debatable and uncertain. The particular specifications of ϕ_ξ listed below are subjectively selected, albeit typical, examples of the type of formulae commonly adopted as the basis of parametrizations for the surface turbulent fluxes in numerical models. For fuller discussions of the variety of postulated, empirical forms of ϕ_ξ see, for example, Chap 6 of McBean et al (1979).

The general behaviour is that ϕ_ξ increases with increasing stability; ie decreasing turbulence decreases the mixing and hence increases the normalised gradient of ξ. Figure 5 illustrates schematically the changing character of the surface-layer wind profile throughout a clear day and a clear night. For details see, for example, Chap 6 of Panofsky and Dutton (1984).

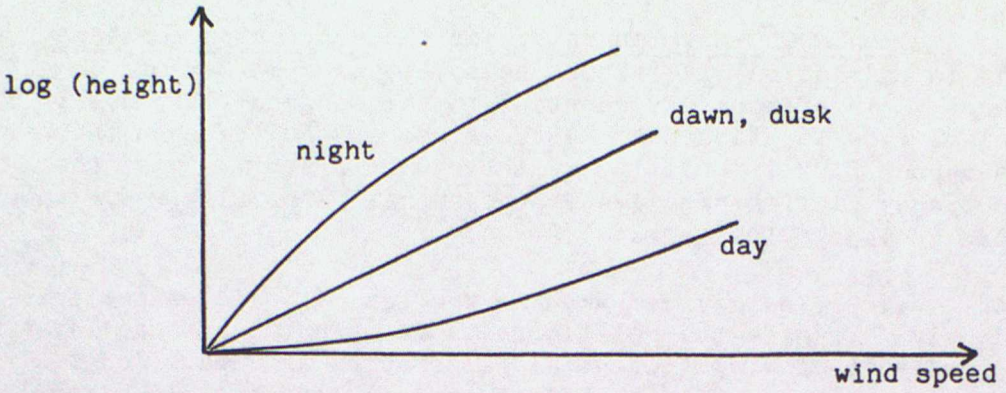

Figure 5. Schematic representation of diurnal variation of surface-layer wind profile.

4.4.1 Unstable and neutral conditions ($z/L \leq 0$)

Dyer and Hicks (1970):

$$\phi_H = \phi_E = \phi_M^2 = (1-16\ z/L)^{-1/2} \quad 0 \geq z/L \geq -1 \qquad (22)$$

where ϕ_M, ϕ_H and ϕ_E are the respective ϕ_ξ for the turbulent transfers of momentum, sensible heat and water vapour. Note that, strictly, the Dyer and Hicks (1970) formulae are limited to $|z/L| \leq 1$ and so other empirical approaches may need to be invoked for more unstable conditions. For a particular choice of extrapolation beyond the Dyer and Hicks limit towards the free-convection limit see Carson (1982, 1986a).

4.4.2 Stable conditions ($z/L > 0$)

Webb (1970):

$$\phi_H = \phi_E = \phi_M = \begin{cases} 1 + 5\ z/L & 0 < z/L \leq 1 \\ 6 & 1 < z/L < 6 \end{cases} \qquad (23)$$

The problem of extending the functional form of ϕ_ξ to highly stable conditions was discussed by Carson and Richards (1978).

4.5 The bulk transfer coefficient, C_ξ, and the aerodynamic resistance, r_ξ

It is standard practice, particularly in AGCMs and NWPMs, to represent the mean vertical surface turbulent flux, F_ξ, by

$$F_\xi = -C_\xi V(z_\ell)\ \Delta\xi(z_\ell) \qquad (24)$$

where

$$\Delta\xi(z_\ell) = \xi(z_\ell) - \xi_o \quad . \qquad (25)$$

z_ℓ is some specified height above the surface and within the boundary layer (and which may be regarded, without loss of generality, as the notional height of a particular numerical model's first level above the underlying surface); $V(z_\ell)$ is the mean horizontal wind speed (ie

$|\underset{\sim}{V}(z)|$) at z_ℓ; $\xi(z_\ell)$ is the value of the property ξ at z_ℓ and ξ_o is its surface value. (Note again that the bar notation to denote mean values (see Eqn (9)) has been omitted to simplify the symbolism). C_ξ is the so-called bulk transfer coefficient, defined in a strictly mathematical sense by Eqn (24), and which, in general, is a complicated function of height, atmospheric stability, surface roughness and, for a vegetated surface, of other physical and physiological characteristics of the surface vegetation.

In bulk-aerodynamic form the surface turbulent fluxes of Eqns (11), (13) and (14) are:

a. Momentum flux $\underset{\sim}{\tau} = \rho C_D V(z_\ell)\, \underset{\sim}{V}(z_\ell)$ (26)

where C_D is the traditional 'drag coefficient'.

b. Sensible heat flux $H = -\rho c_p C_H V(z_\ell)(\theta(z_\ell)-\theta_o)$ (27)

where C_H is the bulk transfer coefficient for heat transfer.

c. Water vapour flux $E = -\rho C_E V(z_\ell)(q(z_\ell)-q_o)$ (28)

where C_E is the bulk transfer coefficient for water vapour transfer.

To determine the fluxes from Eqns (26)-(28) the C_ξ must be prescribed or expressed in terms of modelled variables and parameters and, in addition to the variables modelled explicitly at z_ℓ, the surface temperature and humidity need to be known. The prediction of surface temperature, T_o (simply related to θ_o), is discussed in Section 5. The surface specific humidity, q_o, is not so easy to predict explicitly and its implied value is inextricably linked to the parametrization of the surface hydrology, which is discussed in Section 6. The Monin-Obukhov theory of Sections 4.3 and 4.4 provides a basis for a fairly sophisticated specification of the C_ξ which is described in the next section.

A related approach to Eqn (24) for the representation of the turbulent fluxes at natural surfaces is the so-called resistance approach. Turbulent transfer in the atmospheric boundary layer is seen as a process analogous to the flow of electric current and, in the spirit of Ohm's Law, F_ξ is written as

$$F_\xi = -\frac{\Delta\xi}{r_\xi} \qquad (29)$$

where, in a similar manner to C_ξ in Eqn (22), Eqn (29) can be regarded as defining r_ξ, the aerodynamic resistance to the 'flow' of F_ξ.

The resistance approach has particular appeal when dealing with the complicated and multiple routes for sensible heat transfer and evaporation from vegetated surfaces (see, for example, Monteith (1965), Perrier (1982) or Rosenberg et al (1983)). It was, however, felt instructive to mention it here. Also, comparison of Eqns (24) and (29) yields

$$r_\xi = [C_\xi V(z_\ell)]^{-1} \qquad (30)$$

4.6 C_ξ from Monin-Obukhov similarity theory

For a discussion of the large variety of specifications of C_ξ then in current use in AGCMs see, for example, Carson (1982). However, discussion here is limited to the approach most acceptable to boundary-layer experts and increasingly more prevalent in the current generation of AGCMs and NWPMs, viz, that based on the Monin-Obukhov similarity theory.

From Eqns (24) and (15) it is seen that

$$C_\xi = \left(\frac{u_*}{V(z_\ell)}\right)\left(\frac{\xi_*}{\Delta\xi(z_\ell)}\right) \qquad (31)$$

For Monin-Obukhov theory to be appropriate then z_ℓ must be fully within the surface layer so that Eqn (21) can be invoked in the particular form

$$k\,\frac{\Delta\xi(z_\ell)}{\xi_*} = \int_{\zeta_\xi}^{\zeta_\ell} \frac{\phi_\xi(\eta)}{\eta}\,d\eta \equiv \Phi_\xi(\zeta_\ell, \zeta_\xi) \qquad (32)$$

where $\zeta_\ell = z_\ell/L$ and $\zeta_\xi = z_\xi/L$ is defined such that

$$\xi(z_\xi) \equiv \xi_o \qquad (33)$$

The nature of the similarity formulation implies a logarithmic singularity in Φ_ξ as $z \to 0$. This is avoided by defining the level z_ξ as the virtual height at which the ξ-profile, defined by Eqn (21) and extrapolated towards the surface, attains the actual surface value ξ_o. For momentum transfer, this level, denoted z_o, is defined as the virtual height at which V=0 on the postulated wind profile. z_o is called the surface roughness length and over a bare soil surface is a characteristic of the surface and is usually independent of the flow. There are also corresponding characteristic 'surface roughness lengths' for heat and water vapour transfer. The problems of evaluating effective areal roughness lengths and of discriminating between them for the different properties are complex and it remains common practice in large-scale numerical models to use the estimate for z_o for all three profiles. This aspect of the overall problem is discussed below in Section 4.7.

From Eqns (31) and (32), C_ξ can be specified in terms of finite integrals of the Monin-Obukhov similarity functions, thus,

$$C_\xi = k^2\,\Phi_M^{-1}(\zeta_\ell, \zeta_o)\,\Phi_\xi^{-1}(\zeta_\ell, \zeta_\xi) \qquad (34)$$

where $\Phi_M(\zeta, \zeta_o) = \int_{\zeta_o}^{\zeta} \frac{\phi_M(\eta)}{\eta}\,d\eta = \frac{kV(z)}{u_*}$ (35)

and $\zeta_o = z_o/L$. In general, with ϕ_ξ specified as discussed, for example, in Section 4.4, then Eqn (34) gives C_ξ as a function of ζ_ℓ, ζ_o and ζ_ξ.

It is generally more convenient for modelling purposes to express C_ξ directly as a function of the explictly modelled variables $V(z_\ell)$ and $\Delta\xi(z_\ell)$. This can be achieved by using a bulk Richardson number for the surface layer, Ri_B, instead of ζ_ℓ as the stability indicator, such that

$$Ri_B = \frac{g z_\ell}{T} \frac{[\Delta\theta(z_\ell) + 0.61 T \Delta q(z_\ell)]}{V^2(z_\ell)} \qquad (36)$$

This can be related implicitly to ζ_ℓ through

$$Ri_B = \frac{\zeta_\ell}{k} \frac{C_D}{C_H}^{3/2} \qquad (37)$$

For a full description of the method and the assumptions made, see, for example, Carson and Richards (1978).

As an example, Figure 6 depicts the surface-layer bulk transfer coefficients used in the Meteorological Office 11-layer AGCM which are based on Monin-Obukhov similarity theory and in particular for part of the range of Ri_B (corresponding to a very small section of the abscissa in the Figure), on the specifications of ϕ_ξ given in Eqns (22) and (23). In that particular model z_ℓ = 100 m, z_o over land is 0.1 m and z_o over sea is 10^{-4}m. The bulk transfer coefficients in Figure 6 are used in Eqns (26)÷(28) to provide estimates of the surface turbulent fluxes $\underset{\sim}{\tau}$, H and E, respectively.

4.7 Surface roughness length (z_o)

z_o, like the surface albedo of Section 3, is a land-surface characteristic which has a marked geographical variation. In most of the current generation of AGCMs and NWPMs, z_o has direct and indirect effects on the surface turbulent exchanges of sensible heat and moisture as well as on the surface shearing stress (see comments above in Section 4.6). However, the evaluation of an effective areal surface roughness length for heterogeneous terrain is an important practical issue that poses a variety of as yet unsatisfactorily resolved problems.

The effective areal z_o for natural surfaces is rarely estimated from the wind profile and/or surface shear stress measurements. Instead, it is most likely to be determined indirectly from a knowledge of, for example: terrain relief (elevation, slope, etc); land use; type and distribution of the surface roughness elements. Algorithms, however qualitative, are needed to perform this function sensibly, at least in a fairly local (1 x 1 km^2) sense. The pros and cons of alternative approaches to the question of how to average over larger areas has been discussed by Carson (1986b).

Most standard boundary-layer text books provide a table of values of z_o as a function of terrain type described qualitatively in terms of relief and vegetative characteristics (see, for example, Table 6.2 in Panofsky and Dutton (1984)). Such traditional relationships may well be adequate on the very local scale for the smoother, quasi-homogeneous types of terrain but can be expected to be less well founded for areal averages over rough, heterogeneous terrain, typical say of a European semi-rural landscape with small hills, woods, fields, crops, hedges, towns, lakes, etc. Wieringa (1986) has addressed this problem and produced a table giving effective areal z_o in terms of a terrain classification when there are no significant orographic effects (see Table 3).

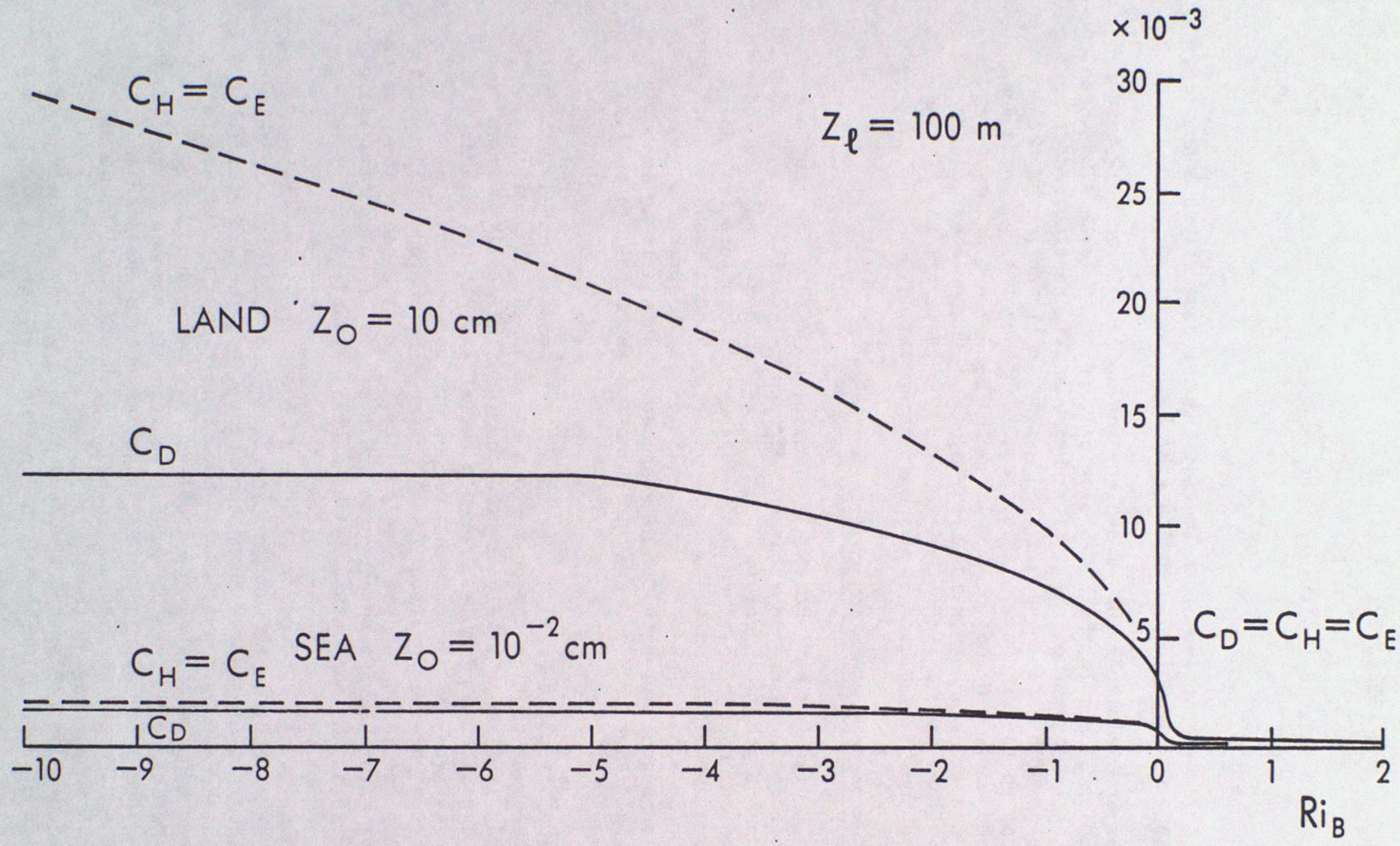

Figure 6. Surface layer bulk transfer coefficients derived from Monin-Obukhov similarity theory and used in the Meteorological Office's 11-layer AGCM.

For fuller discussions of issues concerning the evaluation of effective z_o the reader is referred to the recent papers by Smith and Carson (1977), Mason (1985), Carson (1986b), Wieringa (1986) and André and Blondin (1986).

Land use category	z_o (m)
Sea (minimal fetch 5 km)	0.0002
Small lake, mud flats	0.006
Morass	0.03
Pasture	0.07
Dunes, heath	0.10
Agriculture	0.17
Road, canal (in Dutch landscape tree-lined)	0.24
Orchards, bushland	0.35
Forest	0.75
Residential built-up area ($H \leq 10$ m)	1.12
City centre (high-rise building)	1.6

Table 3. Effective mesoscale surface roughness length, z_o (m), expressed as a function of land use and proposed by Wieringa (1986). H is the height of the major surface obstacles.

5. Soil Heat Conduction and the Land-surface Temperature

In our formulation of the energy flux balance at a bare-soil surface, Eqn (1), G_o the sensible heat flux in the soil is equated to the net imbalance in the energy fluxes between the surface and the atmosphere. If the aim was solely to evaluate G_o, then use of the surface energy balance, as depicted in Eqn (1), would be a legitimate method for obtaining such an estimate. Indeed, in principle, the energy balance method can be invoked to estimate any one of the terms in Eqn (1) if all the others are known by some other means.

The more direct, microphysical approach to understanding the soil heat flux term G_o is through the study of heat transfer in the soil itself, a process which is predominantly that of heat conduction. In general, G_o will depend in a complicated way on the soil's thermal properties which in turn depend on, for example, the type of surface, the type of soil and whether it is wet, dry, frozen or snow-covered, and whether it is bare soil or vegetation. In simple, general terms a thin surface layer of the soil stores heat during the day (strictly, from Eqn (1), when $R_N > H + Q$ ie G_o is positive) and acts as a source of heat energy to the surface at night (strictly, when $R_N - H - Q < 0$ ie G_o is negative). On longer, seasonal and annual time scales deeper soil layers act as a reservoir of heat which may be replenished during warm seasons and depleted during the cold seasons.

Good estimates of the detailed behaviour of G_o throughout the day and throughout the year are now recognised as important to include in NWPMs, which attempt to forecast the characteristic diurnal cycle of land-surface temperatures, and also in climate models which need to simulate realistically and interactively the heat-storage properties of the soil over periods ranging from less than a day to at least several years.

Implicit in a knowledge of heat transfer through the soil is a knowledge of the soil temperature profile with depth. In particular, the land-surface temperature, T_o, features in each of the terms in Eqn (1) and it is now the common practice in AGCMs and NWPMs to invoke the surface energy balance as a diagnostic relation or prognostic equation for evaluating T_o. The variety of techniques commonly used in such models for representing G_o in the surface energy balance has already been reviewed fairly comprehensively by, for example, Bhumralkar (1975), Deardorff (1978) and Carson (1982, 1986a). In order to illustrate the relationships between soil heat flux, soil temperature profile and the thermal properties of the soil, I shall restrict my discussion to those methods which rely on a knowledge of heat conduction in the soil and invoke either simple, one-dimensional, analytical models or attempt to model explicitly the soil heat transfer in a multi-layer soil model.

5.1 Heat transfer in a semi-infinite homogeneous soil

Most parametrizations of G_o are now based on considerations of heat conduction and conservation in the soil. The problem is usually simplified by assuming a semi-infinite, spatially homogeneous soil layer with no horizontal heat transfer and no melting or freezing within it. This restricted and idealised one-dimensional problem is governed by:

a. the soil heat conservation equation

$$\frac{\partial T_g}{\partial t} = -\frac{1}{C}\frac{\partial G}{\partial z_g} \qquad (38)$$

where T_g is the soil (ground) temperature, G is the soil heat flux, C is the volumetric heat capacity of the soil (SI units: J $m^{-3}K^{-1}$), $z_g = -z$ is the vertical co-ordinate in the soil layer and t is time; and

b. the flux-gradient relation for heat conduction

$$G = -\lambda \frac{\partial T_g}{\partial z_g} \qquad (39)$$

where λ is the thermal conductivity of the soil (SI units: $Wm^{-1}\ K^{-1}$).

Substitution of Eqn (39) into Eqn (38), with the assumption of homogeneity, yields the one-dimensional equation for conduction of heat in the soil, viz.

$$\frac{\partial T_g}{\partial t} = \kappa \frac{\partial^2 T_g}{\partial z_g^2} \qquad (40)$$

where κ is the thermal diffusivity of the soil (SI units: $m^2\ s^{-1}$) such that

$$\kappa = \lambda/C = \lambda/\rho_g c_g \qquad (41)$$

where ρ_g is the uniform soil density and c_g is the specific heat capacity (SI units: J kg^{-1} K^{-1}).

The definitions and characteristics of the soil thermal properties C, λ, κ and c_g can be found in standard text books such as Geiger (1965), Sellers (1965), Oke (1978) and Rosenberg et al (1983). The values in Table 4 are given in Oke (1978) and illustrate the typical magnitudes of these terms for a few simple soil types (and for snow) and also indicate their sensitivity to how wet or dry the soil is.

Material	Remarks	ρ_g kg m^{-3} x 10^3	c_g J kg^{-1} K^{-1} x 10^3	C J m^{-3} K^{-1} x 10^6	λ Wm^{-1} K^{-1}	κ m^2s^{-1} x 10^{-6}	δ_d m	δ_a m
Sandy soil (40% pore space)	Dry	1.60	0.80	1.28	0.30	0.24	0.08	1.55
	Saturated	2.00	1.48	2.96	2.20	0.74	0.14	2.73
Clay soil (40% pore space)	Dry	1.60	0.89	1.42	0.25	0.18	0.07	1.34
	Saturated	2.00	1.55	3.10	1.58	0.51	0.12	2.26
Peat soil (80% pore space)	Dry	0.30	1.92	0.58	0.06	0.10	0.05	1.00
	Saturated	1.10	3.65	4.02	0.50	0.12	0.06	1.10
Snow	Fresh	0.10	2.09	0.21	0.08	0.10	0.05	1.00
	Old	0.48	2.09	0.84	0.42	0.40	0.10	2.00

Table 4. Thermal properties of natural materials (from Oke (1978)). ρ_g, c_g, C, λ and κ are defined in Section 5.1. δ_d and δ_a are the e-folding depths of the diurnal and annual soil temperature waves and are defined in Section 5.2.

A standard practice is to combine Eqns (38), (39) and the surface energy balance, Eqn (1), to produce a prognostic equation for T_o (usually assumed equivalent to the soil surface temperature T_{go}). The simplest approaches of this kind introduce the concept of an effective depth of soil D and an effective surface thermal capacity

$$C_{eff} = CD = \rho_g c_g D \qquad (42)$$

defined such that

$$G_o = C_{eff} \frac{\partial T_{go}}{\partial t} \equiv CD \frac{\partial T_o}{\partial t} \qquad (43)$$

Many AGCMs and NWPMs contain rather arbitrary and empirical selections of C_{eff} (see, for example, Carson (1982)) and with G_o replaced by the RHS of the surface energy balance, Eqn (43) can be solved for T_o.

Note however that C_{eff} (and D) can be defined more formally from consideration of the soil heat conservation equation (38). On the assumption that $G \to 0$ as $z_g \to \infty$ then Eqn (38) can be integrated to give

$$G_o = C \int_o^\infty \frac{\partial T_g}{\partial t} \, dz_g \qquad (44)$$

which, when used to replace G_o in Eqn (43), allows D to be defined in a strictly mathematical sense as

$$D = \left(\frac{\partial T_o}{\partial t}\right)^{-1} \int_o^\infty \frac{\partial T_g}{\partial t} \, dz_g \qquad (45)$$

The following section describes a popular analytical approach in which Eqn (45) may be invoked to good advantage.

5.2 One-dimensional heat transfer in a semi-infinite, homogeneous soil whose surface is heated in a simple periodic manner

One simple, attractive and commonly adopted method of determing D in Eqn (43) is by appealing to the theory of heat transfer in a semi-infinite homogeneous medium when the surface is heated in a simple periodic manner (as discussed, for example, in Sellers (1965)).

If it is assumed that the surface temperature

$$T_o \equiv T_g(0, t) = \hat{T}_g + a_o \sin \omega t \qquad (46)$$

where ω is the angular frequency of oscillation, $\hat{T}_g$ is the mean soil temperture (over the period $P = 2\pi/\omega$), assumed to be the same at all depths, and a_o is the amplitude of the surface temperature wave, then the solution of Eqn (40) is

$$\begin{aligned} T_g(z_g,t) &= \hat{T}_g + a(z_g) \sin (\omega t - z_g/\delta) \\ &= \hat{T}_g + a_o \exp (-z_g/\delta) \sin (\omega t - z_g/\delta). \end{aligned} \qquad (47)$$

$$\delta = \left(\frac{\kappa P}{\pi}\right)^{1/2} = \left(\frac{2\lambda}{C\omega}\right)^{1/2} \qquad (48)$$

is the e-folding depth of the temperature wave of period P, ie it is the depth where the amplitude of the oscillation is reduced to $^1/_e$ (ie 0.37) times its surface value. Values of the e-folding depths corresponding to the diurnal and annual periods, respectively, are given for a range of soil types in Table 4.

The effective depth D corresponding to the soil temperature profile Eqn (47) is, from Eqn (45),

$$\begin{aligned} D &= \frac{1}{a_o \cos \omega t} \int_o^\infty a(z_g) \cos (\omega t - z_g/\delta) \, dz_g \\ &= \frac{1}{\cos \omega t} \int_o^\infty \exp (-z_g/\delta) \cos (\omega t - z_g/\delta) \, dz_g \end{aligned}$$

$$= \frac{\delta}{\sqrt{2}} \frac{\sin(\omega t + \pi/4)}{\cos \omega t} \qquad (49)$$

Therefore D as defined in Eqn (43) is not only a function of the thermal diffusivity of the soil and the single frequency assumed for the simple periodic forcing at the surface but also varies with time according to Eqn (49). Substituting for D from Eqn (49) in Eqn (43) gives a prognostic equation for T_o, viz.

$$\frac{\partial T_o}{\partial t} = \frac{\sqrt{2}\, G_o \cos \omega t}{C\delta \sin(\omega t + \pi/4)} \qquad (50)$$

which in turn can be expanded easily to give

$$\frac{\partial T_o}{\partial t} = \frac{2G_o}{C\delta} - \frac{2\pi}{P}(T_o - \hat{T}_g) \qquad (51)$$

This, I believe, is a relatively neat way of deriving Eqn (51) which was proposed by Bhumralkar (1975) and has come to be referred to as the 'force-restore method', a term introduced by Deardorff (1978).

The period of the diurnal temperature oscillation is normally used in Eqn (51) as that appropriate for determining the thermal capacity of the effective surface layer. Additional information about $\hat{T}_g$ is required to solve Eqn (51). $\hat{T}_g$ may be fixed or diagnosed over short periods of a few days but would need to be determined prognostically over the much longer periods of integration involved, for example, in climate modelling. Deardorff (1978) has suggested a second prognostic equation for $\hat{T}_g$ analogous to Eqn (51) but with the appropriate effective depth determined by the e-folding depth of the annual temperature wave. Although there is some useful mileage in extending this simple, analytically-based method further (see, for example, Deardorff (1978) and Carson (1982)), such parametrizations soon become analogous to the more elaborate schemes which explicitly model the temperature profile through several soil layers.

5.3 Multi-layer soil models

The somewhat idealised analytical assumptions underlying the force-restore method and other simpler parametrizations can be avoided in principle by explicit modelling of the soil temperature profile and soil heat conduction with a multi-layer soil model of specified depth and with appropriate vertical resolution and boundary conditions. One approach, for example, would be to invoke Eqn (39) to evaluate G_o explicitly from the modelled soil temperature profile such that

$$G_o = \left[-\lambda \frac{\partial T_g}{\partial z_g}\right]_{z_g=0} \qquad (52)$$

With this representation of G_o, Eqn (1) could then be solved diagnostically for T_o.

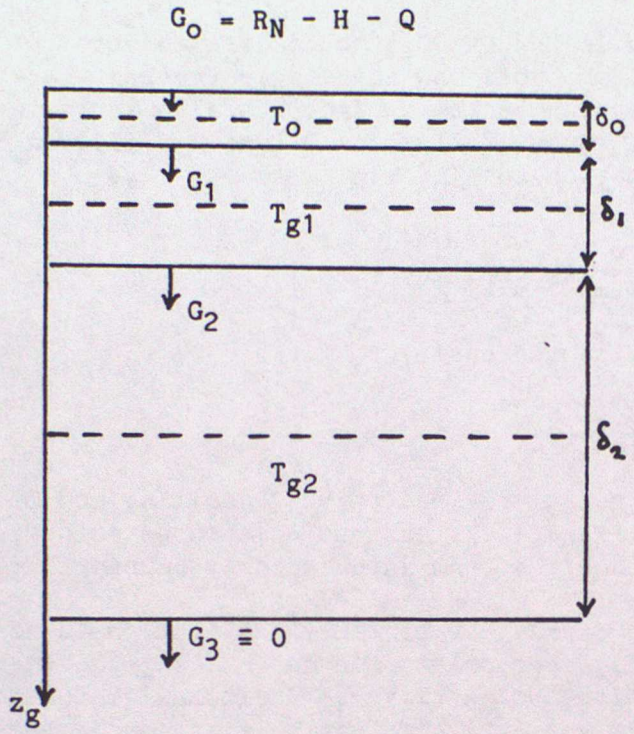

Figure 7. Schematic representation of a 3-layer, soil-temperature, finite-difference model. T_o, T_{g1} and T_{g2} are the representative temperatures in the soil layers of depth δ_o, δ_1 and δ_2, respectively. G_o, G_1, G_2 and G_3 are the corresponding soil heat fluxes at the respective layer boundaries.

An alternative approach is represented schematically for a 3-layer soil-temperature model in Figure 7. Here the surface temperature T_o is represented by the mean temperature of a very thin surface soil layer of depth δ_o. The rate of change of T_o with time is given by the soil heat flux divergence in the surface layer according to a simple finite difference form of Eqn (38), i.e.

$$\frac{\partial T_o}{\partial t} = \frac{G_o - G_1}{C\delta_o} \quad . \tag{53}$$

G_o is as usual the net imbalance of the terms on the RHS of Eqn (1) and G_1, the soil heat flux into the next layer down, is determined from the explicitly modelled soil temperature profile from the heat conduction Eqn (39) written simply as

$$G_1 = \frac{2\lambda(T_o - T_{g1})}{\delta_o + \delta_1} \quad . \tag{54}$$

Therefore, from Eqns (53) and (54),

$$\frac{\partial T_o}{\partial t} = \frac{G_o}{C\delta_o} + \frac{2\kappa\,(T_{g1} - T_o)}{\delta_o(\delta_o + \delta_1)} \quad , \tag{55}$$

and the same general technique is used to provide the corresponding predictive equations for the temperatures of the other soil layers.

In the 3-layer soil model of Figure 7, all three soil temperatures are treated as prognostic variables during integration of the model, with the boundary condition that the soil heat flux is zero at the lower soil boundary (ie $G_3 \equiv 0$ in Figure 7). An alternative, popular lower boundary condition is to hold the bottom-layer soil temperature constant at its initialised value. This latter boundary condition is used, for example, in the 4-layer soil model in the current Meteorological Office fine-mesh operational forecasting model (Carson, 1986a) and also in the 3-layer soil model used at ECMWF (Blondin, 1986).

The selection of 'representative' soil thermal characteristics C and λ (and hence κ) and suitable soil-layer depths, $\delta_0 \ldots . \delta_i \ldots . \delta_{n-1}$ where n is the number of explicitly resolved layers in the soil; remains a difficult, empirical and highly subjective business. On the basis of a comprehensive study of the amplitude and phase responses of multi-layer soil schemes to periodic surface temperature forcing, Warrilow et al (1986) have recommended a 4-layer soil-temperature scheme of the type depicted in Figure 7 for use in the Meteorological Office AGCM. Their paper gives full description of how the appropriate soil-model parameters were selected. For further discussion of values used in specific models see, for example, Blondin (1986) and Carson (1982, 1986a). Table 5 gives values of the main parameters likely to be incorporated into the most recent control version, the so-called 'Fourth Annual-Cycle Version', of the Meteorological Office 11-layer AGCM used for climate modelling research (Warrilow, private communication).

SOIL THERMAL PROPERTIES	Value
Volumetric heat capacity, C ($J\ m^{-3}\ K^{-1}$)	2.34×10^{6}
Thermal conductivity, λ ($W\ m^{-1}K^{-1}$)	0.56
Thermal diffusivity $\kappa = \lambda/C$ (m^2s^{-1})	2.39×10^{-7}
Thermal inertia $\Upsilon = (\lambda C)^{1/2}$ ($J\ m^{-2}K^{-1}s^{-1/2}$)	1145
Soil-layer depths:	
δ_o (m)	0.037
δ_1 $[r_1=\delta_1/\delta_o]$	0.143 [3.91]
δ_2 $[r_2=\delta_2/\delta_o]$	0.516 [14.05]
δ_3 $[r_3=\delta_3/\delta_o]$	1.639 [44.65]
$\sum_{i=o}^{3} \delta_i$	2.335
Depth of the surface layer of soil determined by $\delta_o = (\frac{2\lambda}{C\omega_o})^{1/2}$ where	
ω_o (s^{-1})	3.5509×10^{-4}
$P_o = 2\pi/\omega_o$ (day)	0.2048 (ie 4.8 hr)
Thermal capacity of surface layer of soil: $C\delta_o$ ($J\ m^{-2}K^{-1}$)	8.59×10^{4}

Table 5. Physical properties selected by Warrilow (private communication) for use in the 4-layer soil-temperature model to be used in the Fourth Annual-Cycle version of the Meteorological Office 11-layer AGCM. The general approach is described fully in Warrilow et al (1986).

5.4 The land-surface temperature, T_o

Throughout this paper, following the general practice in AGCMs and NWPMs, it has been assumed that the land-surface temperature is a well-defined and unique property of any natural land surface and that the same 'T_o' is appropriate as: the radiative surface temperature of Eqn (7); the surface temperature as used in the extrapolated atmospheric boundary layer profiles and surface-flux formulae of Section 4; and the surface soil temperature related to the soil heat

flux as introduced above in Section 5. The 'surface temperatures' implied by these different physical processes at the surface must be closely related but they are not necessarily all the same. The ambiguity and difficulty in defining surface temperature become even greater when the surface has a vegetative canopy. Suffice it to state here that at present the problem is very poorly understood and that more observational and theoretical studies are needed before any significant differences between the 'T_o' can be clearly delineated and incorporated sensibly in AGCMs and NWPMs.

6. Surface Hydrology and the Soil Water Budget

Most of the current generation of AGCMs and NWPMs now include some form of 'interactive' surface hydrology, usually of a very rudimentary nature. Such parametrizations are termed 'interactive' in the sense that the soil has some recognised hydrological property that is allowed to vary in response to the model's continuously evolving atmospheric state and surface boundary conditions and which in turn exerts both direct and indirect influences on the surface fluxes themselves. The most common practice is to define a variable 'soil moisture content' for some notional depth of surface soil layer which is constrained at all times to satisfy the surface moisture flux balance as expressed in Eqn (2).

In direct analogy to the need to study heat conduction in the soil to provide a sound physical basis for evaluating the 'surface temperature', so also is there a corresponding need to understand more about the dynamics which govern the movement of water in the soil in order to model changes in the profile of 'soil moisture content'. Since the concepts of 'surface temperature' and 'soil moisture content' have been introduced here independently and in different sections, it is perhaps worth emphasizing again the strong, interactive coupling between the thermal and hydrological properties and processes in the soil. Not only does E (or Q) appear explicitly in both Eqns (1) and (2) but most of the other surface fluxes (including the momentum flux $\underline{\tau}$) depend to varying degrees on both the 'surface temperature' and the 'soil moisture content'. Indeed, in a model with both interactive surface hydrology and interactive land-surface temperature, the value of the 'soil moisture content' has an important bearing on the evaluation of T_o, and vice-versa.

As in the case of the surface radiative fluxes $R_{S\downarrow}$ and $R_{L\downarrow}$ in the context of the surface energy balance (discussed in Section 3), the surface rainfall rate P_r is regarded here as an externally determined component of the surface moisture balance, Eqn (2). Accurate evaluation of P_r is of course of crucial importance in establishing a realistic surface moisture balance and also, through the coupling discussed above, a realistic surface energy balance. The other processes involved in the hydrology of a bare soil, including evaporation, surface runoff, and transport and storage of water in the soil are generally very complex and not so well understood nor as simple to parametrize sensibly as the individual terms in the surface energy balance. The very small-scale spatial inhomogeneities within a typical soil layer appear to be more important in the determination of soil moisture movement than for the heat flow and this presents formidable difficulties when trying to formulate a parametrization based soundly on underlying physical and dynamical hydrological principles. This is particularly so when one-dimensional hydrological models are applied to catchment-sized or typical AGCM/NWPM grid-box areas. Hence the importance of the HAPEX-MOBILHY project (Andrē et al, 1986) aimed at studying the hydrological budget and evaporation flux at the scale of an AGCM grid

square, ie 10^4 km^2. A two-and-a-half-month special observing period should provide detailed measurements of the relevant atmospheric fluxes and intensive remote sensing of surface properties. The main objective of the programme is to provide a data base against which parametrizations of the land-surface water budget can be developed and tested.

A proper discussion of the surface and sub-surface hydrology of natural soils is beyond the scope of this paper. For this the reader is referred to the recent fuller expositions by, for example, Brutsaert (1982a, b), Dooge (1982), Eagleson (1982) and Dickinson (1984) in which the problems of areal representation of hydrological processes are specifically discussed. The remainder of this section is restricted to an introduction to the most simple form of the basic equations which govern the movement of water in the soil and brief descriptions of some specific formulations for soil-water transport, evaporation and surface runoff. These examples although chosen quite subjectively should nevertheless give an indication of the general tenor and level of many of the current attempts to parametrize grid-scale hydrological processes.

6.1 Water transport in a homogeneous soil

There are various inter-related measures of soil moisture content, two of which are:

a. χ, the soil moisture concentration, defined as the mass of water per unit volume of soil. (SI units: kg m^{-3}), and

b. χ_v, the volumetric soil moisture concentration, defined as the volume of water per unit volume of soil and therefore dimensionless.

Therefore

$$\chi = \rho_\omega \chi_v \qquad (56)$$

where ρ_ω is the density of water. These are very appropriate measures in parametrizations based on simulating changes in the water mass of a specified layer of soil.

In general, several different forces are acting to bind the water to the soil and a less direct but nevertheless very useful measure of soil moisture content in the context of water movement is the soil moisture potential Ψ (also termed soil moisture tension, soil moisture suction, etc) which may be thought of as the energy needed to extract water from the soil matrix. It is common practice to express Ψ as a length, in a fashion analogous to the concept of a pressure head in hydraulics, such that at a level z_g in the soil

$$\Psi = \psi - z_g \qquad (57)$$

where z_g represents the gravitational component of the moisture potential and ψ, the so-called matric potential, is the contribution to Ψ due mainly to capillarity and adsorption.

In an analogous fashion to the treatment of soil heat conduction in Section 5.1, consider the grossly simplified hydrology of a spatially homogeneous soil layer with no horizontal water movement and no melting or freezing within it. This restricted and idealised one-dimensional problem is governed by:

a. the equation of continuity

$$\frac{\partial \chi}{\partial t} = \rho_\omega \frac{\partial \chi_v}{\partial t} = - \frac{\partial M}{\partial z_g} \qquad (58)$$

where M is the vertical mass flux of water and χ, χ_v and M are functions of z_g and t; and

b. the flux-gradient relation (Darcy's Law)

$$M = -\rho_\omega K(\psi) \frac{\partial \Psi}{\partial z_g} \qquad (59)$$

$$= -\rho_\omega K(\psi) \left(\frac{\partial \psi}{\partial z_g} - 1\right)$$

where K, the hydraulic conductivity of the soil (SI units: ms^{-1}), is a function of ψ, which in turn is a function of z_g and t. Combining Eqns (58) and (59) yields the Richards' equation for the vertical movement of water in an unsaturated soil, viz.

$$\frac{\partial \chi_v}{\partial t} = \frac{\partial}{\partial z_g} [K(\psi) \left(\frac{\partial \psi}{\partial z_g} - 1\right)] \qquad (60)$$

Solving even the idealised Eqn (60) for reasonable boundary conditions is by no means a trivial matter. Proposals do exist which express ψ and $K(\psi)$ as functions of χ_v, although it should be stressed that these are highly empirical and difficult to justify in all but the most idealised circumstances. In such cases Eqn (60) takes the form of a diffusion equation for soil water

$$\frac{\partial \chi_v}{\partial t} = \frac{\partial}{\partial z_g} (\kappa_\omega(\chi_v) \frac{\partial \chi_v}{\partial z_g}) - \frac{\partial K}{\partial z_g}(\chi_v) \qquad (61)$$

where κ_ω is a moisture diffusivity of the soil (SI units: m^2s^{-1}) defined by

$$\kappa_\omega = K(\chi_v) \frac{\partial \psi}{\partial \chi_v} \qquad (62)$$

Prognostic equations for soil moisture content based on the idealised hydrology of this section are beginning to appear in AGCMs and NWPMs; see, for example, the particular examples discussed in Dickinson (1984) and Warrilow et al (1986). One particular multi-layer soil hydrology scheme which has attracted considerable support from numerical modellers is the force-restore treatment of Deardorff (1978) in which he postulates equations for soil moisture transport of a form directly analogous to the corresponding force-restore equations for soil temperatures (vid. Eqn (51)). An effective 3-layer version of Deardorff's approach is used, for example, in ECMWF models (Blondin, 1986). However, the most common current

approach to modelling soil moisture content is probably still that based on a single surface soil layer and a more detailed discussion of only that example will suffice here.

6.2 Single-layer soil hydrology models

A common, rudimentary approach to the parametrization of the hydrological processes at a bare-soil surface is to monitor the change of soil moisture content in a single, shallow surface layer of soil of notional depth δ_ω, as depicted schematically in Figure 8.

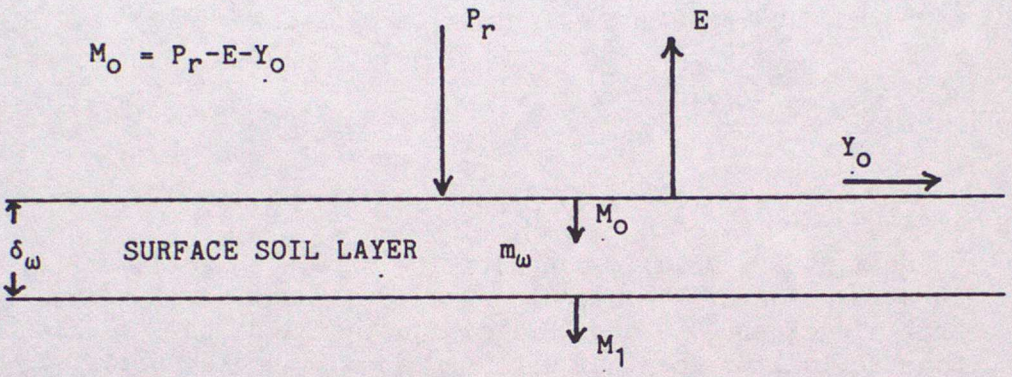

Figure 8. Schematic representation of the moisture balance of a surface layer of soil.

Let m_ω denote the mass of liquid water per unit lateral area in the soil layer of depth δ_ω, ie

$$m_\omega = \int_o^{\delta_\omega} \chi \, dz_g = \hat{\chi} \, \delta_\omega = \rho_\omega \hat{\chi}_v \delta_\omega = \rho_\omega d_\omega \qquad (63)$$

where Eqn (63) also defines a layer-mean soil moisture concentration, $\hat{\chi}$, a corresponding layer-mean volumetric soil moisture concentration, $\hat{\chi}_v$, and d_ω, a representative depth of water in the layer. Integration of Eqn (58) over the layer depth gives, from Eqn (63), the surface layer water mass balance equation in the form

$$\frac{\partial m_\omega}{\partial t} = M_o - M_1$$

$$= P_r - E - Y_o - M_1 \qquad (64)$$

when M_o is substituted from Eqn (2).

M_1 is the vertical mass flux of water at the base of the surface layer. Apart from the surface runoff term Y_o, all other horizontal fluxes of soil water have been neglected. With P_r regarded in the present context as determined externally, then it remains here to illustrate with the aid of specific examples some of the problems of formulating parametrizations for E, Y_o and M_1.

6.3 Evaporation at a bare-soil surface (E)

In principle, the surface evaporation rate E can be obtained as the residual flux from either the surface energy balance, Eqn (1), or the surface moisture balance, Eqn (2), and there are many empirical formulae for estimating E based on such approaches. A very useful introduction to the large variety of methods available can be found, for example, in Rosenberg et al (1983) and for more detailed discussions see, for example, Eagleson (1982) and Brutsaert (1982a, b). However, in this introduction to interactive soil temperature and soil moisture content parametrizations in AGCMs and NWPMs, I have selected the soil-flux terms G_o and M_o as the residual components in the surface balance equations (1) and (2), (see, for example, Eqns (51), (55) and (64)) and assumed implicitly that E can be evaluated in some independent manner.

Indeed, the method of estimating E has already been implied in principle in Section 4 where E as one of the main surface turbulent fluxes was ultimately parametrized in the bulk aerodynamic form of Eqn (28) as

$$E = -\rho C_E V(z_\ell)(q(z_\ell)-q_o) \qquad (65)$$

with the recommendation that the bulk transfer coefficient C_E be evaluated from Monin-Obukhov similarity theory. It was however also noted that the surface value of the specific humidity q_o, required explicitly in Eqn (65) (and also, for example, in determining the bulk Richardson number defined by Eqn (36), and hence C_E) is not easy to determine. To overcome this problem it is standard practice to imply a value of q_o through relations with $q_{sat}(T_o)$, the saturation specific humidity at the surface which is readily determined as a function of surface temperature (and pressure) via the Clausius-Clapeyron relationship

$$\frac{dq_{sat}}{dT} \simeq 0.622 \frac{L_i\, q_{sat}}{R\, T^2} \qquad (66)$$

where T is temperature, R is the specific gas constant for dry air and L_i is the appropriate latent heat (ie L_e when the surface is not frozen).

Two common methods are:

a. to specify a surface relative humidity, r_o, such that

$$q_o = r_o\, q_{sat}(T_o); \qquad (67)$$

b. to evaluate a potential evaporation rate

$$E_p = -\rho C_E\, V(z_\ell)(q(z_\ell)-q_{sat}(T_o)) \qquad (68)$$

and to specify an empirical 'moisture availability function', β, (usually ranging from 0 for an arid surface to 1 for a saturated surface) such that the actual evaporation rate is given by

$$E = \beta\, E_p \qquad (69)$$

The second method is by far the more commonly adopted. For a discussion and comparison of the two approaches see, for example, Nappo (1975) and for examples of their use in specific AGCMs see Carson (1982). It is worth noting in passing that an alternative relation in the spirit of Eqn (69) is used for computational convenience in some models and that is

$$\Delta q(z_\ell) = q(z_\ell) - q_o = \beta(q(z_\ell) - q_{sat}(T_o)) \qquad (70)$$

which implies that

$$q_o = \beta\, q_{sat}(T_o) + (1-\beta) q(z_\ell) \qquad (71)$$

The reasons for preferring Eqn (70) to Eqn (69) are discussed in Carson (1982) (and more fully in Carson and Roberts (1977)).

The most common method now employed is to express β as a simple linear function of the variable soil moisture content in the surface soil layer such that

$$\beta = \begin{cases} \hat{\chi}_v / \hat{\chi}_{v,c} & 0 \le \hat{\chi}_v < \hat{\chi}_{v,c} \\ 1 & \hat{\chi}_v \ge \hat{\chi}_{v,c} \end{cases} \qquad (72)$$

where $\hat{\chi}_{v,c}$ is a critical value of the mean volumetric soil moisture concentration below which $\beta < 1$, and is usually expressed as some fraction of a maximum allowable value of $\hat{\chi}_v$ ie some nominal 'field capacity' $\hat{\chi}_{v,f}$. Eqn (72) for β can of course be simply reformulated in terms of any of the other standard measures of soil moisture content (see Eqn (63)) the most common of which is probably d_ω.

A slight modification of Eqn (72), due to Warrilow et al (1986), is currently used in the Meteorological Office 11-layer AGCM, viz.

$$\beta = \begin{cases} 0 & 0 \le \hat{\chi}_v < \hat{\chi}_{v,\omega} \\ \dfrac{\hat{\chi}_v - \hat{\chi}_{v,\omega}}{\hat{\chi}_{v,c} - \hat{\chi}_{v,\omega}} & \hat{\chi}_{v,\omega} \le \hat{\chi}_v < \hat{\chi}_{v,c} \\ 1 & \hat{\chi}_v \ge \hat{\chi}_{v,c} \end{cases} \qquad (73)$$

where $\hat{\chi}_{v,\omega}$ is called the 'wilting point'.

The critical value $\hat{\chi}_{v,c}$ used in Eqn (73) is not well defined but for simplicity, and in line with previous practice (see, for example, Carson (1982)) it is given by

$$\hat{\chi}_{v,c} = \hat{\chi}_{v,\omega} + \frac{1}{3}(\hat{\chi}_{v,f} - \hat{\chi}_{v,\omega}) \qquad (74)$$

where $\hat{\chi}_{v,f}$ is a nominal 'field capacity' used only to define $\hat{\chi}_{v,c}$. The particular values of $\hat{\chi}_{v,\omega}$ and $\hat{\chi}_{v,f}$ being used globally in the Meteorological Office AGCM, which assumes for hydrological purposes only a single surface layer of soil of nominal depth $\delta_\omega = 1$ m, are listed in Table 6. With these values Eqn (73) reads

$$\beta = \begin{cases} 0 & 0 \le \hat{\chi}_v < 0.08 \\ 20\,\hat{\chi}_v - 1.6 & 0.08 \le \hat{\chi}_v < 0.13 \\ 1 & \hat{\chi}_v \ge 0.13. \end{cases} \qquad (75)$$

For a surface soil layer 1 m deep Manabe (1969), who first introduced interactive surface hydrology with Eqns (69) and (72) into an AGCM, originally selected 15 cm as his field capacity (ie for $d_{\omega,f}$ in terms of d_ω used in Eqn (63)) and took $d_{\omega,c}/d_{\omega,f}$ ($= \hat{\chi}_{v,c}/\hat{\chi}_{v,f}$) = $^3/_4$. Carson's (1982) review of AGCMs indicates field capacities, $d_{\omega,f}$, in the range 10-30 cm and $^1/_3$ - $^3/_4$ for the ratio $d_{\omega,c}/d_{\omega,f}$.

It should be borne in mind that the more complex and real practical issue to be addressed is that of determining the actual evapotranspiration from partially vegetated surfaces and not simply the evaporation from a bare-soil surface.

Depth of the surface layer of soil: δ_ω(m)	1
Characteristics of the mean volumetric soil moisture concentration: $\hat{\chi}_v$	
Wilting point: $\hat{\chi}_{v,\omega}$	0.080
'Critical' point: $\hat{\chi}_{v,c}$	0.130
Nominal field capacity: $\hat{\chi}_{v,f}$	0.230
Saturation value: $\hat{\chi}_{v,s}$	0.445
Saturated hydraulic conductivity: K_s (mmh^{-1})	13.0
Surface infiltration rate: F (SI units: kg $m^{-2}s^{-1}$)	13.0 mmh^{-1} equivalent ($= F/\rho_\omega$)
Exponent in Eqn (82): c	6.6

Table 6. Soil hydrological characteristics used in the Warrilow et al (1986) hydrological scheme in the Meteorological Office 11-layer AGCM.

6.4 Surface runoff (Y_Q)

Surface runoff is yet another of the complex surface hydrological processes which is treated very simplistically in current AGCMs and NWPMs. In models employing the single-layer water mass balance Eqn (64) the simplest approach is the so-called 'bucket model' for runoff

(usually implicitly combining both Y_o and M_1 in Eqn (64) into a single 'total runoff' term). In this case, rainfall (modified by the evaporation loss) is allowed to increase the soil moisture content until the field capacity $d_{\omega,f}$ (or $\hat{\chi}_{v,f}$) is reached. Any further attempt to increase d_ω (or $\hat{\chi}_v$) beyond the field capacity is implicitly assumed to be runoff water (including percolation to deeper layers) which plays no further part in the model's hydrological cycle. This identifies the original rôle played in these simple hydrological parametrizations by the field-capacity term, in addition to its use to define $d_{\omega,c}$ (or $\hat{\chi}_{v,c}$), as in Eqns (72)-(74). For a selection of the crude and highly empirical formulations used in specific AGCMs see, for example, Carson (1982).

A novel, but still relatively simple, parametrization has been developed by Warrilow et al (1986) for use in the Meteorological Office AGCM. It is based, with considerable simplification, on a scheme proposed by Milly and Eagleson (1982). An attempt has been made to allow for the spatial variability of rainfall since use of grid-box averages would give marked underestimation of the surface runoff. The rain is assumed to fall over a proportion μ of the grid-box where at present μ is chosen arbitrarily as 1 for the model's so-called 'large-scale dynamic rain' and as 0.3 for its 'convective rain'. These are thought to be conservatively high values. Eagleson and Qinliang (1985) have explored the likely coverage of a rainfall area for different catchment sizes and suggest that for an AGCM grid-square more appropriate values for μ are 0.6 and 0.05, respectively. The local rainfall rate, $P_{r\ell}$, throughout a grid-area is treated statistically as represented by the probability density function

$$f(P_{r\ell}) = \frac{\mu}{P_r} \exp\left(\frac{-\mu P_{r\ell}}{P_r}\right) \qquad (76)$$

where P_r is the model's grid-point rainfall rate which is taken to represent the average grid-box rainfall.

The local surface runoff, $Y_{o\ell}$, is defined by

$$Y_{o\ell} = \begin{cases} P_{r\ell} - F & P_{r\ell} > F \\ 0 & P_{r\ell} \leq F \end{cases} \qquad (77)$$

where F is a surface infiltration rate, deemed constant for a given soil, and at present given a fixed global value (equivalent to 13 mm h^{-1}). Integration of $Y_{o\ell}$ over all values of $P_{r\ell}$ yields an expression for the total surface runoff rate for a grid-area, viz,

$$Y_o = P_r \exp(-\mu F/P_r) \qquad (78)$$

6.5 The vertical mass flux of water at the base of the surface layer (M_1)

As indicated in the previous section, the simplest single-layer approaches typically assume explicitly that M_1 in Eqn (64) is negligible or implicitly that it combines with Y_o to give a 'total runoff'. In the scheme of Warrilow et al (1986), adapted from Milly

and Eagleson (1982), M_1, referred to as the gravitational drainage from the base of the surface layer, is acknowledged as a separate hydrological component of Eqn (64) that has to be parametrized.

Reference to Eqn (59) shows that

$$M_1 = -\rho_\omega \left[K(\psi)\left(\frac{\partial\psi}{\partial z_g} - 1\right)\right]_{z_g=\delta_\omega} \qquad (79)$$

Warrilow et al (1986) have argued, somewhat speculatively, that for horizontal averaging over a typical AGCM grid-area, the term $[K(\psi)\partial\psi/\partial z_g]_{zg=\delta\omega}$ is small and that M_1 in Eqn (79) can be represented simply by

$$M_1 = \rho_\omega [K(\chi_v)]_{zg=\delta\omega} \qquad (80)$$

with the further assumption that χ_v is effectively spatially homogeneous in the surface soil layer so that

$$M_1 = \rho_\omega K(\hat{\chi}_v) \qquad (81)$$

Their particular prescription of the hydraulic conductivity as a function of $\hat{\chi}_v$, attributed to Eagleson (1978), is

$$K(\hat{\chi}_v) = K_s\left(\frac{\hat{\chi}_v - \hat{\chi}_{v,\omega}}{\hat{\chi}_{v,s} - \hat{\chi}_{v,\omega}}\right)^c \qquad (82)$$

where $\hat{\chi}_{v,s}$ is termed the saturation value of $\hat{\chi}_v$, K_s the saturation conductivity (ie $K(\hat{\chi}_{v,s})$) and c is an empirically derived constant. For particular values of these quantities adopted globally by Warrilow et al (1986) see Table 6.

With the terms E, Y_o and M_1 evaluated according to a particular model's approach selected from the wide range of methods implied and discussed in Sections 6.3-6.5, and with P_r determined by some other parametrization in the model, then Eqn (64) can be solved either in simple explicit fashion or by more subtle implicit methods to determine the change in m_ω (and hence in $\hat{\chi}_v$, $\hat{\chi}$, d_ω, etc). This concludes the introduction to parametrization of land-surface hydrological processes in AGCMs and NWPMs.

7. Snow-covered Surfaces

A particular class of non-vegetated land surfaces which have their own very special characteristics and exercise significant influence on the climate system over a wide range of time-scales is that comprised of snow- (and ice-) covered surfaces. As in the case of land-surface hydrology, it is generally true that little attention has yet been given to the representation in AGCMs and NWPMs of the special physical processes associated with such surfaces. However, I am confident that this particular area of the wider problem will receive increasing attention in the near future.

According to Kuhn (1982), in the course of the year about 50% of the Earth's land surface is covered by snow or ice. He also comments that, although the polar ice sheets contain about 99% of the Earth's fresh-water ice by mass, nevertheless the seasonal snow cover with its large areal extent and its high spatial and temporal variability may have an equal or

even greater impact on the atmospheric circulation. Undoubtedly then, a key issue will be how to deal sensibly with partial and rapidly changing snow cover, particularly in complex terrain, over the area of a typical grid-box in a large-scale numerical model. The proper treatment of the processes associated with snow-covered surfaces is a major topic in its own right. The brief comments here are no more than a postscript to the main discussion of bare-soil surfaces in Sections 2.6. For fuller expositions of the varied and complex characteristics and the effects of snow and its associated physical processes see, for example, Martinelli (1979), Male (1980), Gray and Male (1981) and IGS (1985). For discussions of snow covered surfaces aimed specifically at the AGCM parametrization problem see, in particular, Kuhn (1982) and Kotliakov and Krenke (1982).

7.1 Special conditions at snow- and ice-covered surfaces

Kuhn (1982) has listed the special conditions for snow and ice layers as:

a. the surface temperature cannot exceed the melting temperature of ice;

b. evaporation and sublimation take place at the potential rate;

c. the short-wave albedo is generally high;

d. the medium is permeable to air and water and transparent to visible radiation;

e. the snow pack is a good thermal insulator;

f. the layer has a high storage capacity for heat and water;

g. the roughness of the surface is extremely low (but see comments below at Section 7.2c); and

h. generally, the atmospheric surface layer over snow or ice is stably stratified.

Note that conditions a-h impinge on every aspect of the parametrization problem already discussed in Sections 2-6. The remainder of this section retraces our previous route and indicates briefly where modifications to the parametrizations are typically introduced into AGCMs and NWPMs in recognition of snow (or ice) covering the surface. In general the thermal and hydrological properties of the snow pack are represented very simply and crudely in such models.

7.2 The physical properties of snow- and ice-covered surfaces

a. Short-wave albedo (α). It is firmly established that the physical coupling between snow and ice cover, albedo and the surface temperature is one of the most important feedback mechanisms to include in an AGCM. As indicated on the list above (7.1c), an important characteristic of snow- and ice-covered surfaces is their high reflectivity compared with other natural surfaces such that even a thin covering of fresh snow can alter significantly the albedo of a landscape. The local albedo of a

snow-covered surface is very variable and a complicated function of many factors including the age of the snow pack (α decrease markedly as the snow becomes compacted and soiled), the wavelength and angle of the incident radiation and even diurnal cycles in the state of the snow surface, particularly when conditions are right for surface melting. The albedo may lie anywhere in the range from 0.95 for freshly fallen snow to about 0.35 for old, slushy snow (see, for example, Kondratyev et al (1982)).

At present the coupling between snow and ice and the surface albedo is generally prescribed very simply. Three types of snow- or ice-covered surfaces are generally acknowledged, viz:

(1) surfaces with instantaneously variable depth of snow either predicted or implied;

(2) permanent or seasonally prescribed snow- and ice-covered land surfaces; and

(3) permanent or seasonally prescribed areas of sea-ice.

The third category is not the concern of this paper. For models that 'carry' a snow depth a common approach still used is that of Holloway and Manabe (1971) who, following Kung et al (1964), introduced the following simple dependence of albedo on snow depth into an AGCM:

$$\alpha = \begin{cases} \alpha_\ell + (\alpha_s - \alpha_\ell)\, d_{s\omega}^{1/2} & d_{s\omega} < 1 \text{ cm} \\ \alpha_s & d_{s\omega} \geq 1 \text{ cm} \end{cases} \qquad (83)$$

where α_ℓ is the snow-free land surface albedo (see Section 3.4); α_s is the albedo of a deep-snow surface (assumed in this case to be 0.60); and $d_{s\omega}$ is the water equivalent depth of snow (here expressed in cm). No allowance is usually made for the varying density of a snow pack and $d_{s\omega}$ is assumed typically to be about $^1/_{10}$ of the actual snow depth (see further comments in Section 7.3). Therefore the assumption is that when the grid-point snow depth is greater than about 10 cm, then α is independent of snow depth and equal to 0.60. Eqn (83) is designed supposedly to take account of the fact that as the mean snow depth increases, not only does the snow cover surface irregularities more completely but also the area of the grid-box which is snow-free is likely to decrease.

In some models which predict and monitor snowfall, a single albedo value is used for any non-zero depth of snow (see Carson (1982, 1986a)). The first snowfall on a previously snow-free surface results in an immediate increase in surface albedo which will tend, at least initially, to accelerate the positive feedback of a further lowering of the surface temperature with an enhanced probability of further snow accumulation.

Typical model values for land- and sea-ice are in the range 0.5-0.8 (see Carson (1982, 1986a)).

b. Long-wave emissivity (ε). Kuhn (1982) states that this can be assumed to be unity for all practical purposes.

c. Surface roughness length (z_o). The effective z_o for extensive, uniformly covered snow and ice fields and the 'local' value of z_o for snow-covered, simple heterogeneous terrain may indeed be very small ($O(10^{-3}m)$ or less). However, in general, the effective areal z_o of natural, heterogeneous and complex terrain with varied relief and vegetation is very difficult to determine (see Section 4.7) and may be affected greatly or insignificantly by different degrees of snow cover. There is little scope for useful discussion of this problem in a global, large-scale modelling context except to note that, in principle, snow and ice cover can alter z_o.

d. Thermal properties of snow. As noted above, a snow pack is generally a good thermal insulator for the soil below but to capture this effect in a climate model implies a delineation and explicit modelling of the heat conduction (and the hydrology) in and between the two media. In general the thermal and hydrological properties of snow and ice layers are treated very simply, if at all, in AGCMs and NWPMs (see below). The thermal properties of a snow pack will, like its density and albedo, depend in a complicated fashion on many factors. Values thought to be appropriate for snow are given in Table 4 for comparison with the range of soil values also included there.

7.3 Surface energy and mass flux balances at a snow-covered surface

The surface energy flux balance (Eqn (1)) is modified for complete snow cover such that

$$G_o = R_N - H - Q_s - Q_f \qquad (84)$$

where $Q_f = L_f S$ represents the latent heat flux required to affect phase changes associated with melting or freezing at the surface, where S is the rate of snowmelt (or ice melt) and L_f is the latent heat of fusion;

$Q_s = L_s E_s$ represents the latent heat flux due to surface sublimation by turbulent transfer, where E_s is the rate of sublimation and L_s is the latent heat of sublimation ($L_s = L_e + L_f$);

and G_o is now strictly the flux of heat into the snow layer at its upper surface.

A simple budget equation, corresponding to that used for soil moisture content in a single soil layer (Eqn (64)), is also used for snow on the 'surface', viz.

$$\frac{\partial m_s}{\partial t} = P_s - E_s - S \qquad (85)$$

where P_s, the only undefined term on the RHS, is the intensity of snowfall at the surface and m_s is the mass of snow lying per unit area of the surface. m_s is therefore treated like m_ω as a surface

prognostic variable and is often represented as a snow depth, d_s, or more commonly as an equivalent depth of water, $d_{s\omega}$, (cf Eqn (63)) such that

$$m_s = \rho_s d_s = \rho_\omega d_{s\omega} \qquad (86)$$

where ρ_s is the density of snow. Although it is recognised that the density of a snow pack varies, this again is a complicated issue in its own right and it is quite common practice in large-scale numerical models to assume simply that $\rho_s \simeq 0.1\ \rho_\omega$.

Eqn (85) is usually complemented by the surface-layer balance equation for the soil moisture content (Eqn (64)) modified to include the snowmelt term, ie

$$\frac{\partial m_\omega}{\partial t} = P_r - E + S - Y_o - M_1 \qquad (87)$$

Each model has its own system of checks and algorithms for deciding which of the terms in Eqns (85) and (87) are in force simultaneously. One popular approach is as follows. When snow is lying T_o is not allowed to rise above 273 K and the snow depth accumulates without limit or decreases according to the net value of $(P_s - E_s)$. If, however, snow is lying and the solution of the heat balance Eqn (84), excluding the terms Q_f, produces an interim surface temperature value $T_o' > 273$ K then sufficient snow (if available) is allowed to melt to maintain $T_o = 273$ K. The heat required to melt the snow and reduce T_o to 273 K can be evaluated by specifying an effective surface thermal capacity of the snow pack (cf Eqn (43)) such that

$$Q_f = L_f S = C_{eff,s} \left(\frac{T_o' - 273}{\Delta t}\right) \qquad (88)$$

where Δt is the appropriate model time step. The change in the water equivalent snow depth, $\Delta d_{s\omega}$, resulting from the melting is determined from Eqn (85) and (88) such that

$$\Delta m_s = \rho_\omega \Delta d_{s\omega} = -S\ \Delta t$$

$$= -\frac{C_{eff,s}}{L_f}(T_o' - 273) \qquad (89)$$

It is usually assumed that the snow pack has no moisture holding capacity; all melted snow is added directly to the soil moisture content (through Eqn (87)) following the corresponding reduction ($\Delta d_{s\omega}$) in the snow depth. In all cases it is only when the snow disappears through melting or sublimation that evaporation of moisture is allowed to resume at the surface.

8. Concluding Remarks

It should be evident from Sections 2-7 that, in many respects, the representations of land-surface processes in AGCMs and NWPMs are still rather crude and simple. The demands for improvements will come from both climate modelling studies and numerical weather forecasting. Indeed, the steadily increasing number of studies with AGCM's has already amply demonstrated the sensitivity of such models to surface properties and

processes (see, for example, recent reviews by Mintz (1984), Rowntree (1983, 1984) and Rowntree et al (1985)). Parametrizations thought adequate at present will undoubtedly be seen to be deficient in models which couple interactively further components of the climate system. This is already apparent with respect to air-sea interactions in coupled ocean-atmosphere models. Although the major developments in the longer term are more likely to comé from climate modelling studies, nevertheless valuable feedback is being obtained from the continuous close scrutiny of the various models' performances in the acutely critical arena of operational weather forecasting - especially of local, near-surface variables such as wind and temperatures.

A schematic resumé of the processes, variables and parameters introduced in this discussion of the specification of parametrizations for simple, non-vegetated land surfaces is given in Figure 9.

	Radiative	Thermal	Hydrological	Dynamical
'External forcing'	$R_{S\downarrow}$, $R_{L\downarrow}$		P_r, P_s	
Atmospheric variables		← $\theta(T)$,	q,	$\underset{\sim}{V}$ →
Surface variables	← T_o →		q_o, d_s	
Surface parameters	α, ε	← β		z_o →
Surface fluxes	R_N	H $Q = L_e E$ $Q_f = L_f S$ $Q_s = L_s E_s$ G_o	E, E_s S M_o, Y_o	$\underset{\sim}{\tau}$
Sub-surface fluxes		G	M	
Sub-surface parameters		λ, C	δ K Significant values of χ_v	
Sub-surface variables		T_g	χ_v	

Figure 9. Schematic resumé of the processes, variables and parameters involved in the specification of parametrizations at simple, non-vegetated land surfaces.

REFERENCES

André, J-C and Blondin, C 1986 'On the effective roughness length for use in numerical three-dimensional models', Boundary-Layer Meteorol., 35, 231-245.

André, J-C, Goutorbe, J-P Perrier, A 1986 'HAPEX-MOBILHY: A hydrologic and atmospheric experiment for the study of water budget and evaporation flux at the climatic scale', Bull. Amer. Met. Soc., 67, 138-144.

Beuttner, K J K and Kern, C D 1965 'The determination of infrared emissivities of terrestrial surfaces', J. Geophys. Res., 70, 1329-1337.

Bhumralkar, C M 1975 'Numerical experiments on the computation of ground surface temperature in an atmospheric general circulation model', J. Appl. Met., 14, 1246-1258.

Blondin, C A 1986 'Treatment of land-surface properties in the ECMWF model'. Proceedings of the ISLSCP Conference on Parametrization of Land-surface Characteristics, Use of Satellite Data in Climate Studies, and First Results of ISLSCP, Rome 2-6 Dec 1985, 53-60, ESA SP-248.

Brutsaert, W H 1982a 'Vertical flux of moisture and heat at a bare soil surface', Land Surface Processes in Atmospheric General Circulation Models, Ed. P S Eagleson, 115-168, CUP, Cambridge.

Brutsaert, W H 1982b 'Evaporation into the atmosphere. Theory, history and applications'. D Reidel Publ. Co., Dordrecht.

Carson, D J 1982 'Current parametrizations of land-surface processes in atmospheric general circulation models', Land Surface Processes in Atmospheric Circulation Models, Ed P S Eagleson, 67-108, CUP, Cambridge

Carson, D J 1986a 'Parametrizations of land-surface processes in Meteorological Office numerical weather prediction and climate models', Unpublished Met Office Report, DCTN 37, Met O 20.

Carson, D J 1986b 'Issues concerning the evaluation of effective surface roughness of heterogeneous terrain' Proceedings of the ISLSCP Conference on Parametrization of Land-Surface Characteristics, Use of Satellite Data in Climate Studies, and First Results of ISLSCP, Rome, 2-6 Dec 1985, 77-82, ESA SP-248.

Carson, D J and Richards, P J R 1978 'Modelling surface turbulent fluxes in stable conditions', Boundary-layer Meteorol., 14, 67-81.

Carson, D J and Roberts, S M 1977 'Concerning the evaluation of the turbulent fluxes at unsaturated surfaces'. Unpublished Met Office Report, Met O 20 Tech. Note No. II/103.

Deardorff, J W 1978 'Efficient prediction of ground surface temperature and moisture, with inclusion of a layer of vegetation', J. Geophys. Res., 83, 1889-1903.

Dickinson, R E 1984 'Modelling evapotranspiration for three-dimensional global climate models', Climate Processes and Climate Sensitivity, Geophys. Monograph 29, Maurice Ewing Vol. 5; 58-72, AGU.

Dooge, J C I 1982 'Parametrization of hydrologic processes', Land Surface Processes in Atmospheric Circulation Models, Ed. P S Eagleson, 243-288, CUP, Cambridge.

Dyer, A J and Hicks, B B 1970 'Flux-gradient relationships in the constant flux layer', Quart. J. R. Met. Soc., 96, 715-721.

Eagleson, P S 1978 'Climate, soil and vegetation', Water Resources Research, 14, 705-776.

Eagleson, P S 1982 'Dynamic hydro-thermal balances at mesoscale', Land Surface Processes in Atmospheric Circulation Models, Ed. P S Eagleson, 289-357, CUP, Cambridge.

Eagleson, P S and Qinliang, W 1985 'Moments of catchment storm area', Water Resources Research, 21, 1185-1194.

Geiger, R 1965 'The climate near the ground', Harvard Univ. Press, Cambridge, Mass.

Gray, D M and Male, D H	1981	'Handbook of snow. Principles, processes, management and use', Eds. D M Gray and D H Male, Pergamon Press, Toronto.
Holloway, J L, Jr and Manabe, S	1971	'Simulation of climate by a global general circulation model. I Hydrological cycle and heat balance', Mon. Weath. Rev., 99, 335-370.
IGS	1985	Proc. Symp. Snow and Ice Processes at the Earth's Surface, Sapporo, Japan, 2-7 Sept. 1984, Annals of Glaciology, Vol. 6, Published by IGS, Cambridge.
Kondratyev, K Ya	1972	'Radiation processes in the atmosphere', Second IMO Lecture, WMO - No. 309, WMO, Geneva.
Kondratyev, K Ya, Korzov, V I Mukhenberg, V V and Dyachenko, L N	1982	'The shortwave albedo and the surface emissivity', Land Surface Processes in Atmospheric Circulation Models, Ed. P S Eagleson, 463-514, CUP, Cambridge.
Kotliakov, V M and Krenke, A N	1982	'Data on snow cover and glaciers for for the global climatic models', Ibid., 449-461.
Kuhn, M	1982	'Vertical flux of heat and moisture in snow and ice', Ibid., 227-240.
Kung, E C, Bryson, R A and Lenschow, D H	1964	'Study of a continental surface albedo on the basis of flight measurements and structure of the Earth's surface cover over North America', Mon. Weath. Rev., 92, 543-564.
Male, D H	1980	'The seasonal snow cover', Chap 6 Dynamics of Snow and Ice Masses, Ed. S C Colbeck, Academic Press, New York.
Manabe, S	1969	'Climate and the ocean circulation. I The atmospheric circulation and the hydrology of the Earth's surface', Mon. Weath. Rev., 97, 739-774.
Martinelli, M, Jr	1979	'Snow', Research on Snow and Ice, Martinelli et al, Rev. Geophys. and Space Phys., 17, 1253-1256. (Refs 1266-1271).
Mason, P J	1985	'On the parametrization of orographic drag', To appear in Proc. Seminar on Physical Parametrization for Numerical Models, Reading, 9-13 September 1985, ECMWF.

McBean, G A, Bernhardt, K, Bodin, S, Litynska, Z, Van Ulden, A P and Wyngaard, J C 1979 The Planetary Boundary Layer, Ed. G A McBean, Chairman CAS Working Group on Atmospheric Boundary-Layer Problems, WMO-No. 530, Tech. Note No. 165, WMO, Geneva.

Milly, P C D and Eagleson, P S 1982 'Parametrization of moisture and heat fluxes across the land surface for use in atmospheric general circulation models', MIT Report No. 279, Cambridge, Mass.

Mintz, Y 1984 'The sensitivity of numerically simulated climates to land-surface boundary conditions', The Global Climate, Editor J T Houghton, 79-105, CUP, Cambridge.

Monteith, J L 1965 'Evaporation and environment', Symp. Soc. Exptl. Biol., 19, Swansea, 8-12 September 1964, 205-234.

Nappo, C J, Jr 1975 'Parametrization of surface moisture and evaporation rate in a planetary boundary layer model', J. Appl. Met., 14, 289-296.

Oke, T R 1978 'Boundary Layer Climates', Methuen, London.

Paltridge, G W and Platt, C M R 1976 'Radiative Processes in Meteorology and Climatology', Developments in Atmospheric Science, 5, Elsevier Sci. Pub. Co., Amsterdam.

Panofsky, H A and Dutton, J A 1984 'Atmospheric Turbulence. Models and methods for engineering applications;, John Wiley and Sons, New York.

Perrier, A 1982 'Land surface processes: vegetation', Land Surface Processes in Atmospheric Circulation Models, Ed. P S Eagleson, 395-448, CUP, Cambridge.

Rosenberg, N J, Blad, B L, and Verma, S B 1983 'Microclimate. The Biological Environment', Second Edition, John Wiley and Sons, New York.

Rowntree, P R 1983 'Land surface processes in climate models - parametrization and model sensitivity', Report of the Fourth Session of the JSC, Venice, 1-8 March 1983, Appendix B, 57-75, WCRP, ICSU/WMO.

Rowntree, P R 1984 'Review of general circulation models as a basis for predicting the effects of vegetation change on climate', To appear in Proc. United Nations Univ. Workshop on Forests, Climate and Hydrology - Regional Impacts, Oxford, 26-30 March 1984. Available as Unpublished Met Office Report, Met O 20 Tech. Note No. II/225.

Rowntree, P R, Wilson, M R and Sangster, A B 1985 'Impact of land surface variations on African rainfall in general circulation models', Unpublished Met Office Report, DCTN 30, Met O 20.

Sellers, P J, Mintz, Y, Sud, Y C and Dalcher, A 1986 'A simple biosphere model (SiB) for use within general circulation models', J. Atmos. Sci., 43, 505-531.

Sellers, W D 1965 'Physical Climatology', The Univ. of Chicago Press, Chicago and London.

Smagorinsky, J 1982 'Large-scale climate modelling and small-scale physical processes', Land Surface Processes in Atmospheric Circulation Models, Ed. P S Eagleson, 3-17, CUP, Cambridge.

Smith, F B and Carson, D J 1977 'Some thoughts on the specification of the boundary layer relevant to numerical modelling', Boundary-layer Meteorol., 12, 307-330.

Warrilow, D A, Sangster, A B and Slingo, A 1986 'Modelling of land surface processes and their influence on European climate', Unpublished Met Office Report, DCTN 38, Met O 20.

WCP 1985 Report of the First Session of the JSC Scientific Steering Group on Land Surface Processes and Climate, Geneva, 21-25 Jan 1985, WCP-96, WMO/TD-No 43, WCRP, ICSU/WMO.

Webb, E K 1970 'Profile relationships: the log-linear range and extension to strong stability', Quart. J. R. Met. Soc., 96, 67-90.

Wieringa, J 1986 'Roughness-dependent geographical interpolation of surface wind speed averages', To appear in Quart. J. R. Met. Soc.

Wilson, M F and Henderson-Sellers, A 1985 'A global archive of land cover and soils data for use in general circulation climate models', J Climatol., 5, 119-143.

.nj

Advanced Lecture 5

The Parametrization of the Turbulent Boundary Layer-II: the bulk parametrization approach

5.1 Introduction

In this lecture we shall consider the technique of bulk parametrization of the boundary layer and, in this and the next lecture, some applications in terms of specific models of the atmosphere and ocean.

5.2 Bulk parametrizations of the boundary layer

In this approach, it is assumed that the vertical profiles of mean variables through the boundary layer are similar to one another in character so that meaningful vertical averages through the layer can be formed. Best known are the mixed layer models in which the basic assumption is that conservative variables are independent of height through the whole layer. Thus for the dry, convective boundary layer in the atmosphere, for example, it is assumed that, above the shallow surface layer, the potential temperature and humidity mixing ratio are constant with height to the capping inversion, through which a sharp fall in humidity occurs (Figure 4.1a) and across which there is a marked wind shear. In the upper ocean, too, the surface layers are frequently well mixed down to a depth of several tens of metres or more, yielding temperature (essentially the same as potential temperature to these depths) and salinity profiles which are constant with depth to a marked density discontinuity brought about by a sharp temperature and/or salinity gradient (Figure 5.1). As for the atmosphere, a marked shear in the current is frequently found at the base of the oceanic mixed layer. For the development of bulk parametrizations, such profiles are often idealised to those of Figure 5.2. We illustrate the approach to the derivation of the mixed layer equations by reference to the heat conservation equation written in the form:

$$\frac{D\bar{\theta}}{Dt} + w\frac{\partial\bar{\theta}}{\partial z} = -\frac{\partial}{\partial z}(\overline{w'\theta'}) \qquad (5.1)$$

where here and subsequently $D/Dt = \partial/\partial t + \bar{\mathbf{V}}.\nabla$ and $\bar{\mathbf{V}} = \bar{u}\mathbf{i} + \bar{v}\mathbf{j}$. For simplicity, we shall drop the "bars" in what follows below and take $\mathbf{V}$ and θ to be appropriately meaned values. Note that we are considering turbulent heat transport only. Other diabatic terms, such as radiative heating will be included later. In order to produce an equation for mixed layer potential temperature, θ, we shall integrate (5.1) in the vertical from the surface throughout the whole thickness of the layer. To see how the terms in the integrated equation come about, we shall consider the atmospheric case and take the profile to have the shape shown in Figure 5.3. The discontinuity at $z = h$ is recovered by taking the limit as δ tends towards zero. It will be assumed that turbulent transports at $z = h - \delta/2$ are non-zero but are zero at $z = h + \delta/2$. The region of thickness is therefore referred to as the transition layer. Integration of (5.1) over the depth $h - \delta/2$ gives:

$$(h - \tfrac{\delta}{2})\frac{D\theta_m}{Dt} = [\overline{w'\theta'}]_0 - [\overline{w'\theta'}]_{h-\delta/2} \qquad (5.2)$$

Note that the vertical advection term does not contribute since θ is

constant throughout the range of integration. We can set

$$\left[\overline{w'\theta'}\right]_0 = \frac{H}{\rho c_p} \qquad (5.3)$$

where H is the surface sensible heat flux and c_p specific heat. Thus (5.2) becomes:

$$(h-\tfrac{\delta}{2})\frac{D\theta_m}{Dt} = \frac{H}{\rho c_p} - \left[\overline{w'\theta'}\right]_{h-\delta/2} \qquad (5.4)$$

If we now integrate (5.1) across the transition layer we find:

$$\int_{h-\delta/2}^{h+\delta/2} \frac{D\theta}{Dt}\,dz + \int_{h-\delta/2}^{h+\delta/2} w\frac{\partial\theta}{\partial z}\,dz = -\left[\overline{w'\theta'}\right]_{h-\delta/2} \qquad (5.5)$$

Note that the $\overline{w'\theta'}$ term does not contribute at the upper limit $h + \delta/2$ since it is assumed to be zero there.

We now make the assumption that, in the transition layer, the potential temperature profile is a linear function of z, given by (c.f. Figure 5.3):

$$\theta(z,t) = \theta_m(t) + \frac{\Delta\theta(t)}{\delta}\left(z - (h(t) - \delta/2)\right) \qquad (5.6)$$

Substitution of (5.6) into the lhs of (5.5) enables these integrals to be evaluated. The result is that:

$$-\left[\overline{w'\theta'}\right]_{h-\delta/2} = \left(\frac{Dh}{Dt} - w_{-h}\right)\Delta\theta + \delta\left(\frac{D\theta_m}{Dt} - \frac{1}{2}\frac{D(\Delta\theta)}{Dt}\right) \qquad (5.7)$$

Taking the limit as $\delta \to 0$ then yields an expression for the turbulent heat flux at the top of the mixed layer i.e.

$$\left[\overline{w'\theta'}\right]_h = \left(w_h - \frac{Dh}{Dt}\right)\Delta\theta \qquad (5.8)$$

where $\Delta\theta$ is the difference in θ between the mixed layer and the "free atmosphere" above. The quantity $(w_h - Dh/Dt)$ is known as the entrainment velocity, w_e . It represents the rate at which free atmospheric air is entrained into the boundary layer by turbulent motions at its top. Substitution of (5.7) into (5.4) and again taking the limit as $\delta \to 0$ yields:

$$h\frac{D\theta_m}{Dt} = \frac{H}{\rho c_p} - w_e\Delta\theta \qquad (5.9)$$

where:

$$w_e = w_h - \frac{Dh}{Dt} \qquad (5.10)$$

An expression similar to (5.9) in which q replaces θ and E, the surface evaporation, replaces H can be obtained for the equation for humidity mixing ratio, whilst the momentum equation:

$$\frac{D\underset{\sim}{V}}{Dt} + w\frac{\partial \underset{\sim}{V}}{\partial z} + fk\times\underset{\sim}{V} + \frac{1}{\rho}\nabla p = -\frac{\partial}{\partial z}(\overline{\underset{\sim}{V}'w}) \qquad (5.11)$$

yields:

$$h\frac{D\underset{\sim}{V}_M}{Dt} + hfk\times\underset{\sim}{V} + \frac{1}{\rho}\nabla p_M = \frac{\underset{\sim}{\tau}_0}{\rho} - w_e\Delta\underset{\sim}{V} \qquad (5.12)$$

where $\underset{\sim}{\tau}_0 = \rho u_*^2$ is the surface stress (u_* is the friction velocity) and $\Delta\underset{\sim}{V}$ is the shear across the top of the layer. Note that the variation of density with height has been ignored in the derivation of (5.9) and (5.12).

Considering the horizontal advection of h to be negligible for the present, (5.10) can be rewritten in terms of the local rate of change of boundary layer depth with time as:

$$\frac{\partial h}{\partial t} = w_h - w_e \qquad (5.13)$$

Note that w_e negative implies a downwards incorporation of air into the boundary layer which goes towards deepening it. In this case, in regions of large scale ascent, the boundary layer tends to deepen rapidly since both w_h and $-w_e$ are positive. In regions of large scale descent (w negative) the boundary layer may deepen or thin depending on the sign of $w_h - w_e$. If entrainment of air into the boundary layer exactly balances the tendency for subsidence to advect the inversion layer downwards then $\partial h/\partial t = 0$ and the boundary layer depth does not change. Referring back to equation (5.9), note that the last term on the rhs ($w_e\Delta\theta$) represents a downward heat flux across the inversion, whilst, with the shear across the inversion layer positive, the $w_e\Delta\underset{\sim}{V}$ term in (5.12) represents a downward flux of momentum across the layer which goes to offset the effects of the stress at the surface. Figure (5.4) shows an example of the upward sensible and latent heat fluxes through the convectively unstable boundary layer derived, in this instance, from the change in the temperature and moisture profiles over several hours. Here the boundary layer is being heated by both the upward flux at the ground and a downward heat flux at the inversion due to entrainment of warmer air from aloft whilst the magnitude of the entrainment is such as to allow the boundary layer depth to continue to grow against large scale subsidence from aloft. In this case entrainment brings just enough dry air into the boundary layer from above to balance the latent heat flux at the surface so that the mean value of the mixing ratio in the layer remains constant. The effects of horizontal advection in this instance were negligible.

By integrating the continuity equation:

$$\frac{\partial u}{\partial x} + \frac{\partial v}{\partial y} + \frac{\partial w}{\partial z} = 0 \qquad (5.14)$$

over the depth h of the mixed layer, it is easy to see that:

$$w_h = h(\nabla . V_m) \qquad (5.15)$$

In order now to close the system of equations (5.9), (5.10), (5.12) and (5.15) (together with the equation for the moisture variable, if included) it is necessary to provide an equation for the entrainment velocity, w_e. This is usually done via the turbulent kinetic energy equation:

$$\left(\frac{D}{Dt} + w\frac{\partial}{\partial z}\right)\left[\tfrac{1}{2}\rho\left(\overline{\underset{\sim}{V}'^2 + w'^2}\right)\right] = \frac{g}{\theta}\overline{w'\theta'} - \rho\,\overline{\underset{\sim}{V}'w'}\cdot\frac{\partial \underset{\sim}{V}}{\partial z} - \frac{\partial}{\partial z}\left[\overline{w'\left(\tfrac{1}{2}\rho\left(\underset{\sim}{V}'^2 + w'^2\right) + p'\right)}\right] - \varepsilon \qquad (5.16)$$

As noted in the previous lecture, this relates the total rate of change of the TKE to a buoyancy term, a shear production term, a flux convergence term and the dissipation. In order to derive a version of this equation which includes the entrainment velocity, w_e, we integrate it in the vertical from the surface to just above the top of the mixed layer Hence, writing e for the TKE, we have:

$$\int_0^{h+\delta_2} \frac{De}{Dt}\,dz + \int_0^{h+\delta_2} w\frac{\partial e}{\partial z}\,dz = \int_0^{h+\delta_2} \frac{g}{\theta}\overline{w'\theta'}\,dz - \int_0^{h+\delta_2} \rho\,\overline{\underset{\sim}{V}'w'}\cdot\frac{\partial \underset{\sim}{V}}{\partial z} - \int_0^{h+\delta_2} \frac{\partial}{\partial z}\left[\overline{w'\left(\tfrac{1}{2}\rho\left(\underset{\sim}{V}'^2 + w'^2\right) + p'\right)}\right]dz - \int_0^{h+\delta_2} \varepsilon\,dz \qquad (5.17)$$

In order to see how the integrated TKE equation is formulated, we shall briefly consider each of the above integrals in turn:

(i) The total rate of change of TKE:

$$\int_0^{h+\delta_2} \frac{De}{Dt}\,dz + \int_0^{h+\delta_2} w\frac{\partial e}{\partial z}\,dz \qquad (5.18)$$

Assuming a linear decrease of TKE with height at the top of the mixed la yer from its constant value, e_m, within the layer to a value e_A above, evaluation of the integrals yields, in the same way as the treatment of the corresponding term in (5.1):

$$\int_0^{h+\delta_2} \left(\frac{De}{Dt} + w\frac{\partial e}{\partial z}\right)dz = h\frac{De_m}{Dt} - w_e(e_A - e_m) \qquad (5.19)$$

Lt $\delta \to 0$

(ii) Buoyancy term:

$$\int_0^{h+\delta_2} \frac{g}{\theta}\overline{w'\theta'}\,dz \simeq \frac{g}{\theta_m}\int_0^{h+\delta_2} \overline{w'\theta'}\,dz. \qquad (5.20)$$

By multiplying the heat transfer equation (5.1) by z, integrating by parts and introducing the integrated heat transfer equation (5.9) one obtains, as $\delta \to 0$:

$$\frac{g}{\theta_m}\int_0^{h+\delta_2} \overline{w'\theta'}\,dz = \frac{h}{2}\frac{g}{\theta_m}\left(\frac{H}{\rho c_p} + w_e\Delta\theta\right) \qquad (5.21)$$

(iii) Shear production term:

$$\int_0^{h+\delta_2} \rho \overline{\underset{\sim}{V}'w'} \cdot \frac{\partial \underset{\sim}{V}}{\partial z}\, dz \qquad (5.22)$$

Integration of the shear production term brings in contributions from the two high shear layers found near the ground and at the top of the mixed layer. It is convenient, therefore to split the integral into three parts:

$$\int_0^{h+\delta_2} \rho \overline{\underset{\sim}{V}'w'} \cdot \frac{\partial \underset{\sim}{V}}{\partial z}\, dz = \int_0^{\delta_0} \rho \overline{\underset{\sim}{V}'w'} \cdot \frac{\partial \underset{\sim}{V}}{\partial z}\, dz + \int_{\delta_0}^{h-\delta_2} \rho \overline{\underset{\sim}{V}'w'} \cdot \frac{\partial \underset{\sim}{V}}{\partial z}\, dz + \int_{h-\delta_2}^{h+\delta_2} \rho \overline{\underset{\sim}{V}'w'} \cdot \frac{\partial \underset{\sim}{V}}{\partial z}\, dz \qquad (5.23$$

where δ_0 is the thickness of the surface layer. Since $\partial V/\partial z$ is assumed zero in the mixed layer, the second term does not contribute. The first term involves the stress and shear at the surface and scales as u_*^3. It is conventional to write it as:

$$\int_0^{\delta_0} \rho \overline{\underset{\sim}{V}'w'} \cdot \frac{\partial \underset{\sim}{V}}{\partial z}\, dz = -\lambda \rho u_*^3 \qquad (5.24)$$

where λ is an empirical constant. The quantity $\lambda \rho u_*^3$ is often referred to as the power of the wind or the "windmixing energy". At the boundary layer top, evaluation of the third integral of (5.23) gives, as $\delta \rightarrow 0$:

$$\int_{h-\delta_2}^{h+\delta_2} \rho \overline{\underset{\sim}{V}'w'} \cdot \frac{\partial \underset{\sim}{V}}{\partial z}\, dz = \tfrac{1}{2} \rho w_e |\Delta \underset{\sim}{V}|^2 \qquad (5.25)$$

Hence:

$$-\int_0^{h+\delta_2} \overline{\underset{\sim}{V}'w'} \cdot \frac{\partial \underset{\sim}{V}}{\partial z}\, dz = \lambda \rho u_*^3 - \tfrac{1}{2} \rho w_e |\Delta \underset{\sim}{V}|^2$$

(iv) Flux divergence term:

$$\int_0^{h+\delta_2} \frac{\partial}{\partial z} \left[\overline{w' \left(\tfrac{1}{2} \rho \left(\underset{\sim}{V}'^2 + w'^2 \right) + p' \right)} \right] dz \qquad (5.26)$$

Assuming the flux of turbulent kinetic energy and work done by pressure fluctuations to fall to zero above the mixed layer, we obtain:

$$-\int_0^{h+\delta_2} \frac{\partial}{\partial z} \left[\overline{w' \left(\tfrac{1}{2} \rho \left(\underset{\sim}{V}'^2 + w'^2 \right) + p' \right)} \right] dz = \left[\overline{w' \left(\tfrac{1}{2} \rho \underset{\sim}{V}'^2 + w'^2 \right) + p'} \right]_0 \qquad (5.27$$

(v) Dissipation term:

$$\int_0^{h+\delta_h} \varepsilon \, dz \qquad (5.28)$$

The initial scale of the turbulence depends upon the generating mechanism but, whatever this initial scale, turbulent fluctuations will decrease in size until viscous dissipation becomes an important mechanism. The dissipation terms in the TKE equation represent this loss of turbulent energy to heat. The parametrization of this term is clearly important, as the picture of turbulent motions, generated at some initial scale and cascading to smaller scales where they are dissipated, is central to the understanding of any turbulent process. In mixed layer models, various bulk parametrizations have been used. These tend to be very simple. Particular representations will be discussed subsequently.

Combining the above results therefore gives:

$$h\frac{De_M}{Dt} + w_e \Delta e = \tfrac{1}{2} h \frac{g}{\theta_M}\left(\frac{H}{\rho c_p} + w_e \Delta\theta\right) + \lambda \rho u_*^3 - \tfrac{1}{2}\rho w_e |\Delta \underset{\sim}{V}|^2 + \left[\overline{w'\left(\tfrac{1}{2}\rho(\underset{\sim}{V}'^2 + w'^2) + p'\right)}\right]_0 - D \qquad (5.29)$$

where D represents the vertical integral of the dissipation. Thus, in a well stirred boundary layer, there are three distinct mechanisms that produce turbulence and possibly entrainment:

(a) the surface heat flux,

(b) friction at the surface, associated with the friction velocity, u_*

(c) shear generation of turbulence by wind shear at the top, associated with the velocity jump $\Delta \underset{\sim}{V}$ over the entrainment zone.

Opposed to these turbulence-producing mechanisms are the dissipation and the entrainment of relatively warm air through the boundary layer top, which has to be brought down at the expense of turbulent kinetic energy. Closure schemes attempt to simplify the treatment of the TKE equation further by means of appropriate parametrizations of the rate of change, surface turbulent flux and dissipation of TKE terms, as well as, where appropriate, neglecting suitable terms in (5.29) itself. We shall illustrate the approach in an application of a bulk turbulence parametrization to an atmospheric model described below. One common simplification is to ignore the D /Dt term in (5.29) so that, gathering together all of the bulk parametrization equations derived so far, we have:

$$h\frac{D\theta_M}{Dt} = \frac{H}{\rho c_p} - w_e \Delta\theta \qquad (5.9)$$

$$h\frac{D\underset{\sim}{V}_M}{Dt} + hf\underset{\sim}{k}\times\underset{\sim}{V}_M + \frac{h}{\rho}\nabla p_M = \frac{\underset{\sim}{\tau}_0}{\rho} - w_e \Delta \underset{\sim}{V} \qquad (5.12)$$

$$w_h = h(\nabla \cdot \underset{\sim}{V}_M) \qquad (5.15)$$

$$\frac{Dh}{Dt} = w_h - w_e \qquad (5.10)$$

$$w_e \Delta e = \frac{1}{2} h \frac{g}{\theta_m} \left(\frac{H}{\rho c_p} + w_e \Delta\theta \right) + \lambda \rho u_*^3 - \frac{1}{2} \rho w_e |\Delta \underset{\sim}{V}|^2 + \left[\overline{w' \left(\tfrac{1}{2} \rho (\underset{\sim}{V}'^2 + w'^2) + p' \right)} \right]_0 - D \qquad (5.30)$$

where

$$\Delta e = e_A - e_m$$

$$\Delta\theta = \theta_A - \theta_M \qquad (5.31)$$

$$\Delta \underset{\sim}{V} = \underset{\sim}{V}_A - \underset{\sim}{V}_M$$

and $\tau_0 = \rho u_*^2$. Parameters with subscript A represent values in the free air above the mixed layer. Additional equations, representing conservation of moisture, for example, may also need to be specified.

5.3 Application of the bulk parametrization approach to representation of the boundary layer in an atmospheric GCM.

The bulk approach to parametrization of the atmospheric boundary layer in an atmospheric GCM has been followed, in particular, by Suarez, Arakawa and Randall (1983) who applied it to the UCLA model. Suarez et al. used the approach for both the cloud topped and cloud free boundary layers. We shall consider only the cloud free case here, deferring discussion of the cloud topped case until lecture 7. As noted in lecture 4, a particular problem with the bulk approach is the difficulty of coupling such parametrizations into the large scale models, since the predicted boundary layer height will not, in general, correspond to the model layer boundaries. Suarez et al. solved this problem by making the variable boundary layer depth an integral part of the model's structure. This was done by introducing a sigma-coordinate system in which both the boundary layer top and the earth's surface were chosen as coordinate surfaces. The arrangement is shown in Figure 5.5. This leads to algebraic complications in the formulation of the equations which we shall not consider here. However, the basic equations used for the parametrization were essentially as summarised above ((5.9, (5.10), (5.12), (5.15), (5.29) and (5.30)) , with the addition of a moisture equation and a term for the net radiative heat flux divergence across the layer to the heat conservation equation (5.9). In order to close the system of equations, the TKE equation in the form (5.30) was first simplified, however, by assuming, as above, (5.31), that the D /Dt term is negligible, that the flux of TKE by the turbulence itself at the surface is also negligible and that $e_A = 0$. Additionally, they took the surface shear production term as $\rho u_*^2 |\underset{\sim}{V}_m|$. With these assumptions, the TKE equation (5.30) then becomes:

$$w_e e_m = \frac{1}{2} h \frac{g}{\theta_m} \left(\frac{H}{\rho c_p} + w_e \Delta\theta \right) + \rho u_*^2 |\underset{\sim}{V}_m| - \frac{1}{2} \rho w_e |\Delta \underset{\sim}{V}|^2 - D \qquad (5.32)$$

The vertically integrated dissipation rate, D, was then assumed to be given by a term of the form:

$$D = \rho\sigma^3 \qquad (5.33)$$

where σ is a so-called dissipation velocity scale, and e_M by

$$e_M = a_1\sigma^2 \qquad (5.34)$$

where a_1 is a constant. Thus the dissipation velocity scale is taken proportional to the rms turbulence velocity. Hence the TKE equation becomes:

$$-a_1 w_e \sigma^2 = \tfrac{1}{2} h \frac{g}{\theta_m}\left(\frac{H}{\rho c_p} + w_e \Delta\theta\right) + \rho u_*^3 |\underset{\sim}{V}_m| - \tfrac{1}{2}\rho w_e |\Delta\underset{\sim}{V}|^2 - \rho\sigma^3 \qquad (5.35)$$

This says, in effect, that any net production from the source/sink terms is used to make laminar air turbulent, or, in the case of net dissipation, to make turbulent air laminar. The problem then is to relate σ to other known quantities. This was done by dividing the shear production and buoyancy terms into positive and negative contributions, whose totals are denoted by P and -N, and assuming that the dissipation is proportional only to P. i.e.

$$D = a_2 P \qquad (5.36)$$

P represents the sum of the vertical integral of the buoyancy terms in the basic TKE equation (5.16) over those regions where the buoyancy is upward and the vertical integral of the shear production terms. The former is given by area B_+ in Figure 5.6, from which, by simple geometry, it can be deduced that:

$$B_+ = \frac{\left(\frac{H}{\rho c_p} + w_e \Delta\theta\right)}{\left(1 + \left(\frac{w_e \Delta\theta}{H/\rho c_p}\right)^2\right)} \qquad (5.37)$$

Hence, in essence, Suarez et al. take:

$$D = \rho\sigma^3 = a_2 P = \left(\rho u_*^3 |\underset{\sim}{V}_m| - \tfrac{1}{2}\rho w_e |\Delta\underset{\sim}{V}|^2 + \frac{\tfrac{1}{2} h \frac{g}{\theta_m}\left(\frac{H}{\rho c_p} + w_e \Delta\theta\right)}{\left(1 + \left(\frac{w_e \Delta\theta}{H/\rho c_p}\right)^2\right)}\right) \qquad (5.38)$$

Guided by Deardorf's (1974) numerical results, the constants a_1 (in equation (5.34) and a_2 were chosen to be $a_1 = 0.163$ and $a_2 = 0.96$. With the dissipation velocity scale, σ, determined by (5.38), equation (5.35) can be solved for w_e, i.e. the system of mixed layer equations can be closed. Note that Suarez et al. define the entrainment rate to be $E = -w_e$.

Suarez et al. point out a number of different possible situations. Thus, given the definition of P, the positive part of the total "production" terms and -N, the negative part, note that the TKE equation (5.35) can be written as:

$$-a_1 w_e \sigma^2 = P(w_e) - N(w_e) - a_2 P(w_e). \qquad (5.39)$$

Hence:

$$-a_1 w_e \sigma^2 + N = (1 - a_2)P$$

i.e. $(1 - a_2)P$, the excess of the positive part of the"production" terms over the dissipation, is partitioned between $a_1 w_e \sigma^2$ and the negative production, N. The nature of the partitioning depends on the forcing of the boundary layer, by surface heating or cooling, and on the structure of the free atmosphere into which the boundary layer grows. For a cloud free mixed layer growing into a stably stratified free atmosphere, the entrainment rate is limited by the stratification and so $a_1 w_e \sigma^2$ is neligible compared to N, the negative production associated with the entrainment of warm air. On the other hand, if the free atmosphere is neutrally stratified, as would be the case if the boundary layer is rising through a mixed layer left behind from the previous afternoon, then N = 0 and $a_1 w_e \sigma^2$ is dominant in (5.40). Finally if N is large, say as a result of surface cooling, then (5.40) demands that w_e becomes positive. This Suarez et al. interpret as the boundary layer "shallowing" as air loses its turbulent character. In this case, they take $|\Delta \underset{\sim}{V}|$ to be zero to ensure that the sum of the shear production terms is non-negative. In fact the treatment of the shallowing case, as for the stable boundary layer per se, is by no means straight forward (see, e.g. Driedonks (1986)) and in this case the TKE equation is often considerably further simplified by simply setting w_e =0, as we shall see in applications of the mixed layer equations to the boundary layer of the oceans in the next lecture.

Results illustrative of the dry convective case are shown in Figure 5.7 for a North African point from a July to August integration of the UCLA model carried out by Suarez et al. The model resolution used was 5 degrees in longitude and 4 degrees in latitude with 9 layers in the vertical. The model was integrated for a total of 45 days. Composite results for an arbitrarily chosen 9 day period during the last 30 days of the integration are shown. The diurnal cycle is very prominant at this North African location , where there is little evaporation and therefore a large diurnal swing in the ground temperature. It should be noted that a maximum depth of 15% of the mass of the atmosphere below 100 mb was imposed on the growth of the boundary layer (and a minimum depth of 10 mb) which was, in fact reached at this location during the day. The gradual morning deepening of the boundary layer associated with negative entrainment velocities (air being entrained into the boundary layer) is followed by an afternoon of nearly steady depth, then a rapid evening transition associated with large positive entrainment velocities (the boundary layer "detraining"). The ground temperature has its minimum near 0600 and its maximum near 1400 local time. The surface sensible heat flux attains large upward values in daytime, with its maximum near local noon, and only small, negative, values at night. This reflects the strong stability dependence of the surface transfer coefficients.

****

.nj

Advanced Lecture 5-References

Cattle, H. and K.J.Weston, 1975, Budget studies of heat flux profiles in the convective boundary layer over land. Q.J.R.Met.Soc., 101, pp 353-364

Davis, R.E., R.de Szoeke, D.Halpern and P.Niiler, 1981, Variability in the upper ocean during MILE. Part I: The heat and momentum balances. Deep-Sea Res., 28A, pp 1427-1451.

Deardorf, J.W., 1974, Three-dimensional numerical study of turbulence in an entraining mixed layer. Bound-Layer Meteor., 7, 81-106.

Driedonks, A.G.M., 1986, Bulk boundary layer schemes. Vol. 1, Seminar on physical parametrization for numerical models of the atmosphere. ECMWF.

Suarez, M.J., A. Arakawa and D.A. Randall, 1983, The parametrization of the planetary boundary layer in the UCLA general circulation model: Formulation and results. Mon. Wea. Rev., 111, pp 2224-2243.

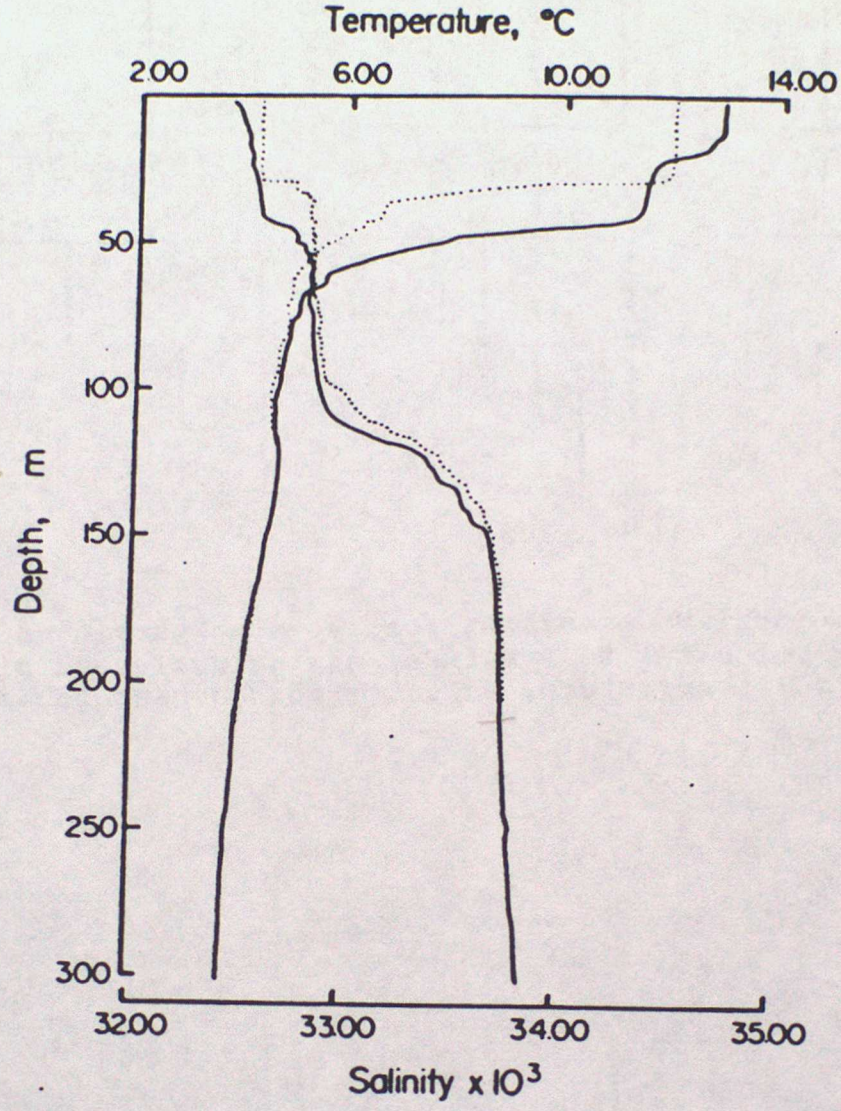

Figure 5.1 Profiles of temperature and salinity at 49°35'N,145°08'W, 0845 GMT, 21 August 1977 (solid) and 49°38'N,145°08'W, 1320 GMT, 24 August 1977 (dashed) (from Davis, de Szoeke, Halpern and Niiler, 1981)

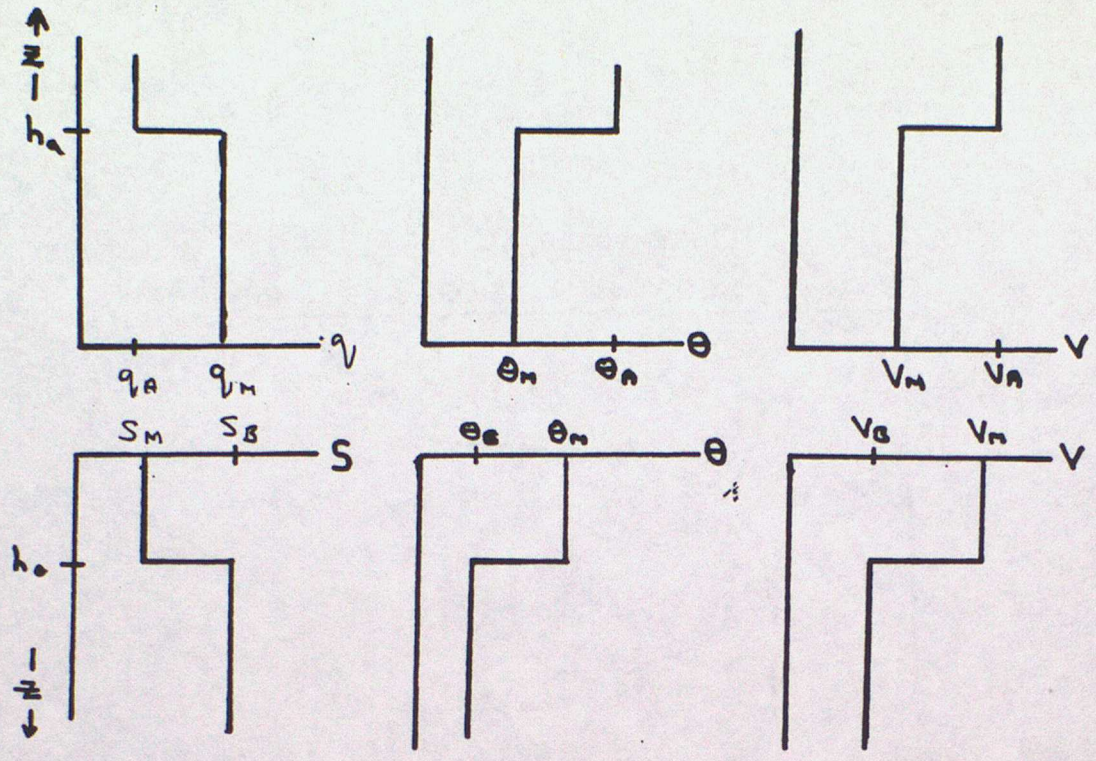

Figure 5.2 Idealised profiles for the atmospheric and oceanic mixed layers for potential temperature, mixing ratio and wind (atmosphere) and potential temperature, salinity and current (ocean)

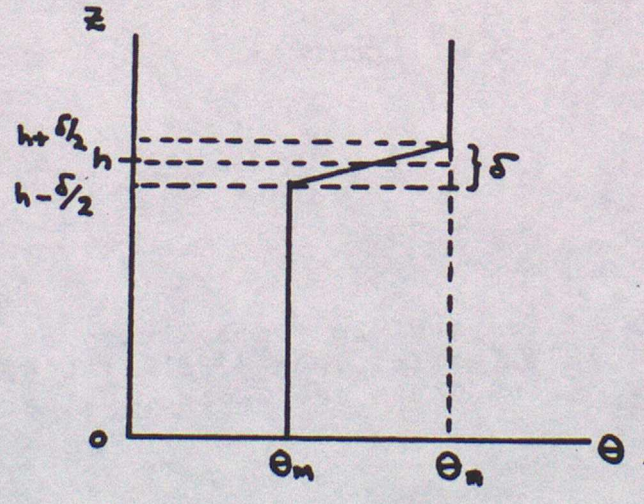

Figure 5.3 Assumed profile shape for vertical integration.

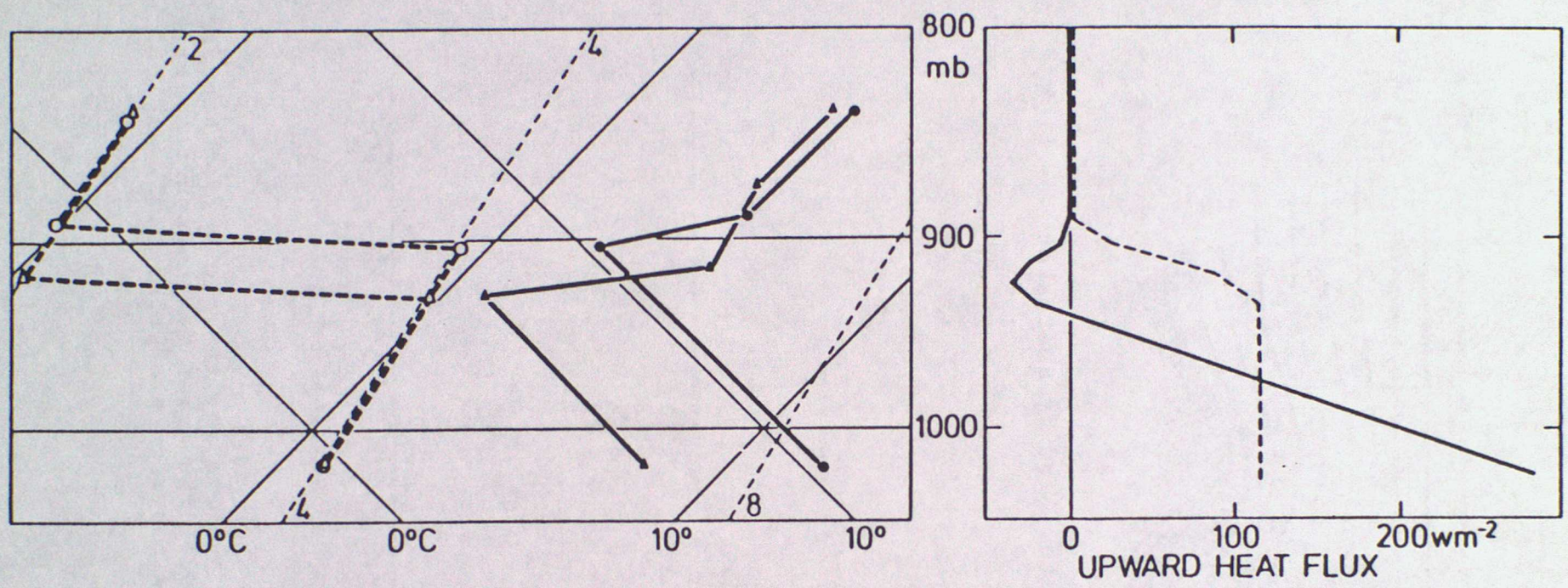

Figure 5.4 Representative smoothed soundings through the boundary layer for 1030 GMT (triangles) and 1330 GMT (circles) on 24 March 1972 and the associated mean profiles of upward sensible heat flux (solid line) and of upward latent heat flux (dashed line) deduced respectively from the change in temperature and moisture profiles between these times (from Cattle and Weston, 1975).

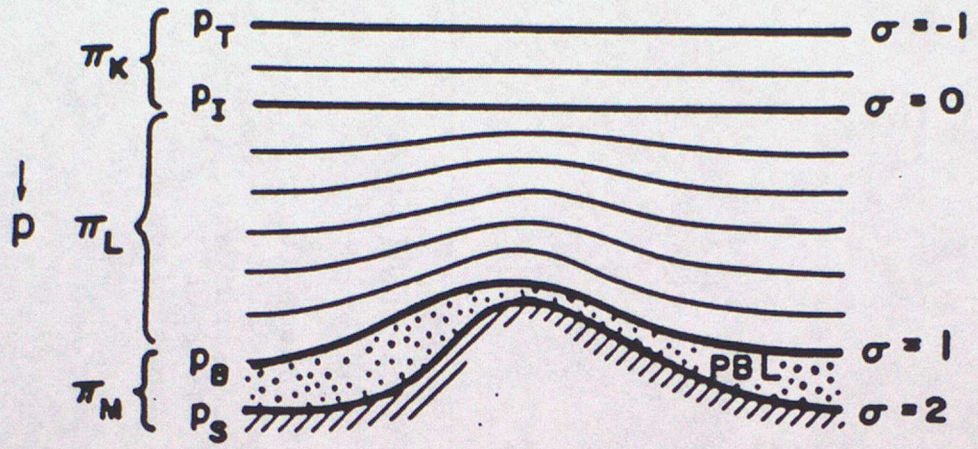

Figure 5.5 Sigma-coordinate system used by Suarez et al. (i983) in the UCLA model.

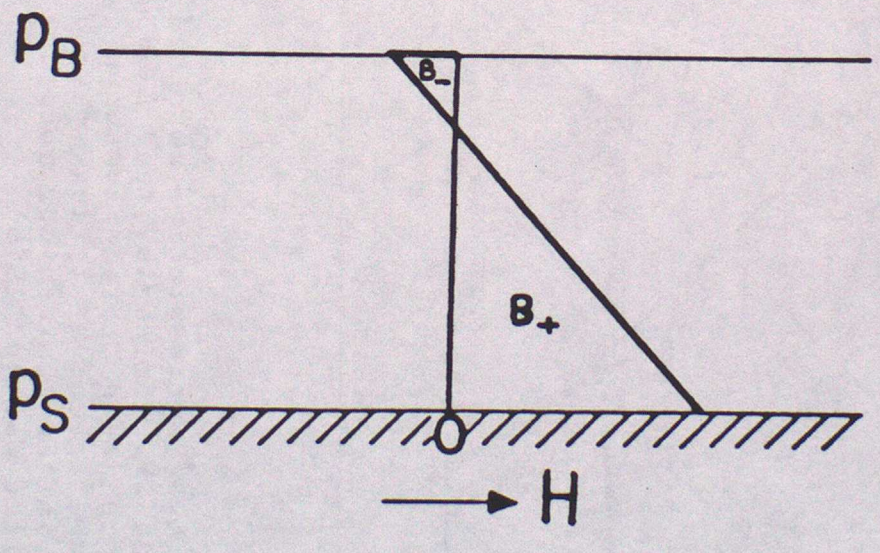

Figure 5.6 Assumed heat flux profile for the cloud free boundary layer as used by Suarez et al. (1983). The areas that measure positive and negative contributions to the buoyancy are shown as B_+ and B_-.

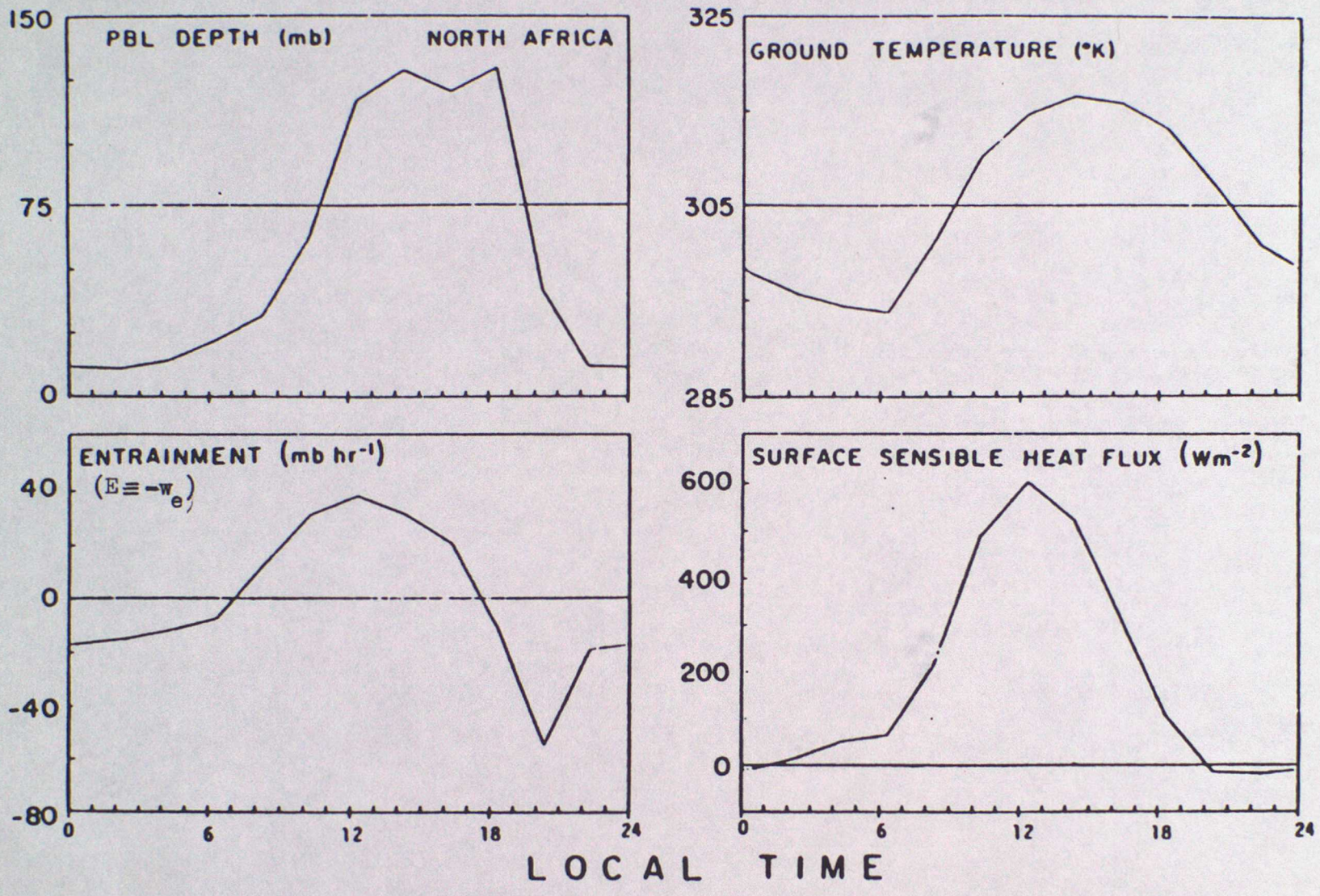

Figure 5.7 9-day average diurnal composites of boundary layer depth, ground temperature, entrainment and sensible heat flux, shown for a North African point from an integration of the UCLA model by Suarez et al. (1983).